Some "simple" strategies for modeling magnetically confined plasmas

David Mascali – Laboratori Nazionali del Sud, CATANIA

Many thanks to Lorenzo Neri, Giuseppe Castro and Federico Di Bartolo for their support in lectures preparation

INFN
Istituto Nazionale di Fisica Nucleare

OUTLINE

1st Part

1. General properties of plasmas and magnetic confinement
2. Applications of plasma physics in the field of magnetic confinement fusion and ion sources for particles accelerators
3. Electron Cyclotron Resonance Ion Sources: the most performing devices for accelerator feeding with high intensity an high charge state ion beams

2nd Part

1. Modeling of magnetically confined plasma
2. Monte-Carlo code for simulation of confinement, heating, beam formation
3. Ray tracing calculation and balance equations
4. Impact of modeling on ion sources development

Plasma

3 states of matter: solid – liquid - gaseous

But what about heating much more strongly!!!!

steam… gaseous …

Plasma: the 4th state of matter





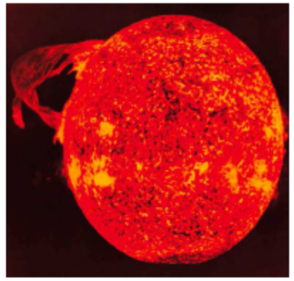

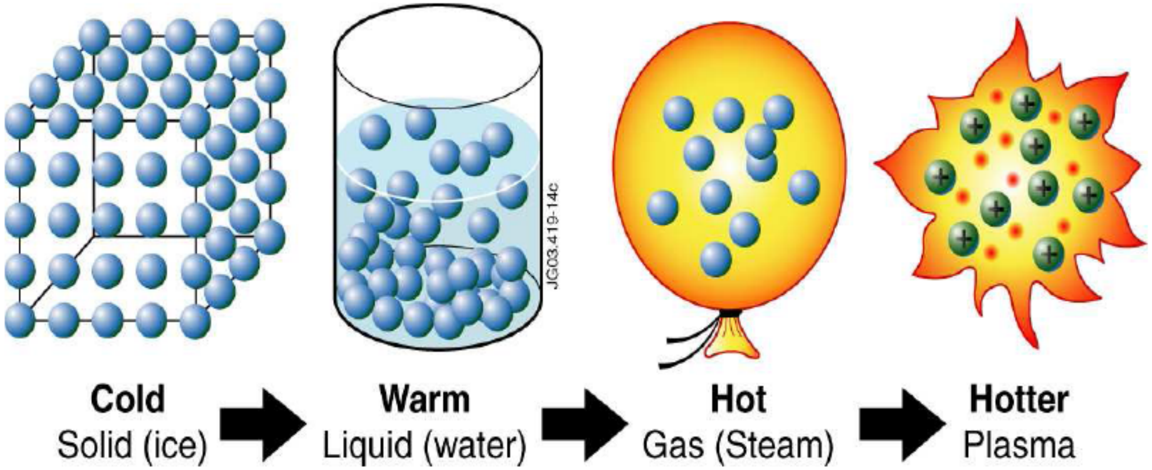

Aumentando la temperatura

Un plasma e' un ottimo conduttore di elettricita'

This is Plasma

Some Applications

Light
(see lamps und projector)

Plasma Monitor
(Television)
large, well resolving, flat

Surface
Hardening

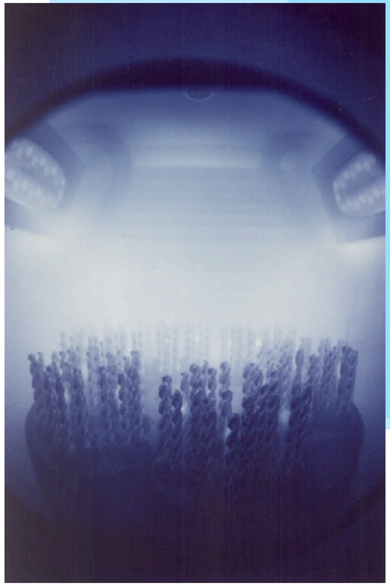

cold
plasm

Surface
Refinement

Plasma treated roof
of the cathedral
„Christ the Saviour"
in Moscow. Steel tiles
covered with films
of Titanium Nitride
and diamond-like carbon

Main Plasma Constituents

- positively charged ions
- electrons
- neutrals

Key Plasma Properties

- quasineutrality
- collective behavior

Electron Temperature and Distribution Functions

Weakly ionized plasma is a mixture of different gases:

neutral gas, ion gas and electron gas.

Under the action of electromagnetic fields electrons gain much more energy from the EM-field than ions. Their mean energy exceeds by far the mean energy of the ions and the neutrals. Thus

$$T_e >> T_+, \mathrm{T}_n$$

In plasma temperatures are measured in eV:

kT = 1eV corresponds to T = 11600 K

Typical values: kT_e = 1… 10^4 eV for electrons

kT_+ = 0.03…0.1eV for *ions*

Why are magnetic fields applied to plasmas?

Stabilization of electron and ion confinement is mandatory for plasma ignition or multicharged ions production

The problem of Coulomb barrier tunneling

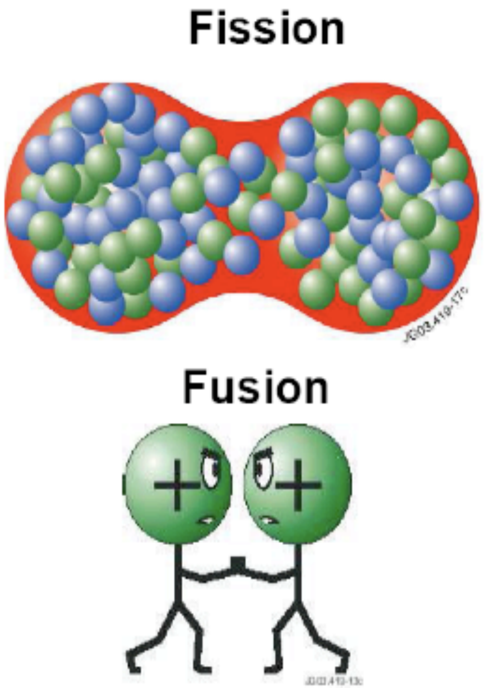

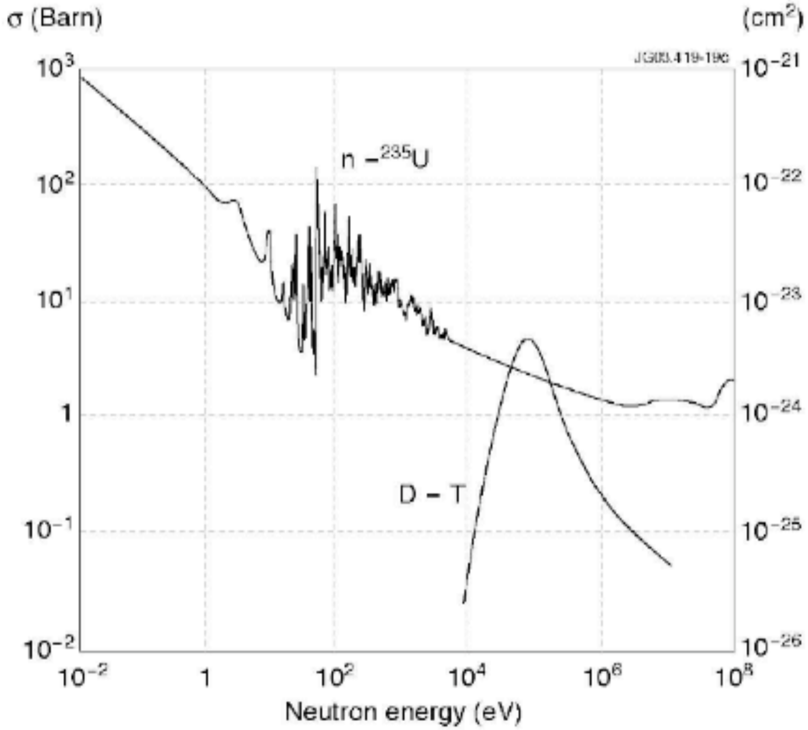

A sufficiently high energy must be transferred to nucleons in order to lead to nuclear fusion (on the order of 10^2 keV). This energy corresponds to temperatures of the order of 100 million of Celsius degrees. At these temperatures the matter is PLASMA

High density – long lifetimes are required for Ion Sources also!!

$$I_{ext} \propto \frac{n_e}{\tau_i} \; ; \qquad < q > \propto n_e{}^{*}\tau_i$$

Plasmas at high electron density and characterized by long ion lifetimes are specifically required. They can be produced by high intensity electron beams or sustained by microwaves

Principles of magnetic confinement

Stabilization of electron and ion confinement is mandatory to achieve ignition (FUSION) or highly charged ions (INJECTORS FOR ACCELERATORS)

How do plasmas can be confined?

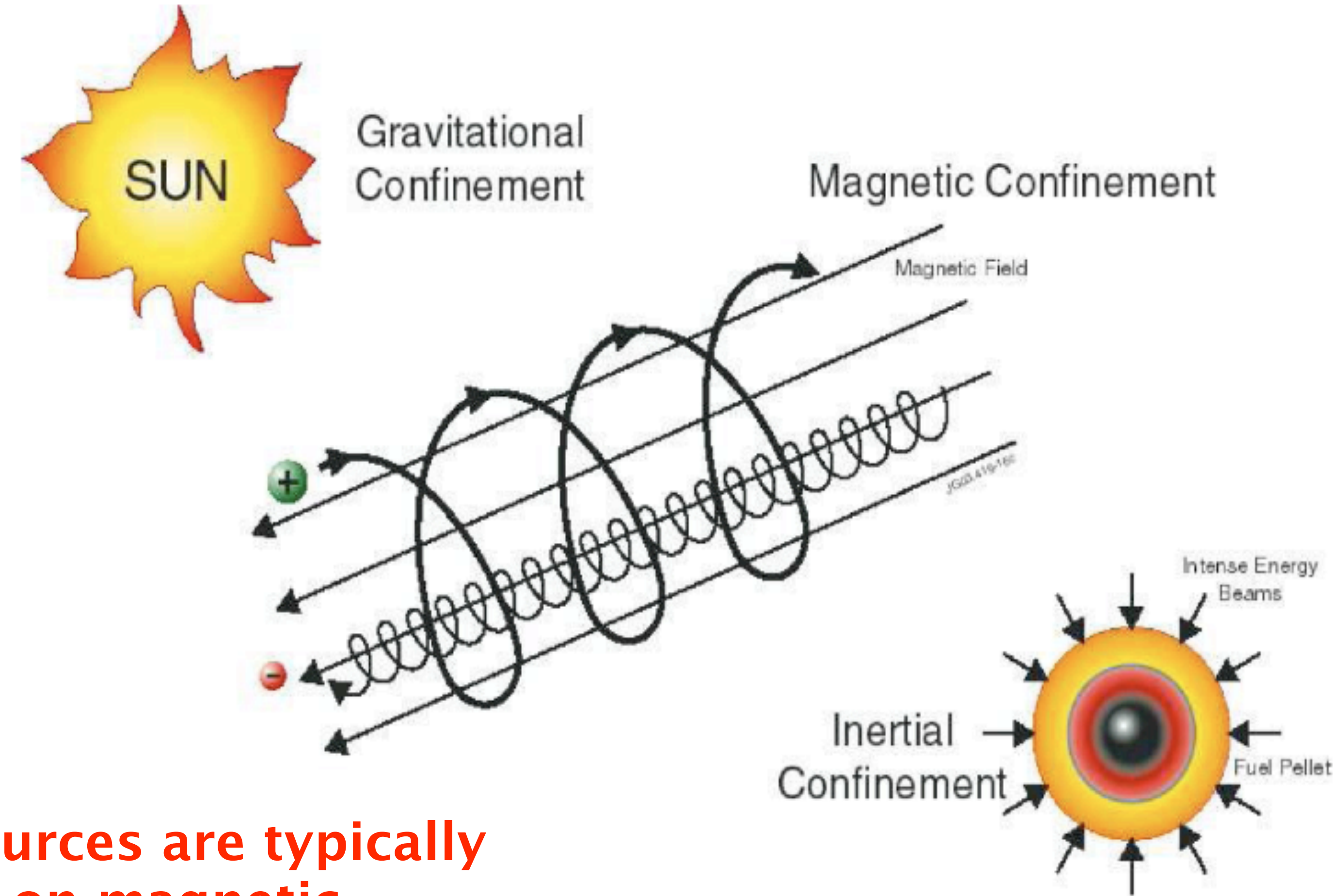

Ion sources are typically based on magnetic confinement

Gyration of ions and electrons under the action of a static magnetic field

❖The Lorentz force $\boldsymbol{F}_L$ exerted by a static magnetic field of induction B on particles of mass m bearing an elementary charge e causes a circular motion.

❖The radius (cyclotron radius) r_B of the circular trajectory is given by $r_B = mv/eB$

❖The corresponding cyclotron frequency ω_B does not depend on the particle velocity v: $\omega_B = eB/m$

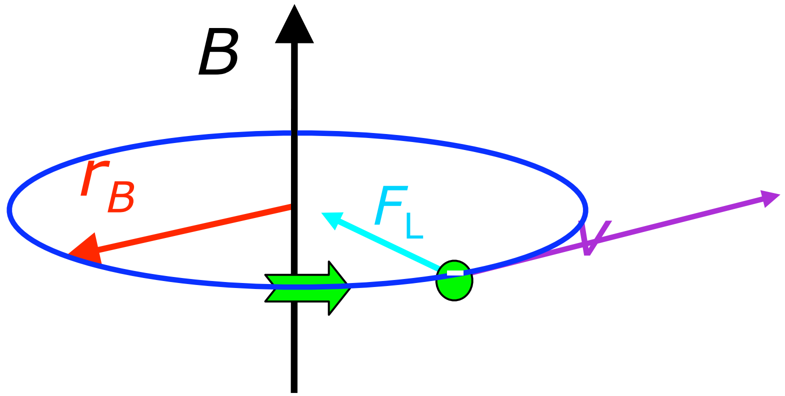

$$F_L = qv \times B$$

Magnetic Confinement

Magnetic fields intrinsically force charged particles to reduce freedom degrees: electrons spiralyze around the field lines and can be trapped for several ms in mirror machines or toroidal structures.

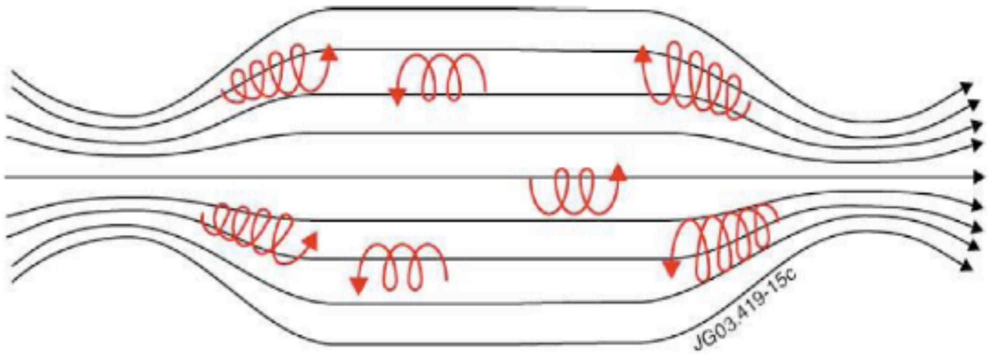

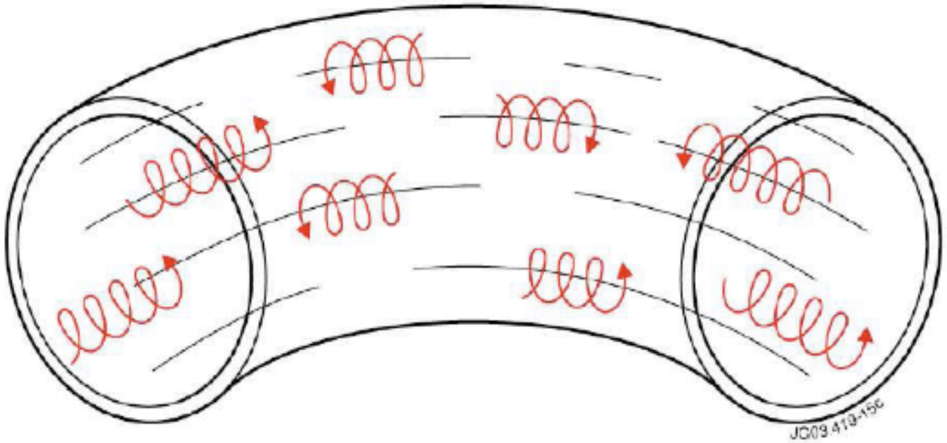

MIRROR STRUCTURES have axial symmetry and can be produced by sequences of room temperature or SC coils. They are commonly used in ion sources field

TOROIDAL CONFINEMENT is typical of Fusion Machines like TOKAMAKS or STELLARATORS

The ideal confinement requires some stringent conditions on plasma equilibrium and stability

Plasma can also be viewed as fluids. Therefore the confinement and its equilibrium and stability can be investigated by looking to the equilibrium between the plasma kinetic pressure and the magnetic (confining) field pressure.

$$p + \frac{B^2}{2\mu_0} = costante$$

The stability of the confinement can be studied as a function of the β parameter, which is the ratio between the kinetic and magnetic pressures.

$$\beta \equiv \frac{\sum nkT}{\frac{B^2}{2\mu_0}}$$

The condition for a magnetically stable plasma is that $\beta << 1$

Stability of magnetic confinement

The magneto-hydro-dynamics equation gives:

$$\nabla p = \frac{1}{\mu_0}(\nabla \times \boldsymbol{B}) \times \boldsymbol{B} = \frac{1}{\mu_0}\left[(\boldsymbol{B}\cdot\nabla)\boldsymbol{B} - \frac{1}{2}\nabla \boldsymbol{B}^2\right]$$

$$\Rightarrow \quad \nabla\left(p + \frac{B^2}{2\mu_0}\right) = \frac{1}{\mu_0}(\boldsymbol{B}\cdot\nabla)\boldsymbol{B}$$

In case B is smoothly variable along its own direction, the right hand term can be neglected, yielding:

$$p + \frac{B^2}{2\mu_0} = \text{costante}$$

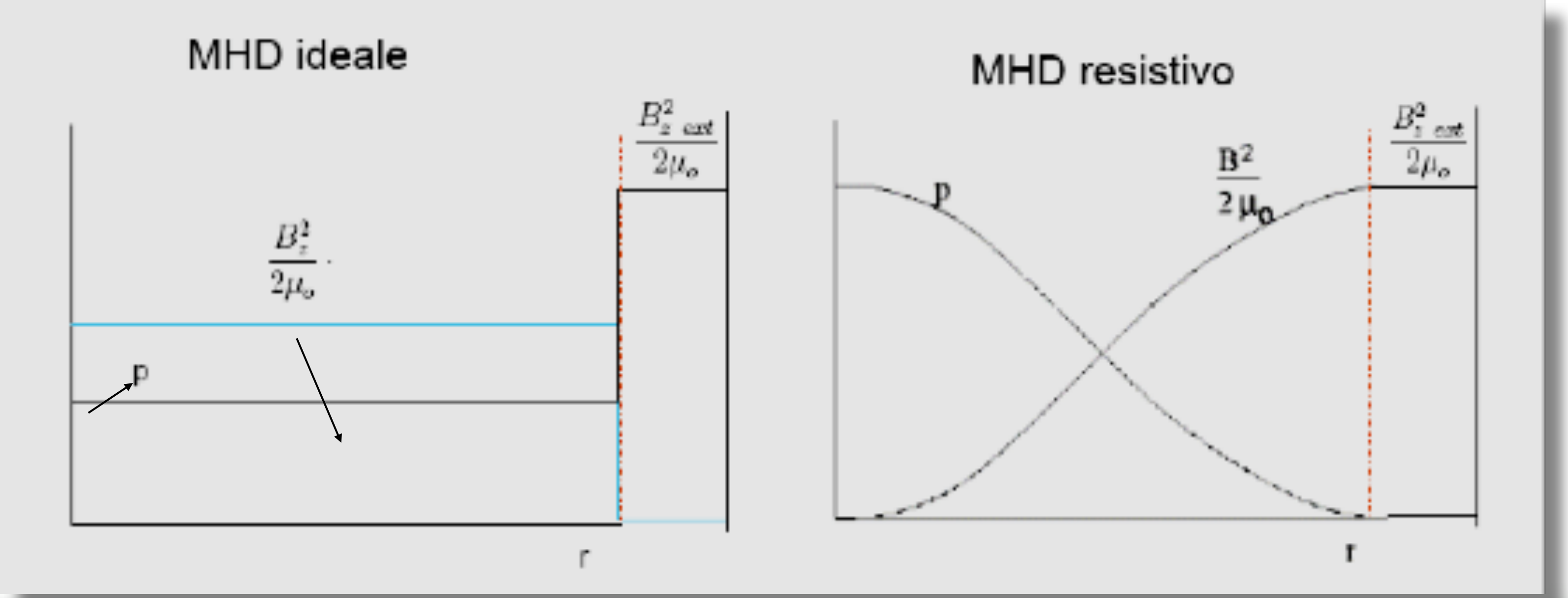

Principles of magnetic mirrors

Magnetic mirrors are largely employed in ion sources field since allow the construction of compact-size machines. Some ingredients are needed to ensure efficient trapping:

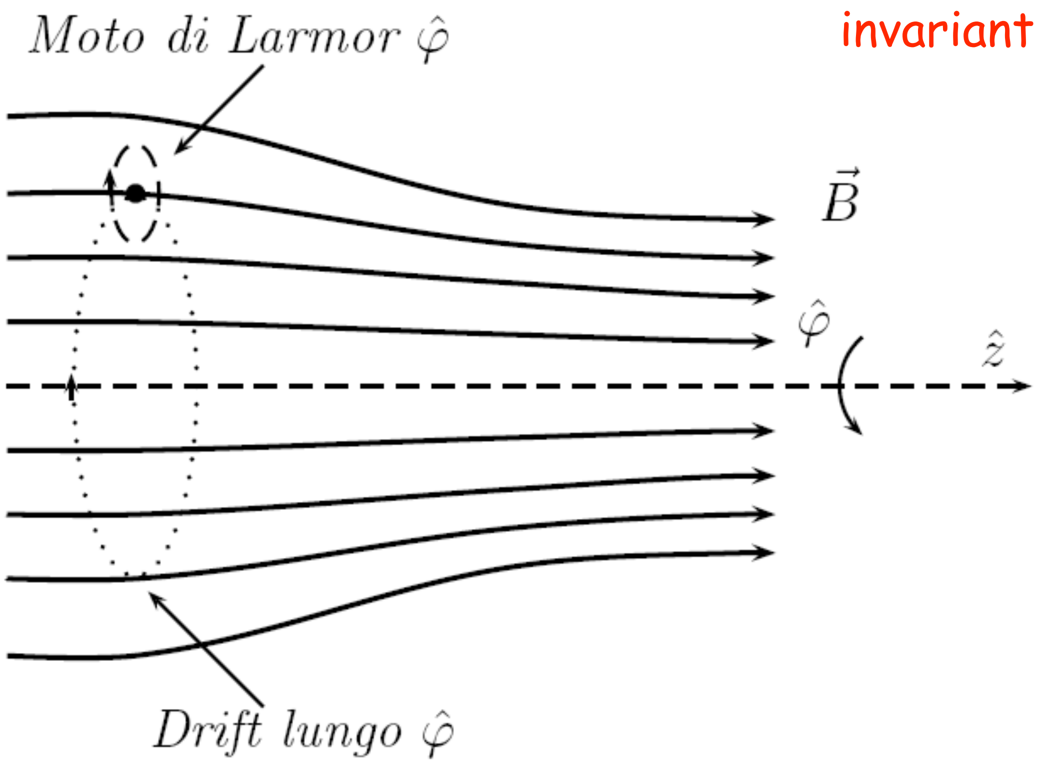

Adiabatic invariant

✓ A magnetic gradient must exist along the direction of B:

$$\vec{F}_{\parallel} = -\mu \frac{\partial B}{\partial s} = -\mu \vec{\nabla}_{\parallel} B$$

$$\mu \equiv \frac{1}{2} \frac{m v_{\perp}^2}{B}$$

✓ Radial component of the magnetic field;

✓The angle formed by the particle velocity w.r.t B must be as large as possible.

The mirror effect is a direct consequence of μ invariance.

Principles of magnetic mirrors

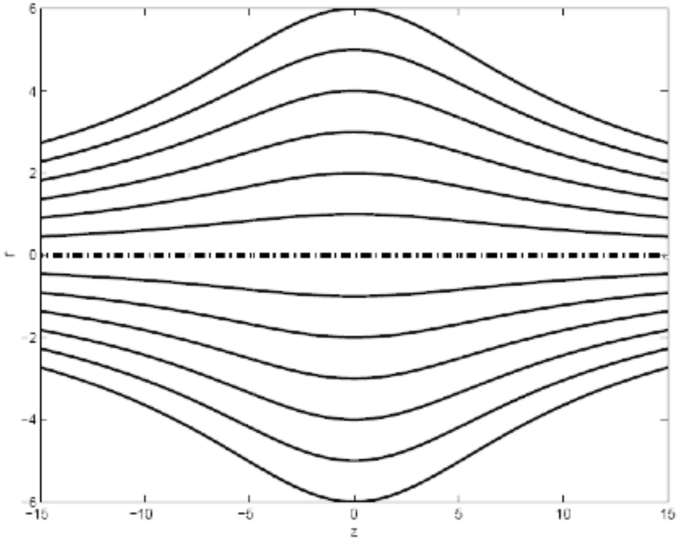

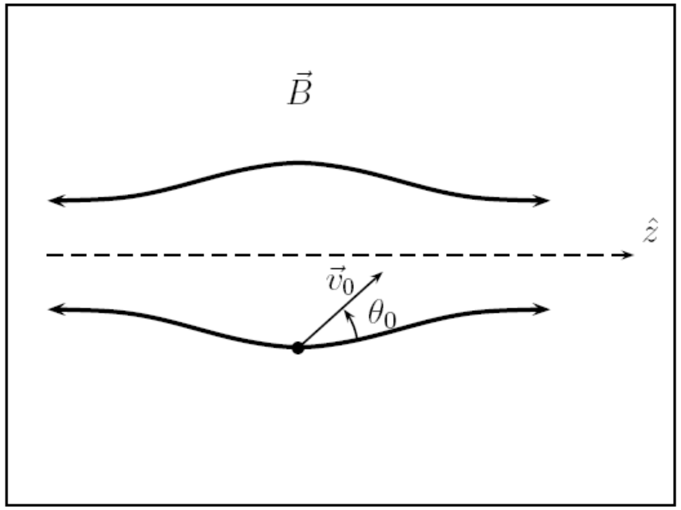

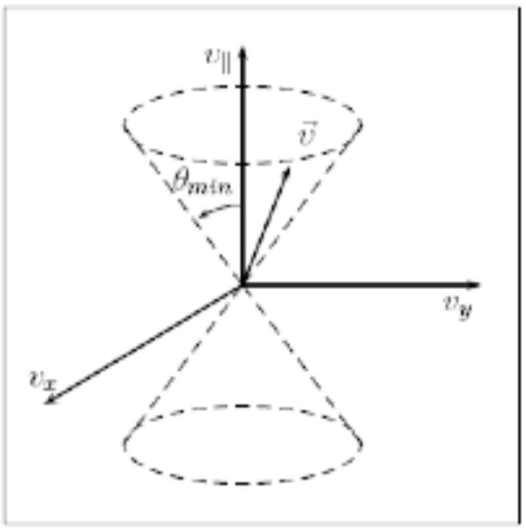

$$\theta_{min} = \arcsin\sqrt{\frac{B_0}{B_m}}$$

✓Efficient confinement by a single-particle point of view.

✓Considering a fluid approach, MHD instability arises because of the bad curvature of the field lines in the midplane, causing the onset of flute instability.

Effects of Magnetic Field

$$\vec{F}_{\perp} = q\vec{v} \times \vec{B} = qv_{\perp}B \Rightarrow \textit{precession around } B \text{ field}$$

$$\vec{F}_{=} = -\mu\nabla\vec{B} = -\frac{1}{2}mv_{\perp}^{2}\frac{\nabla\vec{B}}{B} \Rightarrow \text{confinement}$$

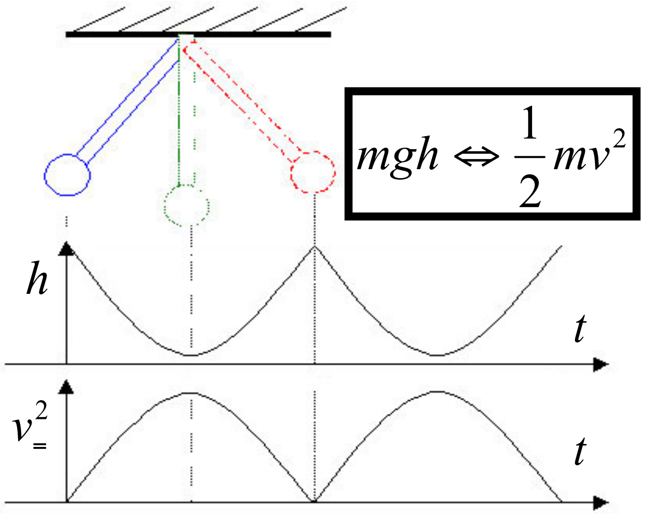

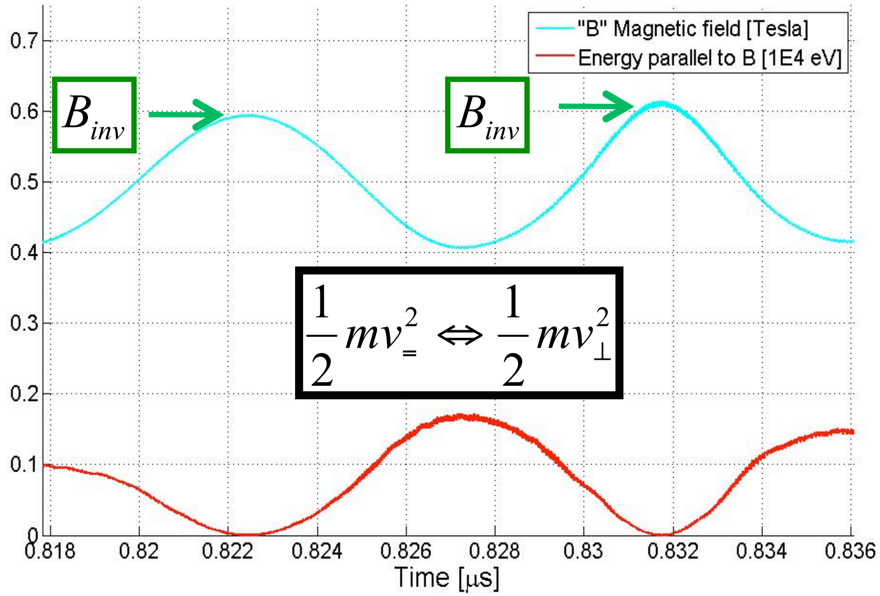

$$E_{tot} = mgh + \frac{1}{2}mv^2$$

$$E_{tot} = \frac{1}{2}mv_{=}^{2} + \frac{1}{2}mv_{\perp}^{2}$$

Principles of magnetic mirrors

- *The necessity of the minimum B structure*

Fluid instabilities generate lateral flows which reduce the plasma lifetime

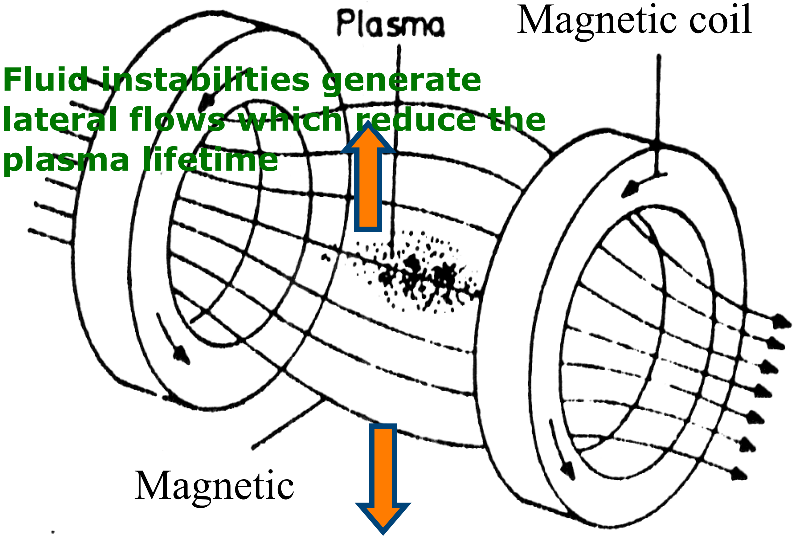

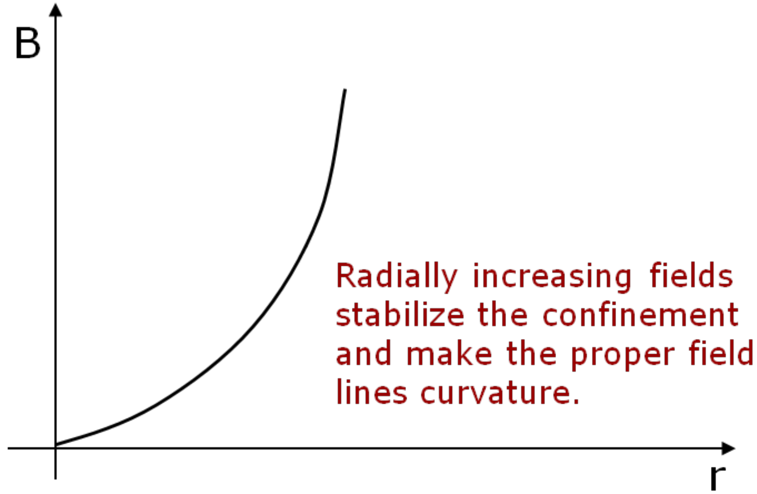

Radially increasing fields stabilize the confinement and make the proper field lines curvature.

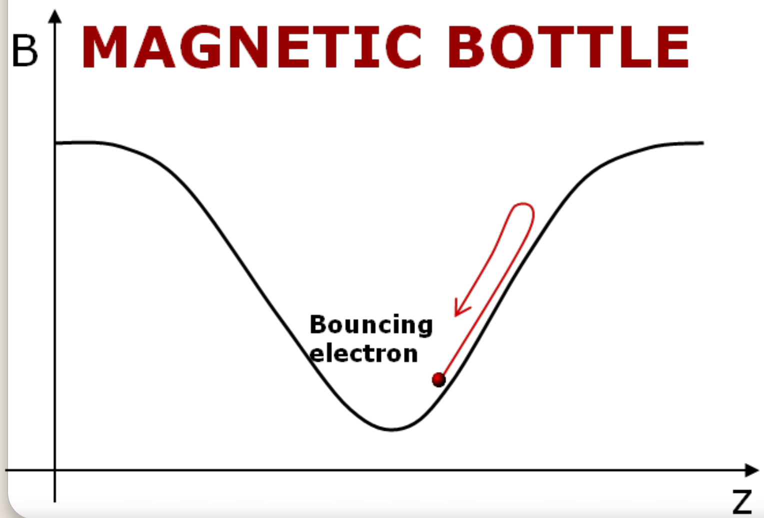

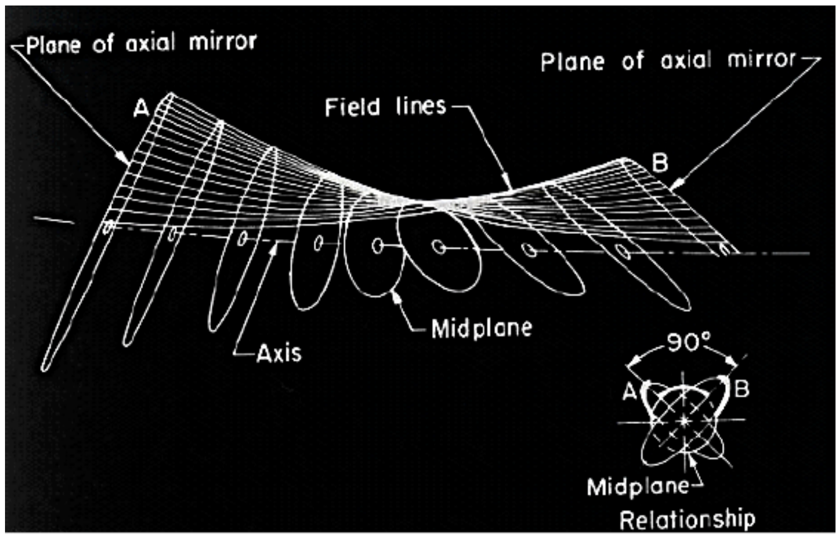

ECRIS magnetic structure

The necessity of the minimum B structure

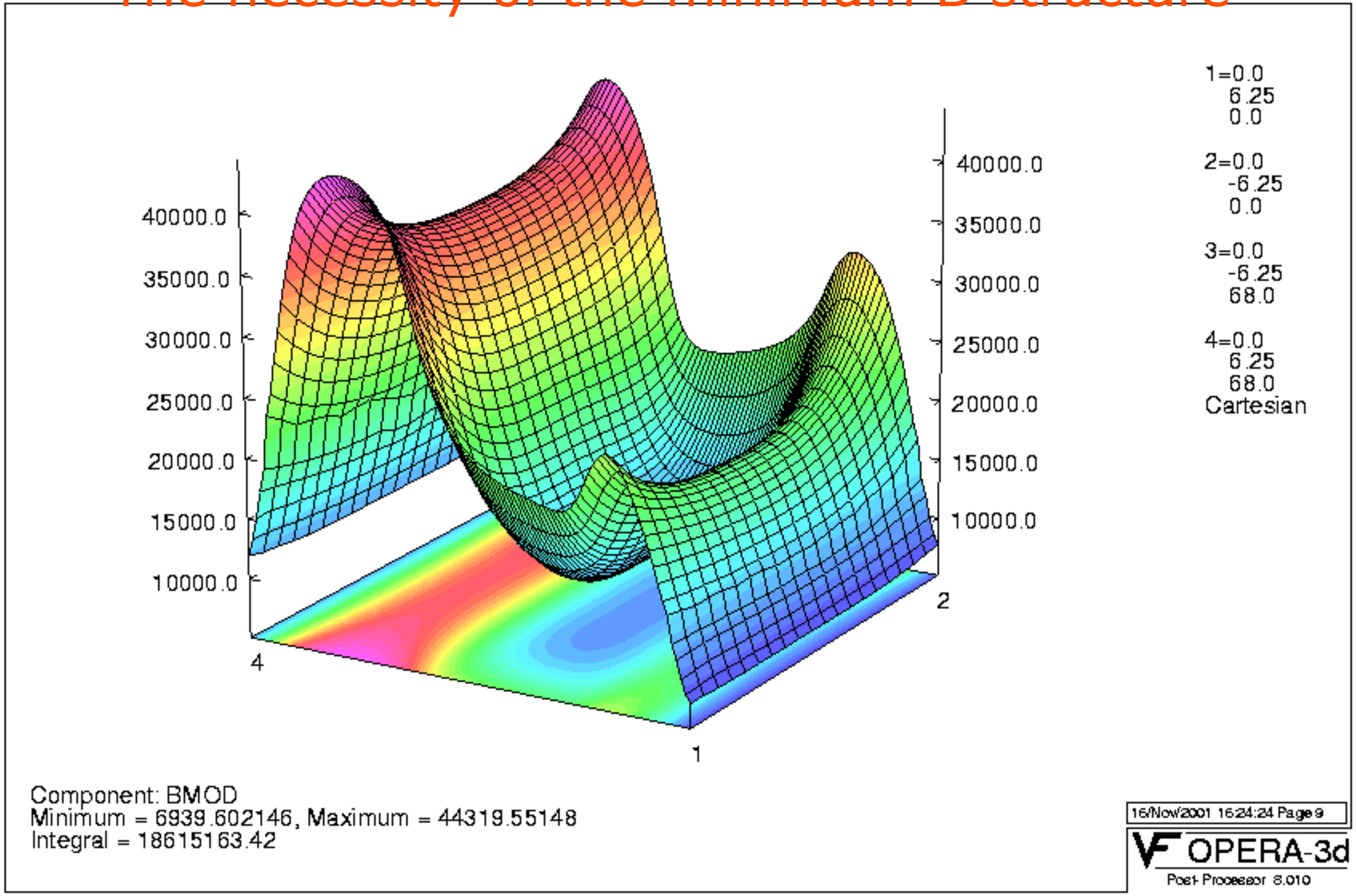

TOKAMAK-like magnetic structure

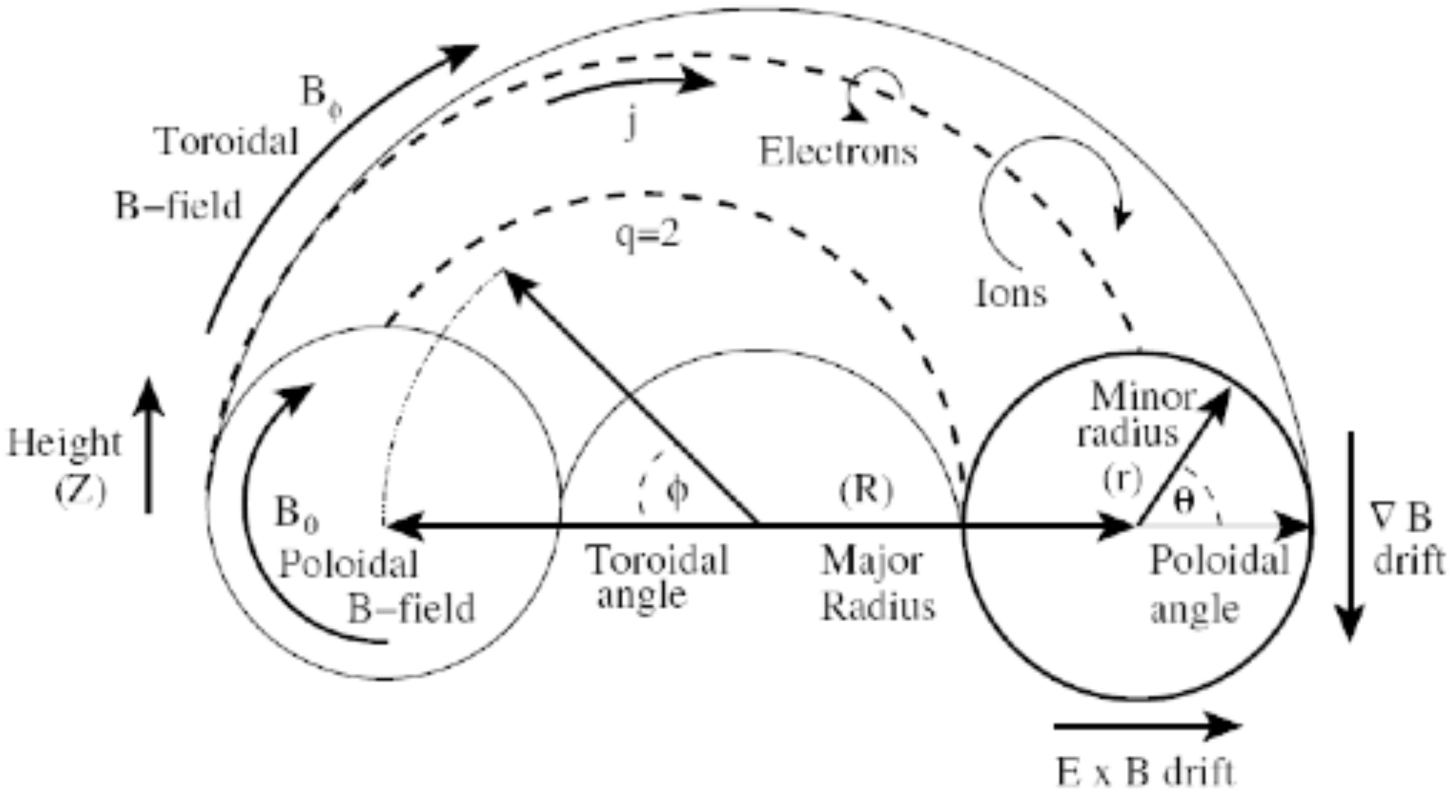

TOKAMAK-like magnetic structure

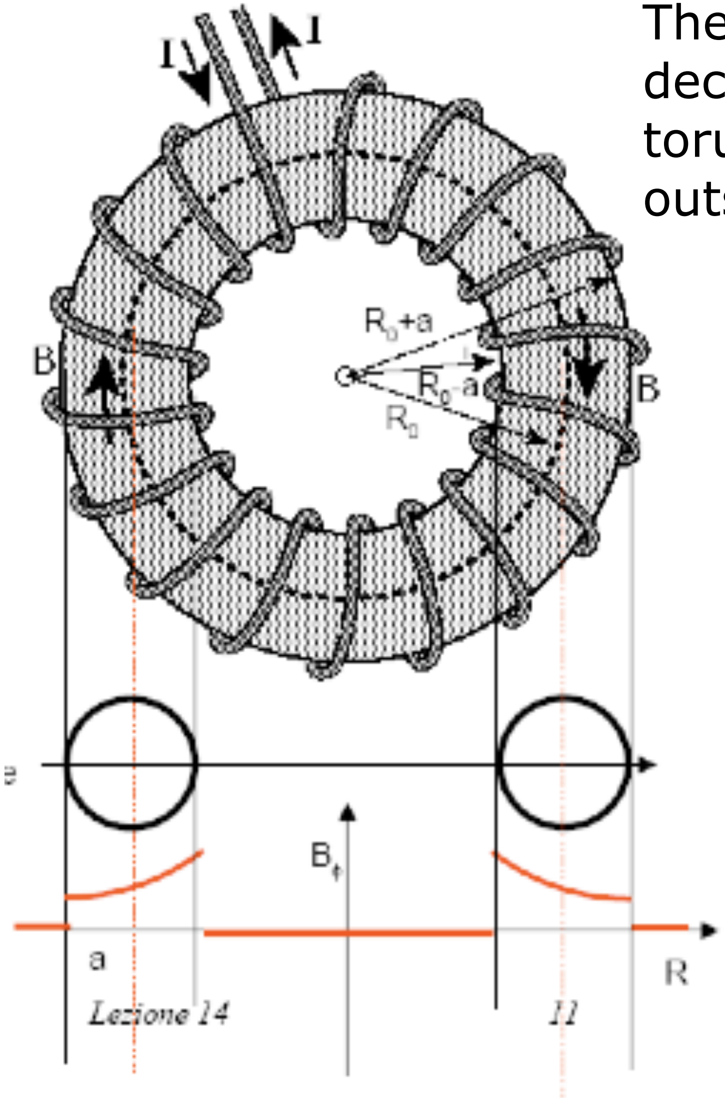

The magnetic field inside the solenoid decreases as 1/R, where R is the main torus radius. The magnetic field is zero outside from the solenoid.

$$\mathbf{B}(R) = \mu_0 \frac{NI}{2\pi R}$$

$$\mathbf{B}(R_0) = \mu_0 \frac{NI}{2\pi R_0}$$

$$\mathbf{B}(R_0) = B_0 \frac{R_0}{R}$$

Single Particle confinement in TOKAMAKS

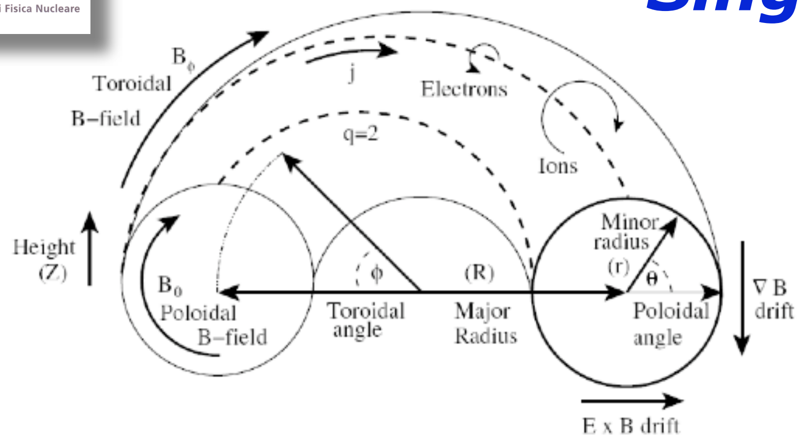

The simple toroidal field is not enough to guarantee the stable confinement of the plasma.

The B gradient induces a drift of the charged particles, which move away from the torus center:

$$\vec{V}_{DG} = \frac{\mu}{q}\frac{\vec{B}\times\vec{\nabla}B}{B^2}c$$

Being the drift due to the gradient oppositely directed for electrons and ions an electric field arises, which in turn produce an additional deconfining drift:

$$\vec{V}_{DE} = c\frac{\vec{E}\times\vec{B}}{B^2}$$

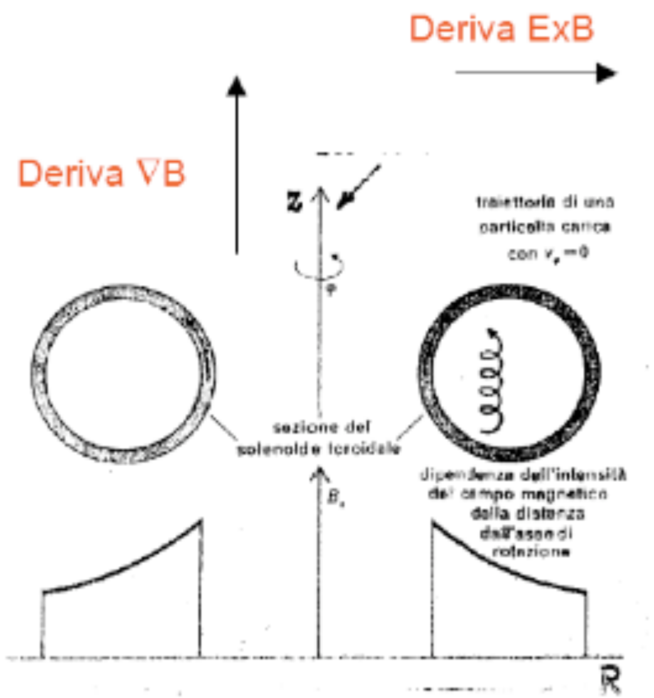

A stable confinement can be ensured only by a proper combination of poloidal and toroidal fields.

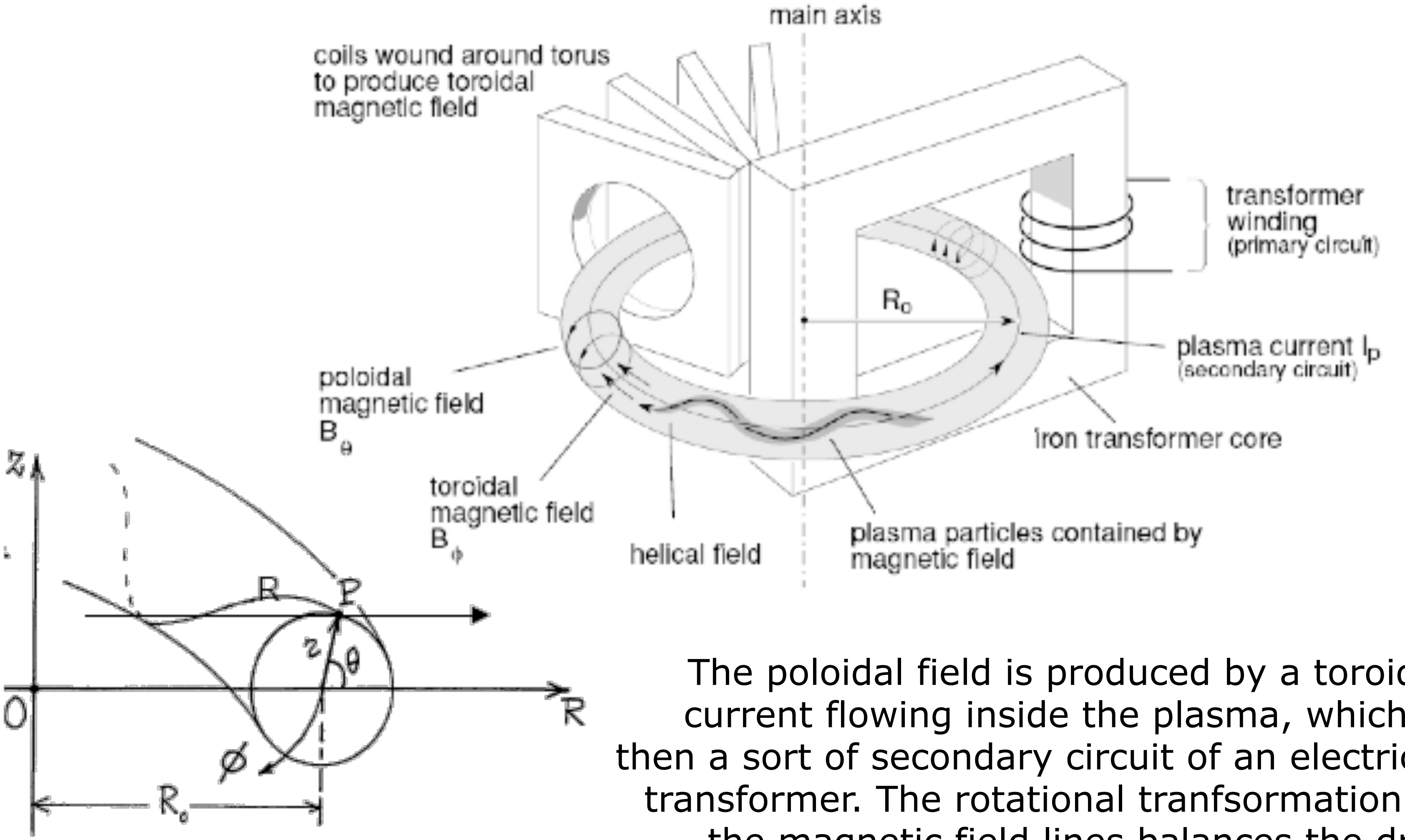

The poloidal field is produced by a toroidal current flowing inside the plasma, which is then a sort of secondary circuit of an electrical transformer. The rotational tranfsormation of the magnetic field lines balances the drift motions and stabilizes the plasma.

TOKAMAK-like magnetic configuration

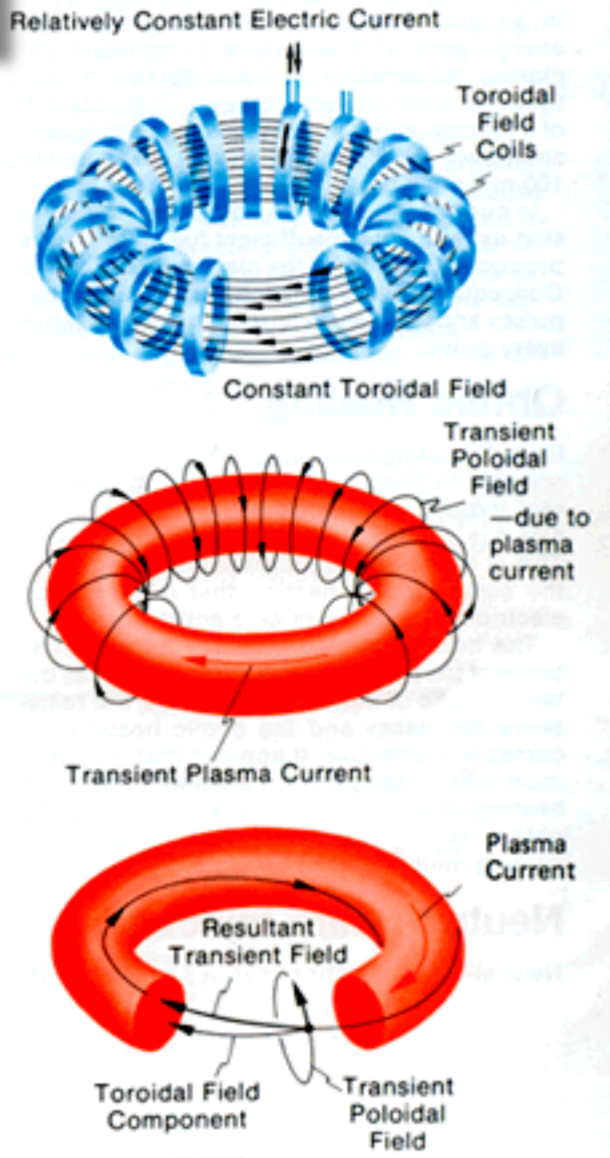

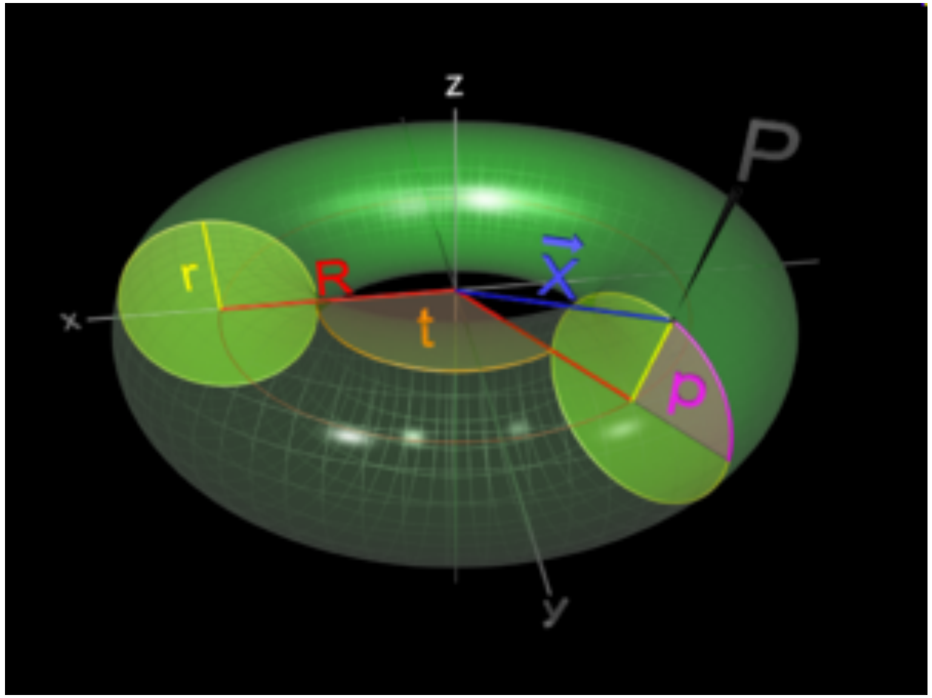

TOKAMAK coordinates

Global composition of the magnetic fields in TOKAMAKS

TOKAMAK

JET – Joint European Tokamak

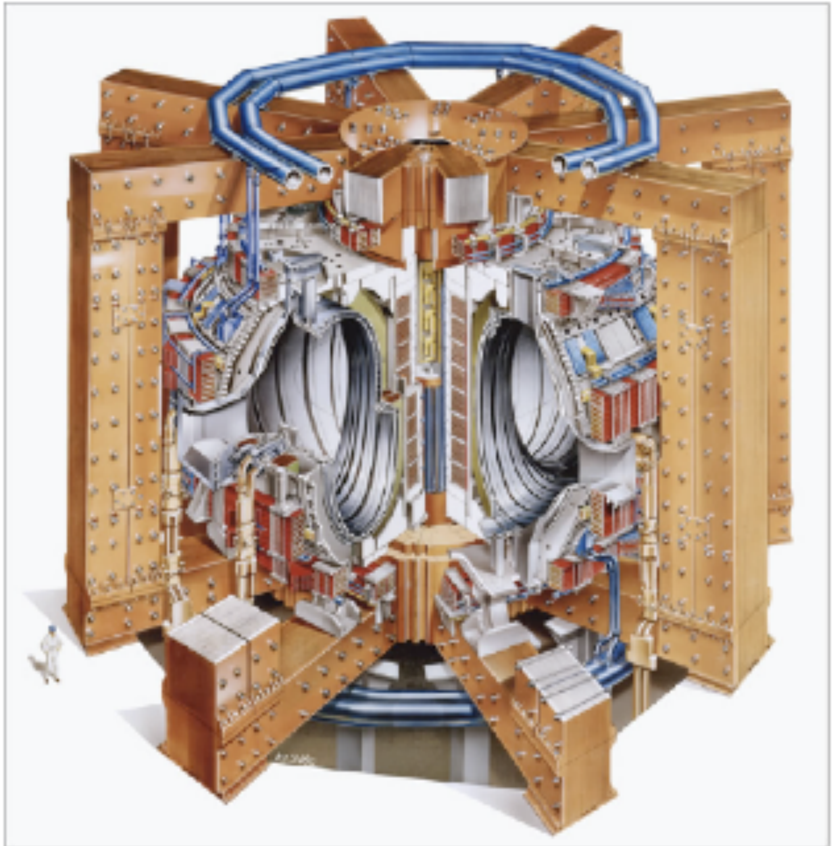

ITER

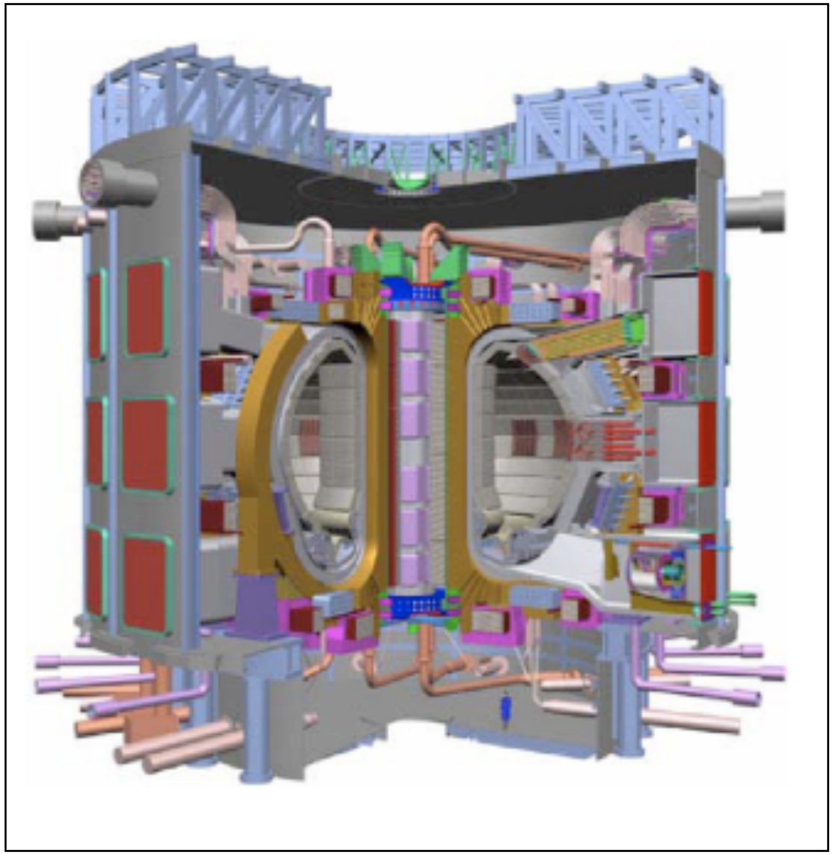

A tokamak is a machine producing a toroidal magnetic field for confining a plasma which is characterized by azimuthal (rotational) symmetry and the use of a plasma-borne electric current to generate the helical component of the magnetic field necessary for stable equilibrium.

JET: il Tokamak Europeo

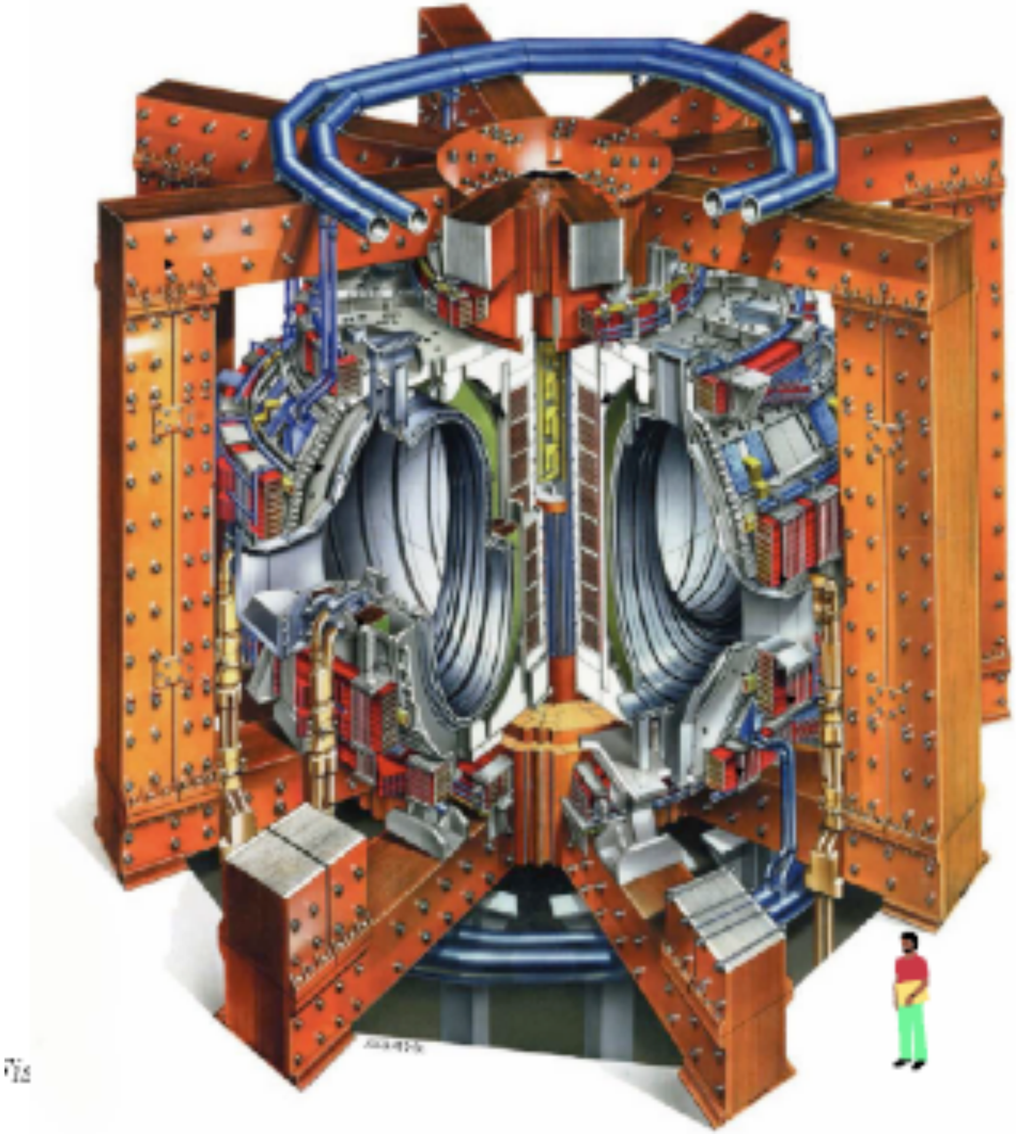

STELLARATOR-like systems

The poloidal field is produced by additional magnets which envelope the torus. The torus is adequately twisted in order to create nested magnetic surfaces. In this case the plasma heating is not governed by inner flowing currents, but it is due to RF heating.

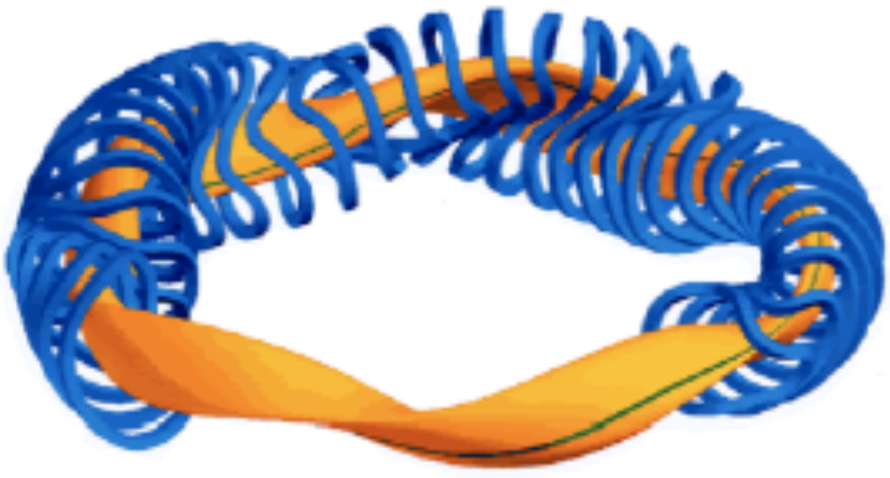

W7-SX Stellarator

1-helical coils, 2-toroidal field coils, 3-vertical field coils

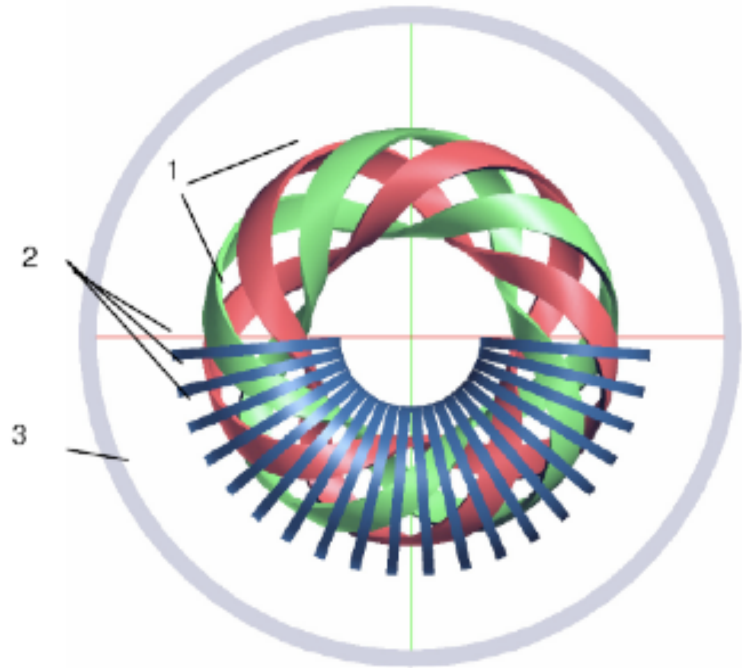

WEGA Stellarator @ Max Planck Institute for Plasma Physics

Fundamental aspects of ion generation and ion sources

The main goal of ion sources is the production of high quality ion beams to be injected into particle accelerators, minimizing beam losses and maximizing the overall reliability

The requirements of Ion sources employed for accelerators like LINACS or Cyclotrons are:

- ❑ **High stability and long-time operations without significant maintenance**
- ❑ **Production of intense beams of highly charged ions**
- ❑ **Low emittance.**
- ❑ **For pulsed operations, the number of particles per pulse must be as high as possible.**

MOTIVATIONS

ION SOURCES:

Their development is crucial to boost the accelerator performances

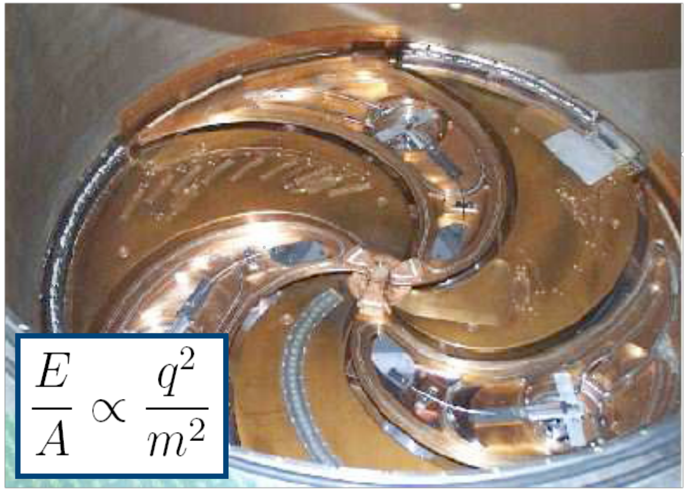

$$\frac{E}{A} \propto \frac{q^2}{m^2}$$

INFN-LNS Cyclotron

Increase of Ion Charge States → Higher energies attainable by Accelerators

Increase of Ion Current → Decrease of acquisition times for rare events

Increase of Ion Sources performances allow to enhance the Accelerators ones without hardware modifications

Atomic Physics background in Ion Sources Science

General Principles for the generation of multicharged ions

Atomic physics of Ion Sources

The ionization up to high charge state is a step by step process

If τ_i is the ion confinement time, then:

$$\boxed{n_e \tau_i \geq \frac{1}{[S_z(T_e)]}} \longrightarrow$$

Multiply charged ion formation criterion

By taking into account the electron temperature:

$$\boxed{n_e \tau_i \geq 5 \cdot 10^4 \left(T_e^{opt}\right)^{\frac{3}{2}}}$$

(we need warm electrons but cold ions!!)

$T_e^{opt} \simeq 5W_{thr} \longrightarrow W_{thr}$ the ionization energy of the particular charge state to be achieved

For fully stripped light ions

$$\boxed{n_e \tau_i \cong 10^{10}\ cm^{-3} \sec \qquad T_e^{opt} = 5\,keV}$$

Atomic physics background in ECRIS

Step by step ionization

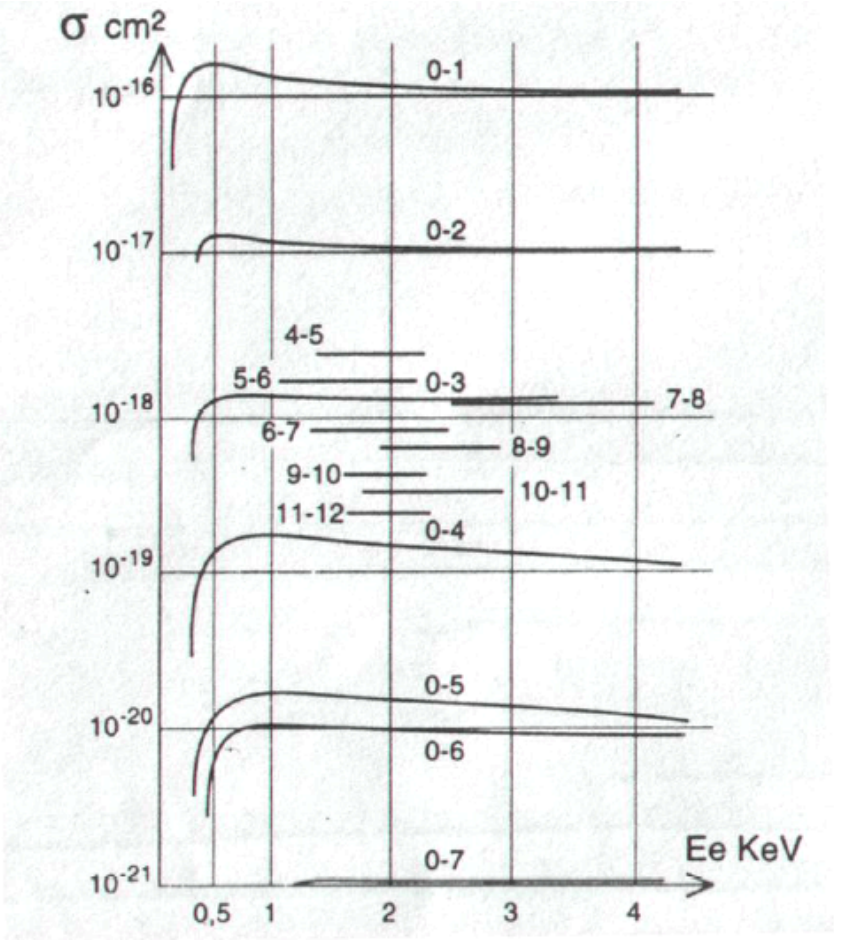

The cross section for ionizing processes like $z \rightarrow z{+}x$ as a function of energy features a maximum value when $x=1$. This means that the ionization proceeds expelling one by one electrons from atomic shells.

The ionization mechanism is therefore a slow process which requires long plasma lifetime to produce highly charged ions

Dynamical (Non-stationary)) balance equations for multi-charged ions (Shirkov 1991)

$dn/dt \neq 0$

$$\frac{dn_0}{dt} = \frac{S}{V}v_0(n-n_0) - n_0\left(\sum_{i=2}^{z}\sigma_i^{ex}n_iv_i + \sum_{i=3}^{z}\sigma_i^{2ex}n_iv_i(\sigma_1^i+\sigma_1^{2i})n_ev_e\right)$$

$$\frac{dn_1}{dt} = n_0\left(\sigma_1^i v_e n_e + \sigma_2^{ex}n_2v_2 + \sigma_2^{2ex}n_3v_3 + \sum_{i=2}^{z}\sigma_i^{ex}n_iv_i\right) - n_1\left(\sigma_2^i v_e n_e + \sigma_2^{2i}v_en_e + \frac{1}{\tau_1}\right)$$

$$\frac{dn_2}{dt} = n_0\left(\sigma_1^{2i}v_en_e + \sum_{i=3}^{z}\sigma_i^{2ex}n_iv_i\right) + n_1\sigma_2^iv_en_e + (\sigma_3^{ex}n_3v_3 + \sigma_4^{2ex}n_4v_4)n_0 - n_2\left((\sigma_3^i+\sigma_3^{2i})v_en_e + (\sigma_2^{ex}+\sigma_2^{2ex})v_2n_0 + \frac{1}{\tau_2}\right)$$

$$\frac{dn_i}{dt} = \sigma_i^iv_en_en_{i-1} + \sigma_{i-1}^{2i}v_en_en_{i-2} + (\sigma_{i+1}^{ex}n_{i+1}v_{i+1} + \sigma_{i+2}^{2ex}n_{i+2}v_{i+2})n_0$$

$$\boxed{3 \le i \le z-2} \quad - n_i\left((\sigma_i^{ex}+\sigma_i^{2ex})v_in_0 - (\sigma_{i+1}^i + \sigma_{i+2}^{2i})v_en_e + \frac{1}{\tau_i}\right)$$

$$\frac{dn_{z-1}}{dt} = (\sigma_{z-1}^in_{z-2} + \sigma_{z-2}^{2i}n_{z-3})v_en_e + \sigma_z^{ex}n_zv_z\,n_0 - n_{z-1}\left(\sigma_z^iv_en_e + (\sigma_{z-1}^{ex}+\sigma_{z-1}^{2ex})v_{z-1}n_0 + \frac{1}{\tau_{z-1}}\right)$$

$$\frac{dn_z}{dt} = (\sigma_z^in_{z-1} + \sigma_{z-1}^{2i}n_{z-2})v_en_e - n_z\left((\sigma_z^{ex}+\sigma_z^{2ex})v_zn_0 + \frac{1}{\tau_z}\right)$$

$$\frac{dn_e}{dt} = \left(\sum_1^{z-1}\sigma_i^i\,n_{i-1} + 2\sum_1^{z-2}\sigma_i^{2i}\,n_{i-1}\right)v_en_e - \frac{n_e}{\tau_e}$$

$$\Delta\phi = \frac{p}{2}en_eR^2f\left(1+2\ln\frac{l}{R}\right) \qquad f = \frac{\sum_{i=1}^{z} in_i - n_e}{n_e}$$

n_0 = density of neutrals inside the plasma
n = density of neutrals outside the plasma
τ_e = electron lifetime determined by the loss cone of the longitudinal magnetic field
l and R = length and radius of the cylindrical source
$\Delta\phi$ = potential
f = factor of plasma neutralization
v_0, v_i and v_e = mean velocities of neutrals, ions and electrons

σ_i^{ex} and σ_i^{2ex} = single – and double – charge – exchange cross sections for the ions with charge state i

σ_i^i and σ_i^{2i} = single – and double – ionization cross sections of the ions with charge state $i-1$

Typical Charge State Distribution

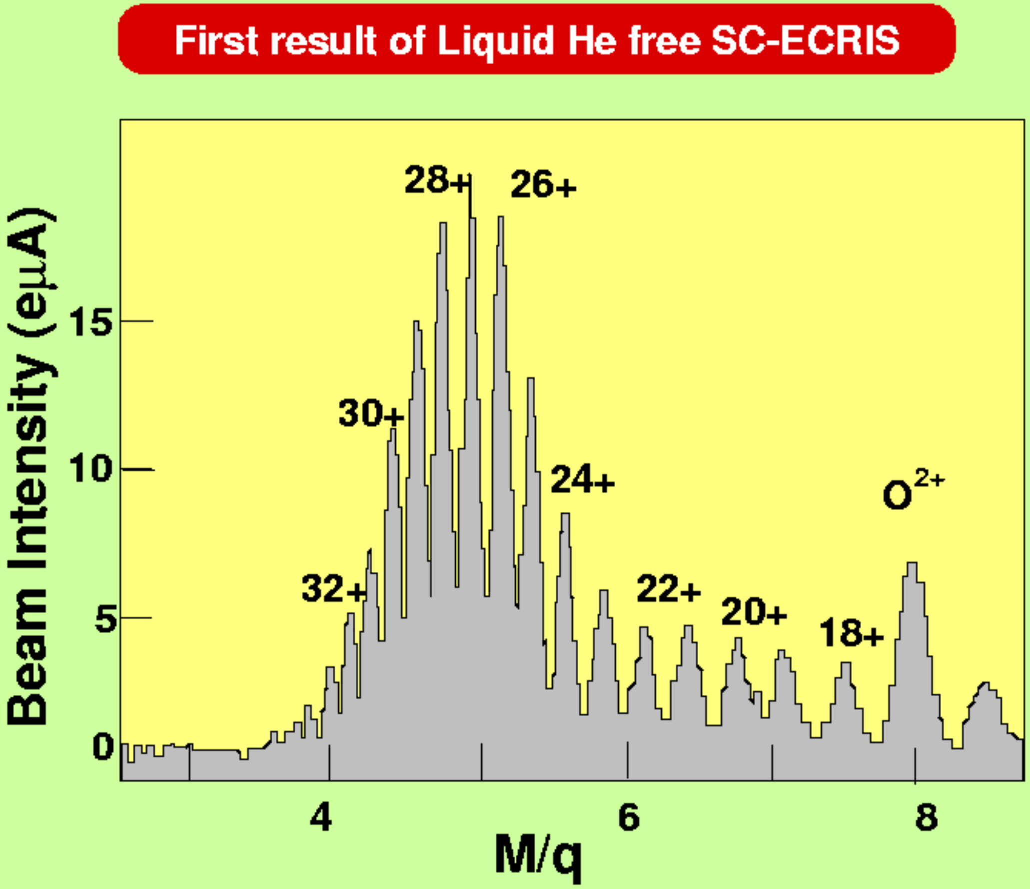

Parameters

Gas
^{136}Xe(85% enriched)+ O_2

Vacuum
- injection 1.9x10^{-7}Torr
- extraction 9.4x10^{-8}Torr

Magnetic field
- B_{inj} 1.84 T
- B_{center} 0.396 T
- $B_{extraction}$ 1.24 T

RF
- Freq 14.5 GHz
- Power 771W

extraction 15kV

Bias Disc
- voltage -225 V
- position 0.5 cm

Four types of ion sources for multicharged ions production or single-charged intense ion beams

EBIS (Electron Beam Ion Sources): easy production of beams at high charge states (very long plasma lifetime), unavailable for high intensity - single charge ion beams (too long plasma lifetime)

MDIS (Microwave Discharge Ion Sources): simplified version of ECRIS for high intensity proton (or single charge state ions) beams.

LIS (Laser Ion Sources): intense beams of medium and high charge states, production of metallic ions from refractive materials, but unable to produce beams in CW mode

ECRIS (Electron Cyclotron Resonance Ion Sources): intense beams of low charge states, moderate intensity of highly charged ions

BEST COMPROMISE **for production of intense beams of highly charged ions**

ECRIS magnetic structure

The necessity of the minimum B structure

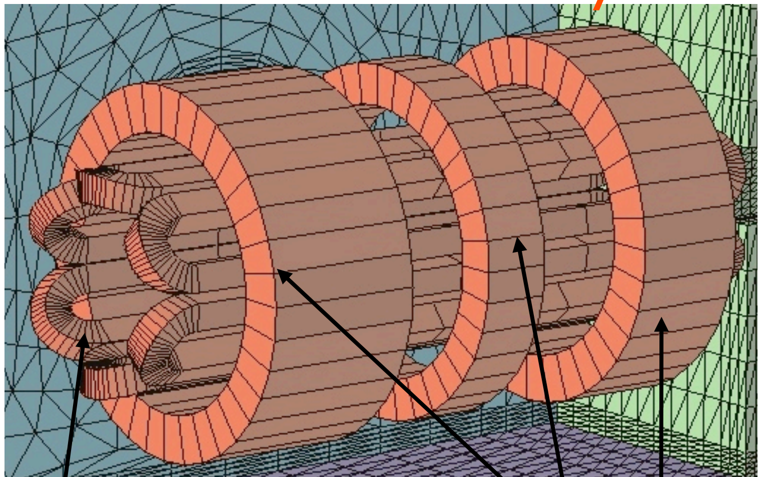

Hexapole for radial confinement

Solenoids for axial confinements

$$
\begin{aligned}
B_x &= -B_1 xz + 2Sxy \\
B_y &= -B_1 yz + S\left(x^2 - y^2\right) \\
B_z &= B_0 + B_1 z^2
\end{aligned}
$$

$$\vec{\nabla} \cdot \vec{B} = 0$$

Minimum B magnetic field structure

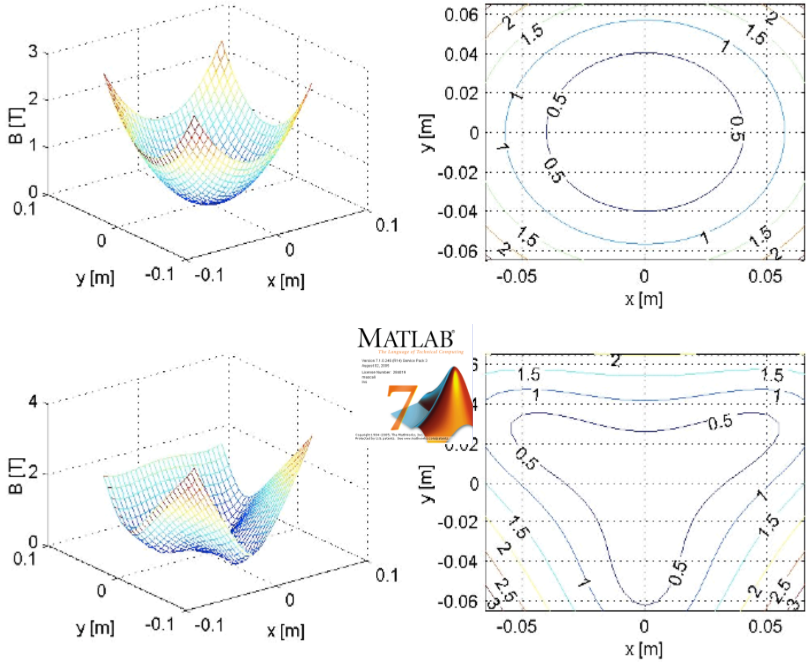

ECRIS subsystems

Ion beams are usually extracted from plasmas. In ECRIS the plasma is sustained by microwaves confined by means of magnetic fields

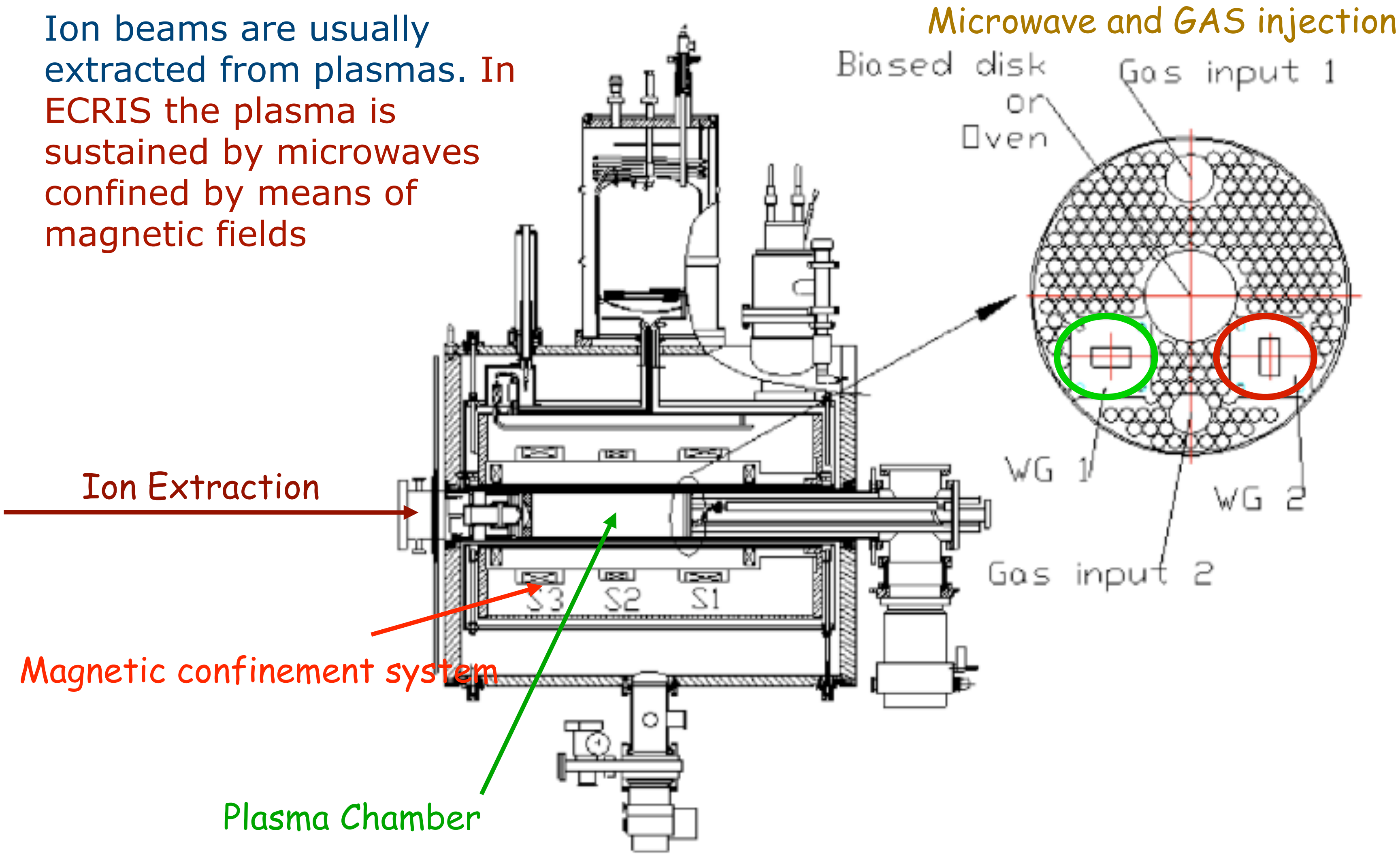

Wave propagation in magnetized plasmas

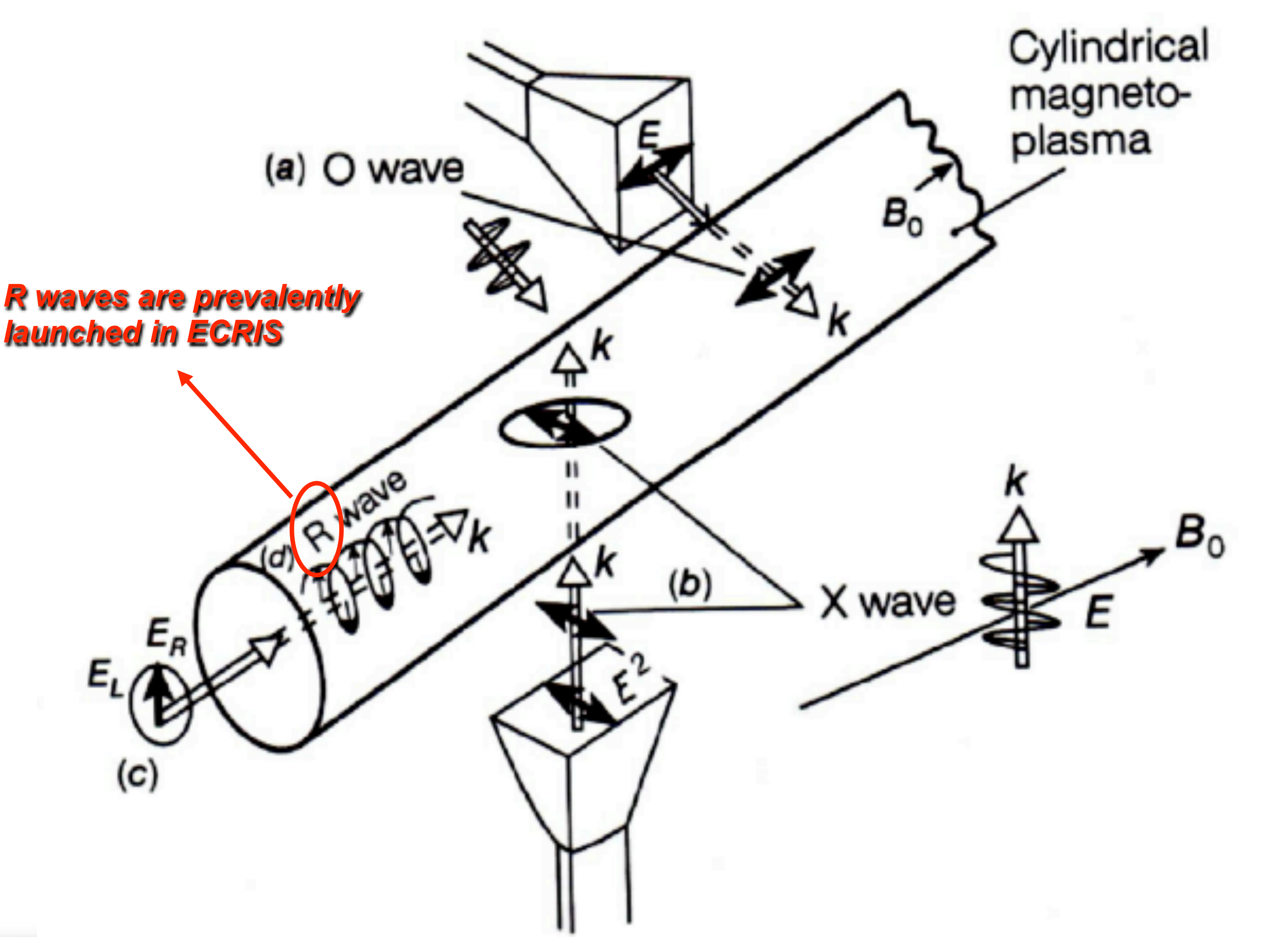

The creation of the ECR Plasma

During the plasma start-up an exiguous number of free electrons exist

Magnetic Field

Electrons turn around the magnetic field lines with the frequency:

$\omega_g = qB/m$

A circulary polarized electromagnetic wave transfer energy to the electrons by means of the ECR :

$\omega_{RF} = \omega_g$

The energetic electrons ionize the gas atoms and create a plasma.

The ionization up to high charge state is a step by step process which requires long ion confinement times and large electron densities

Up to 100 μA of Xe^{30+} can be obtained in 3rd generation ECRIS

ECRIS: classification in terms of "generations"

1st generation:
f=6-14 GHz, P=0.5 kW, I<mA, q=6-12 for Ar

2nd generation:
f=14-18 GHz, P=1-2 kW, I=1-2 mA, q=8-16 for Ar

3rd generation:
f=24-28 GHz, P=5-10 kW, I=20-40 mA, q=14-18 for Ar

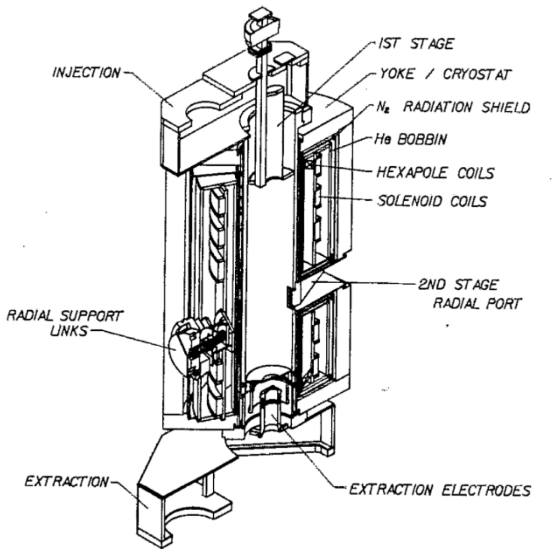

SC-ECRIS, MSU-NSCL

SERSE, INFN-LNS

VENUS, LNBL-USA

The cutoff density

$$\epsilon(\omega) \sim 1 - \frac{\omega_p^2}{\omega^2}$$

The propagation of e.m. waves is possible if $\varepsilon > 0$

$$\omega_p^2 = \frac{4\pi n_e e^2}{m_e}$$

The plasma frequency is connected to self-generated plasma oscillations which strongly affect the wave propagation.

Above the cutoff the wave cannot propagate:

$$n_{cutoff} = 4\pi^2 \frac{m\epsilon_0}{e^2} f_p^2$$

INFN Istituto Nazionale di Fisica Nucleare

ECRIS Standard Model

Scaling Laws

(R. Geller-1987):

For many years they represented the guideline for ECRIS development

$$I \propto \frac{\omega_{RF}^{2}}{M} \qquad \langle q \rangle \propto \log \omega_{RF}^{3.5}$$

1. We have to increase the Microwave frequency to attain higher electron densities
2. No considerations about the confinement

High-B Mode

(G. Ciavola-S.Gammino, 1990)

It doesn't conflict with Scaling Laws, but it limits their efficiency to high confined plasmas

High mirror rations ensure the MHD stability exploiting the density increase.

$$\boxed{\frac{B}{B_{ECR}} > 2}$$

B>4T for future ECRIS !

Overcoming the current limits of ECRIS

Unsolved problems coming out from the Standard Model (Scaling Laws):

1. **High Frequency Generators** (…but hot electrons grow dramatically when increasing the frequency, causing safety problems for the magnet's cryostat);
2. **High Magnetic Fields** (magnetic field scaling is close to saturation);

Limitations come from rising cost of technology, but not only!!

PLASMA OVERHEATING FOR GROWING PUMPING WAVE FREQUENCY IS A PHYSICAL LIMITATION!!

Plasma Heating

Modeling electron heating driven by microwaves

Heating Models

- **Single particle approach** (SPA): predicts the endpoint energy scaling with L, Prf, E.
- **Diffusive approach** (DA): in agreement with SPA about boost of heating for long L.
- **Importance of turbulence**: rarely taken into account, is at the basis of overbarrier heating in multi-mirror devices.

Heating Models

Fluid oscillation

adiabatic

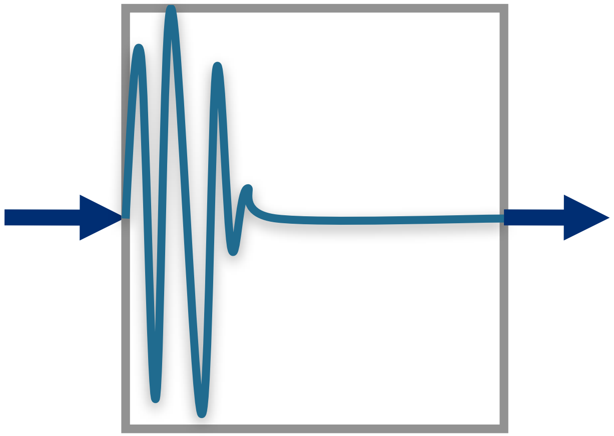

nonadiabatic

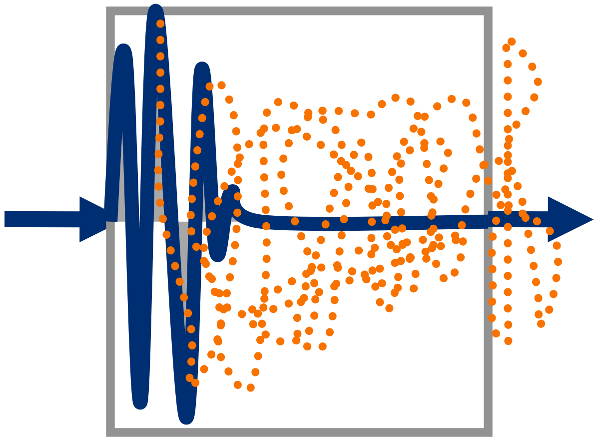

Heating

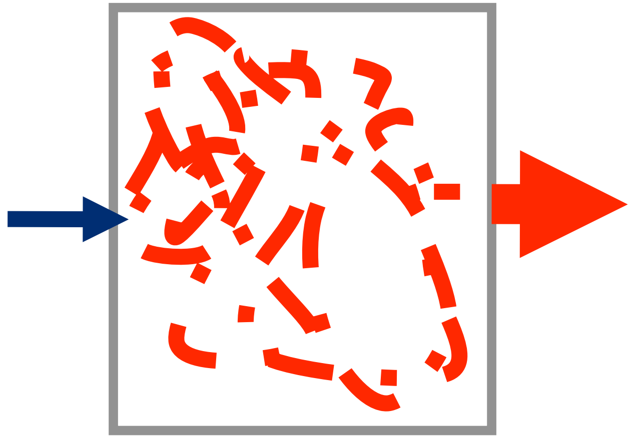

Electron heating requires the momentum randomization.

In thermodynamical systems, the heating proceeds through interparticle collisions.

but…

Plasmas are often collisionless!!

The Single Particle Approach

M. A. Lieberman and A. J. Lichtenberg, *Plasma Phys.* **15** 125 (1973)

The stochastic heating theory

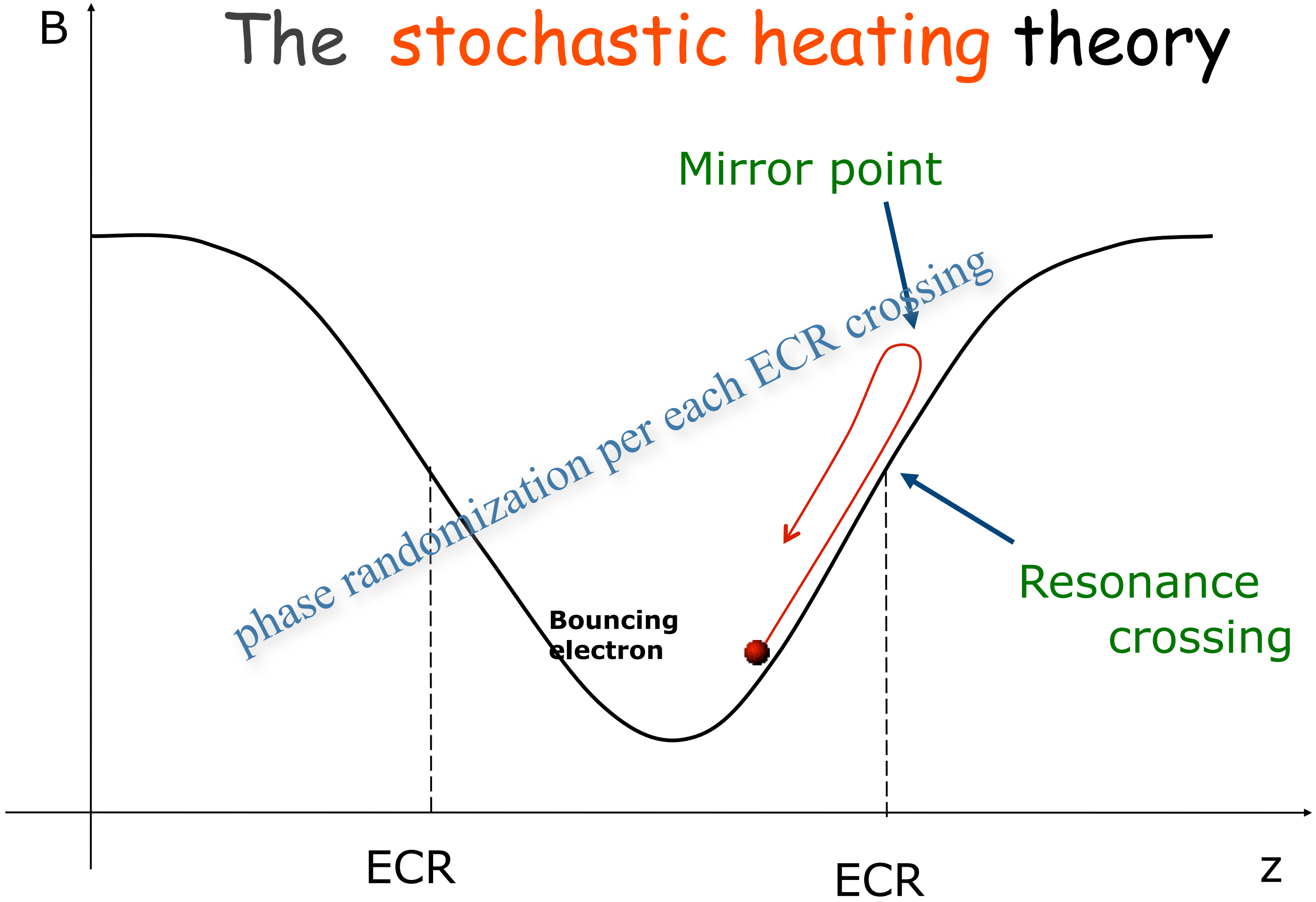

Bouncing Frequency: $\boxed{\omega_b}$

The Single Particle Approach

The stochastic heating theory & the "pendulum model"

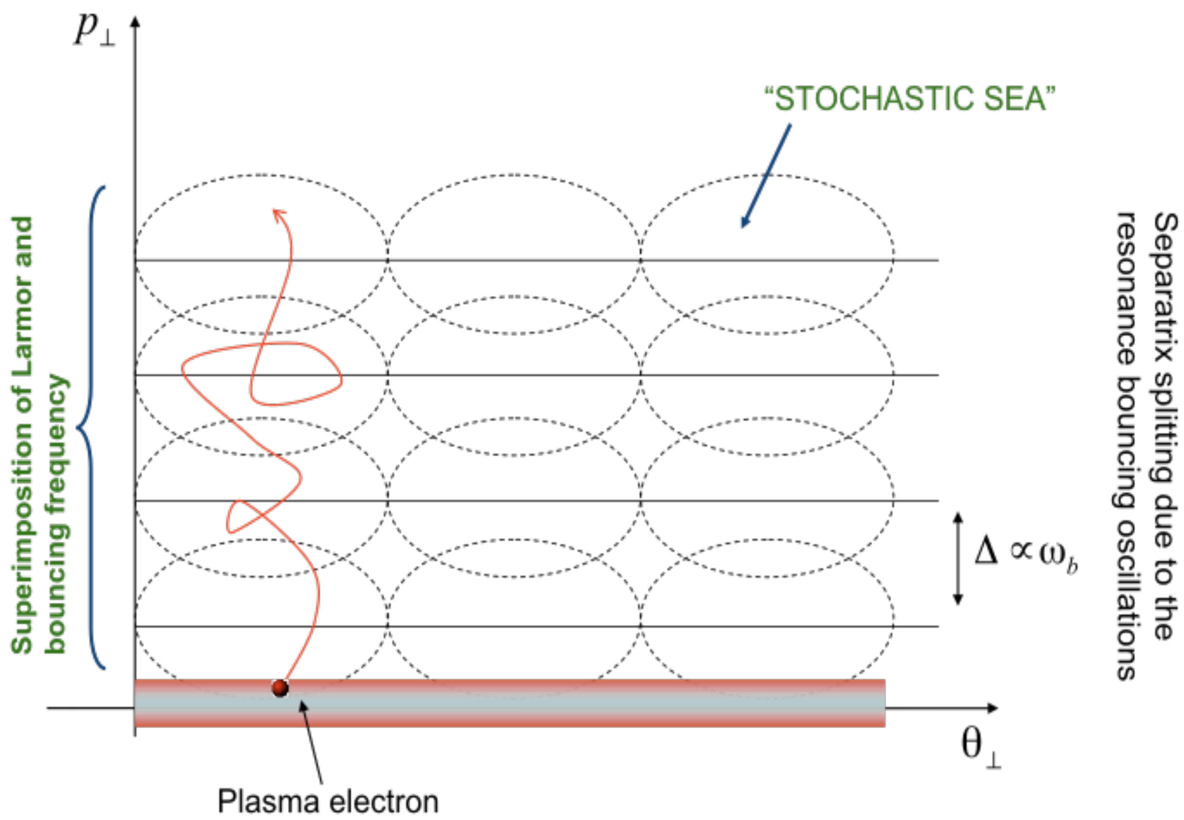

Since the electron rebounces inside the trap:

$$z = z_0 \cos\left(\omega_b t + \psi_0\right)$$

with ω_b bouncing frequency

Assuming, in a simplified picture, that the electron interacts with a linearly polarized plane wave:

$$E_\perp\left(t, z, r, \theta\right) = E_{\perp_0} \cos\left(\omega t - kz + \theta_\perp\right)$$

$$\boxed{E(r,\theta,z,t) = E_0 \cos\left[\left(\omega_{RF} t + \theta_\perp - k z_0 \cos(\omega_b t + \psi_0)\right)\right]}$$

This formula accounts for the composition of the bouncing and cyclotron frequencies, leading to an effective multi-waves interaction

The Single Particle and Diffusive Approach

Trend of the perpendicular velocity for through resonance multi-passing electrons

$$\varepsilon = \varepsilon_i + \Delta\varepsilon + 2\cos(\phi_0 - \phi_p)\sqrt{\varepsilon_i \times \Delta\varepsilon}$$

$\Downarrow$

STOCHASTIC TERM

$$D_{vv} = \frac{\Delta v^2}{2\Delta t} = \pi\left(\frac{eE}{2m_e}\right)^2 \frac{L}{d\omega}$$

$$D_{\mu\mu} = \frac{\Delta\mu^2}{2\Delta t} = D_{vv}\left(\frac{v}{v_\phi}\right)^2$$

For longitudinal B fields like:

$$\begin{cases} \boxed{B = B_{\min}(1 + z^2/L^2)} \\ L = \left(\nabla B/B\right)^{-1} \end{cases}$$

$$\boxed{W_b \approx 5W_s = \left[m_e L\left(1 + \frac{l^2}{L^2}\right)\right]^{1/4} l\omega^{1/2}(eE)^{3/4}}$$

$$\boxed{n_e \propto \omega_{RF}^2}$$

$$\boxed{E_{char} \approx 1/2 m_e v_\phi^2}$$

Absolute stochastic barrier (ABS)
(the phase randomization stops):

[Lieberman&Lichtenberg, *Plasma Phys.* 15 125 (1973); A. Girard et al. Phys Rev E]

Unexplained experimental results

Models are in **qualitative agreement with experiments as concerns the large frequency and B field variation**, but **they do not explain extreme sensitivity of X-ray production to slight *L* adjustments**, or output **currents and emittance dependence on the fine frequency tuning**

FINE TUNING OF ECRIS PARAMETERS (B , f)

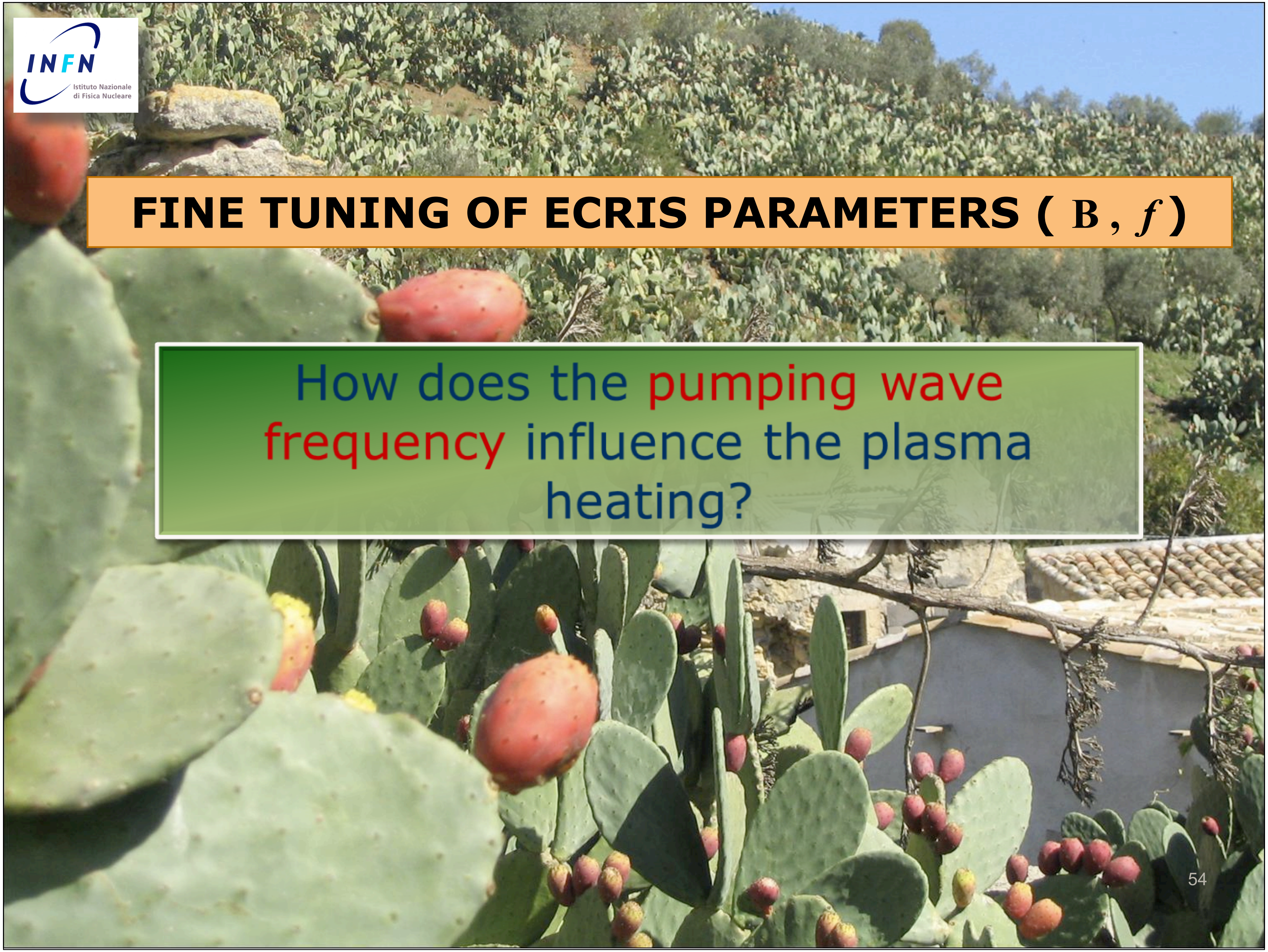

How does the pumping wave frequency influence the plasma heating?

Signs about the importance of the frequency tuning effect came already in 2001-2004 from an experiment carried out on SERSE [L. Celona et al., ECRIS04]

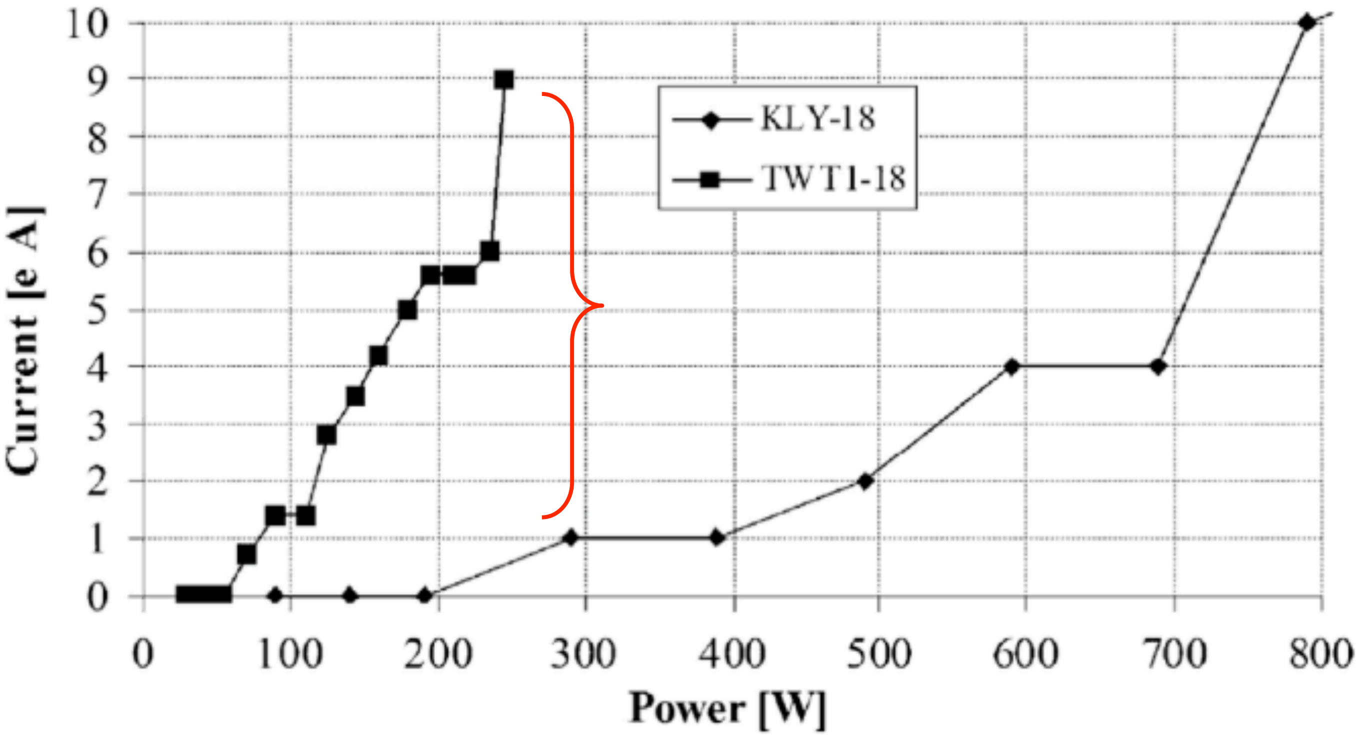

Comparison between trends of O^{8+} at 18 *GHz* for klystron (up to 800 W) and TWT1 operating in the same range of frequency.

TWT worked better than klystron: why?

Relationship between X-ray spectra and CSD: the experiment at LNS

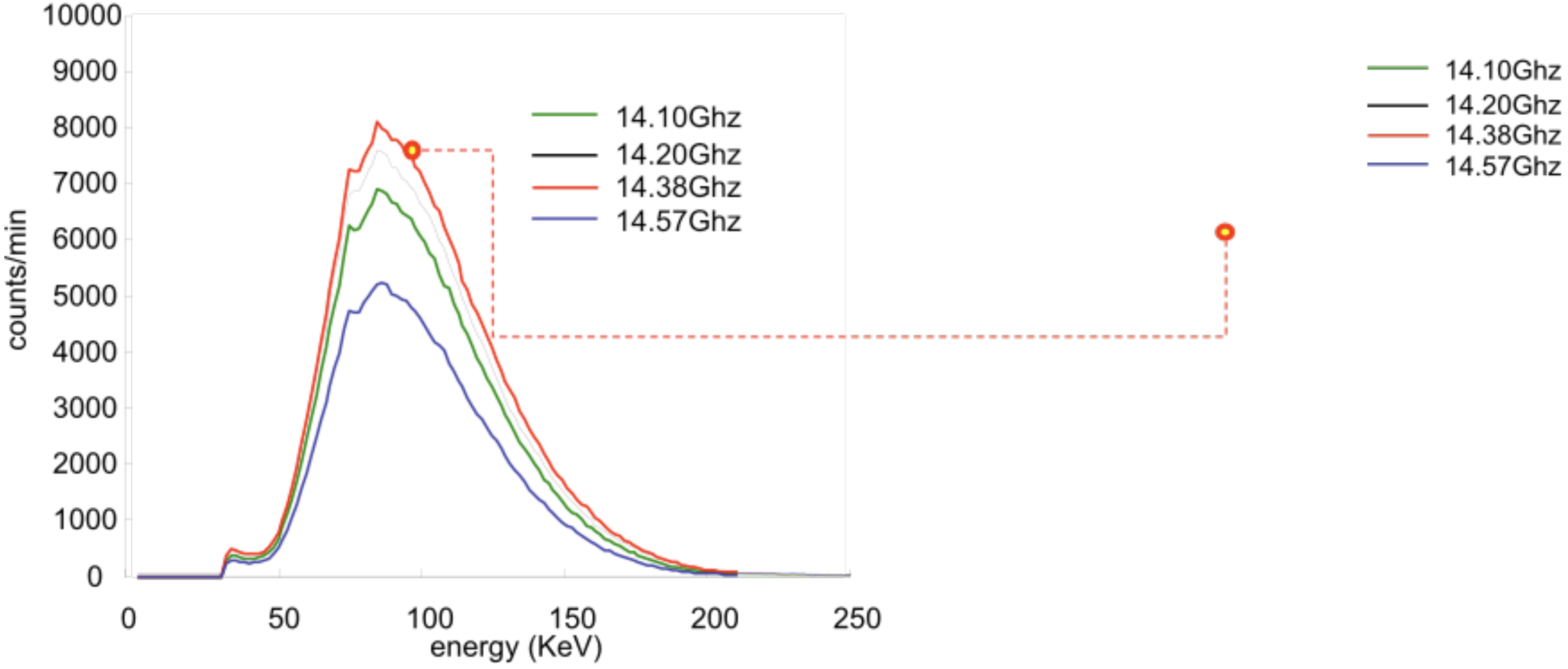

Measurements with CAESAR at LNS reveal that X-ray spectra are not strictly related to frequency tuning.

Frequencies producing large numbers of counts do not necessarily produce optimal CSD

Impact of the frequency on ion beam structure

[L. Celona, et al. Observations of the frequency tuning effect in the 14 GHz CAPRICE ion source. *Rev. Sci. Instrum.*, Feb. 2008. vol. 79, no. 2, p. 023 305.]

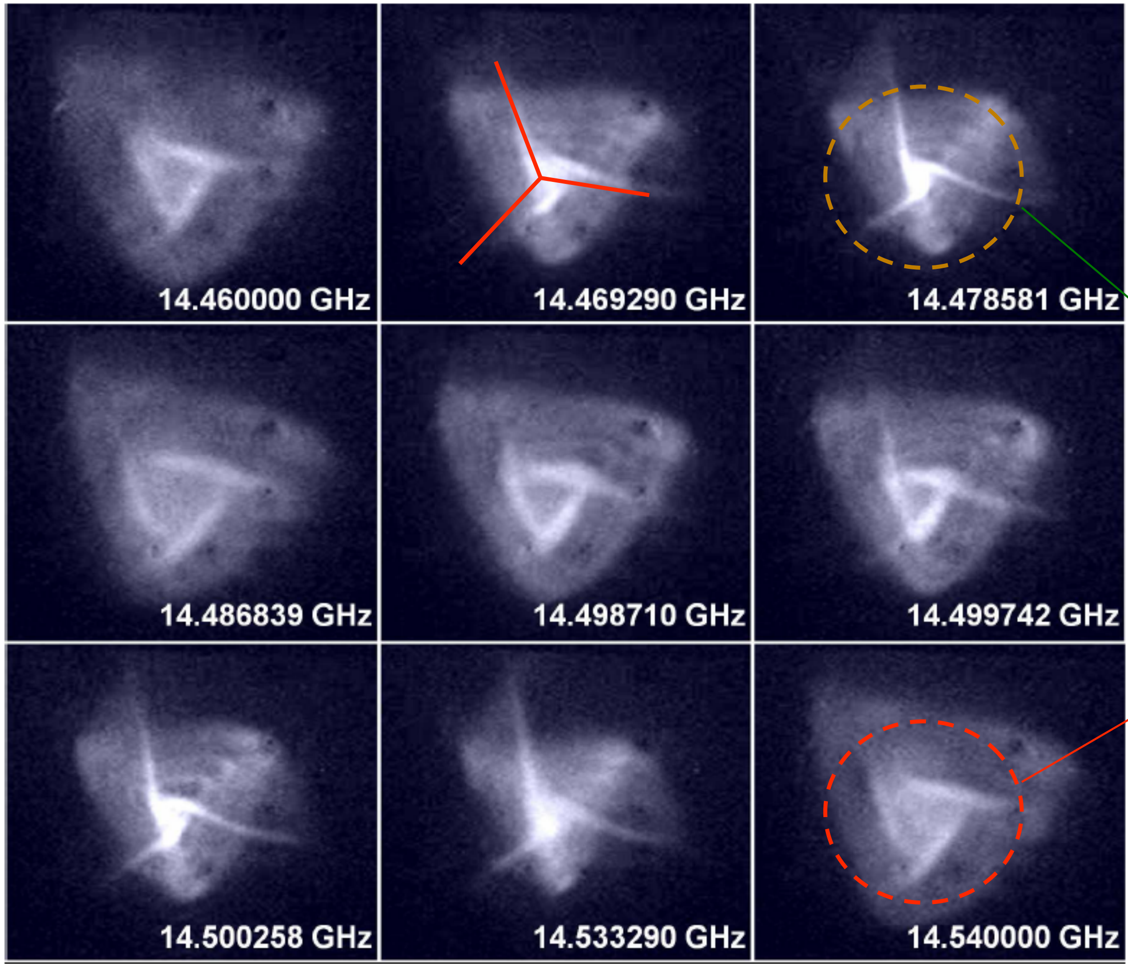

Frames of the extracted beam for different frequencies

"three cusp" shape of the extracted beam according to the magnetic structure

Well focused and high brightness beam

Broadened, low brightness beam

The Frequency Tuning strongly affects also the beam shape and brightness

Additional hypothesis for a better modelling

1. Heating models do not account for resonant modes in low-Q cavities.
2. They additionally do not take into account possible non-linear wave-plasma interaction

We implemented cavity modes in our fully 3D MonteCarlo calculations.

Parametric decay and generation of plasma modes were also considered to explain sensitivity to B profile variations.

Numerical Approaches for palsma modeling in Ion Sources

- **RF coupling**
- **Single particle kinetics**
- **Self-consistent strategies**
- **Propagation of electromagnetic waves**
- **Extraction**
- **Transport**

Montecarlo code for plasma Simulation

A new 3D code for calculation of particles trajectories, density and energy distribution, trapping efficiency and direct ECR-heating

Advantages

- Single particle calculation
- Simulation of collisions and prediction on average particles lifetime
- Simple tuning of parameters

Limitations

- No evidences of fluid instabilities
- Difficult feedback evaluation on waves dynamics
- Parameterized calculation of charge state distribution

"Physics" included into the equations

- External Magnetic Filed;
- Relativistic electron mass variation;
- RF power source (resonant cavity model);
- Physical plasma chamber walls (total absorption model);
- Electrostatic (Spitzer) collisions at 90°;
- Particle tracing and accumulation of density in 3D grid

Simulation of stationary system

Simulation of Simeto river

1° Simulation of all involved particles
+
Continuous creation and destruction of particles

2° Simulation of well defined
statistical sample
+
Accumulation and statistical information for
all the life of the sample

Picture of a stationary plasma

1° We need the calculation of al particle for all here life and we have to consider all the particle that born at different time

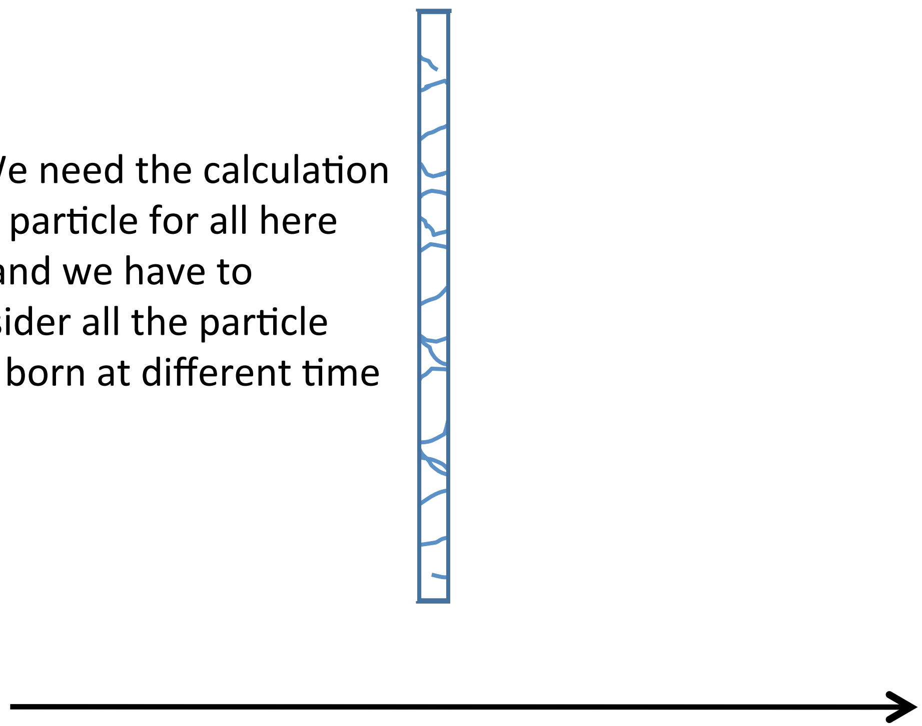

Modeling of electron and ion dynamics with Monte-Carlo calculations

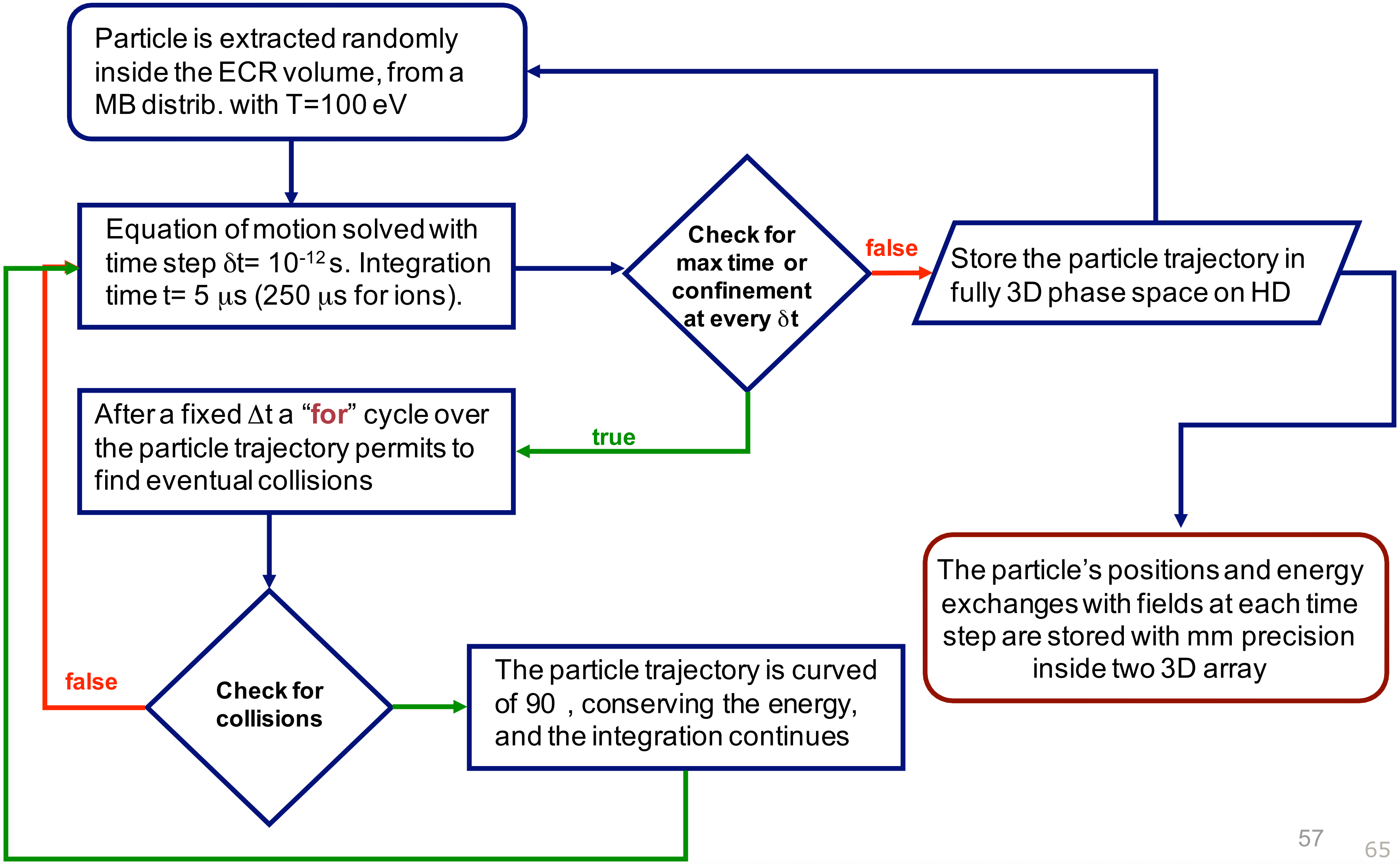

Modeling of electron and ion dynamics with Monte-Carlo calculations: ELECTRONS

A MATLAB code solves the equation of motion of a single particle:

$$\frac{d\vec{v}}{dt} = \begin{cases} \frac{q}{M}\left[\vec{v}\times\vec{B}+\vec{E}_s\right] & (i) \\ \frac{q}{m}\left(1-\frac{v^2}{c^2}\right)^{3/2}\left[\vec{v}\times\vec{B}_S+\vec{v}\times\vec{B}_{em}+\vec{E}_{em}-\frac{1}{c^2}\left(\vec{E}_{em}\cdot\vec{v}\right)\vec{v}\right] & (e) \end{cases}$$

$$\begin{aligned}
\dot{x} &= v_x \\
\dot{y} &= v_y \\
\dot{z} &= v_z \\
\dot{v}_x &= \boxed{F(v)}[(v_y B_z - v_z B_y) + (v_y B_{em_z} - v_z B_{em_y}) + E_{em_x} - \\
&\quad - \frac{1}{c^2}\left(E_{em_x} v_x + E_{em_y} v_y\right) v_x] \\
\dot{v}_x &= F(v)[(v_z B_x - v_x B_z) + (v_z B_{em_x} - v_x B_{em_z}) + E_{em_y} - \\
&\quad - \frac{1}{c^2}\left(E_{em_x} v_x + E_{em_y} v_y\right) v_y] \\
\dot{v}_z &= F(v)[-B_x v_y + v_x B_y - B_{em_x} v_y + v_x B_{em_y} - \\
&\quad - \frac{1}{c^2}\left(E_{em_x} v_x + E_{em_y} v_y\right) v_z]
\end{aligned}$$

Magnetostatic field for the plasma confinement

Magnetic and electric fields associated with the pumping wave

MATLAB solves the six first order ODEs by means of the "*ode45*" Runge-Kutta routine.

- 3000 electrons/week, 8 CPU
- δt = 10^{-12} s ~ 10 points of integration per Larmor radius
- **Collisions are taken into account**
- **Fully 3D calculations with B-min structure**

Code's structure for solving the single particle equation of motion

```
tspan=0:Tstep:Tstep*(double(nPunti)-1);     % fixes temporal domain

    options=odeset('RelTol',1e-7,'Events',@eventStop);
% relative error tolerance and "events" routine for stopping integration when some
conditions are valid (particle deconfinement)

    [t,X]=ode45(@functionSimulazioneECRH,tspan,X0(:),options);
%ODE solver in t interval, with X0 array of initial conditions

X0=[X Y Z normrnd(0,sigma,1,3)];          % array of initial conditionsc
```

Routine for extraction of three random number from three normal distributions having a given σ and μ

```
function [value,isterminal,direction]=eventStop(t1,x,t2,t3,t4)

cond_x=sqrt(x(1)^2+x(2)^2)-0.032;
cond_z=abs(x(3))-0.10;

value=cond_x*cond_z;                      % event function

isterminal=1;%Stop the integration when the particle reach the plasma chamber walls.
direction=0; Stop the integration when the zero crossing occurs from every direction.
```

Ordinary Differential Equations (ODE) solver in MATLAB

Parameters	ode45
RelTol, AbsTol, NormControl	√
OutputFcn, OutputSel, Refine, Stats	√
NonNegative	√
Events	√
MaxStep, InitialStep	√
Jacobian, JPattern, Vectorized	—
Mass MStateDependence MvPattern MassSingular	√ √ — —
InitialSlope	—
MaxOrder, BDF	—

Numerical error setting

Helps in fixing boundaries for trapping

Refine and fixes integration steps

Best compromise as concern rapidity of calculation and error tolerance.

Solver	Problem Type	Order of Accuracy	When to Use
ode45	Nonstiff	Medium	Most of the time. This should be the first solver you try.
ode23	Nonstiff	Low	For problems with crude error tolerances or for solving moderately stiff problems.
ode113	Nonstiff	Low to high	For problems with stringent error tolerances or for solving computationally intensive problems.
ode15s	Stiff	Low to medium	If ode45 is slow because the problem is stiff.
ode23s	Stiff	Low	If using crude error tolerances to solve stiff systems and the mass matrix is constant.
ode23t	Moderately Stiff	Low	For moderately stiff problems if you need a solution without numerical damping.
ode23tb	Stiff	Low	If using crude error tolerances to solve stiff systems.

$$B_x = -B_1 xz + 2Sxy$$

$$B_y = -B_1 yz + 2S(x^2 - y^2)$$

$$Bz = -B_0 + B_1 z^2$$

Terms for longitudinal trap asymmetrization

```
if x(3)<=0
    B0=0.387;
    B1=64.5;
else
    B0=0.387
    B1=57;
 end
```

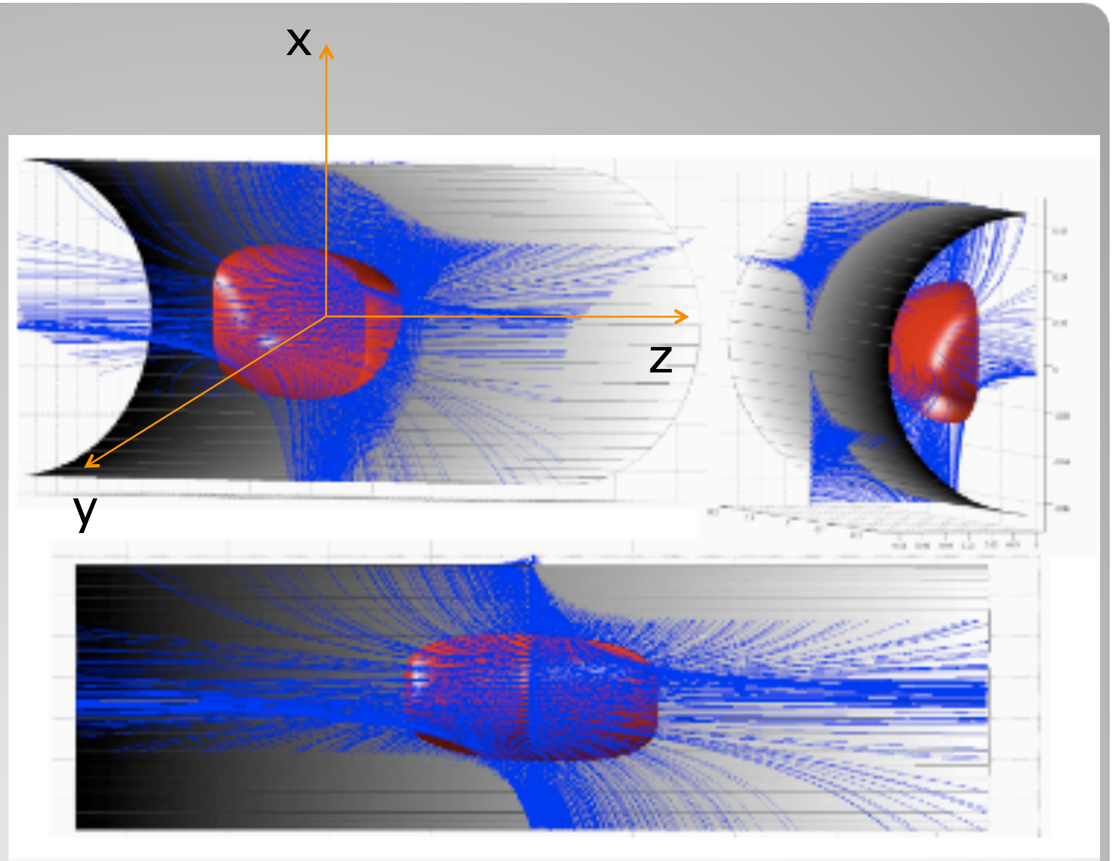


```
S=1100;
Bx=-B1.*x(1).*x(3)+2*S.*x(1).*x(2);
By=-B1.*x(2).*x(3)+S.*(x(1).^2-x(2).^2);
Bz=B0+B1.*x(3).^2
```

x= x(1); vx = x(4)
y= x(2); vy = x(5)
z= x(3); vz = x(6)

$\underline{x}$= x(1)
x(2)
...
x(6)

Magnetic Field

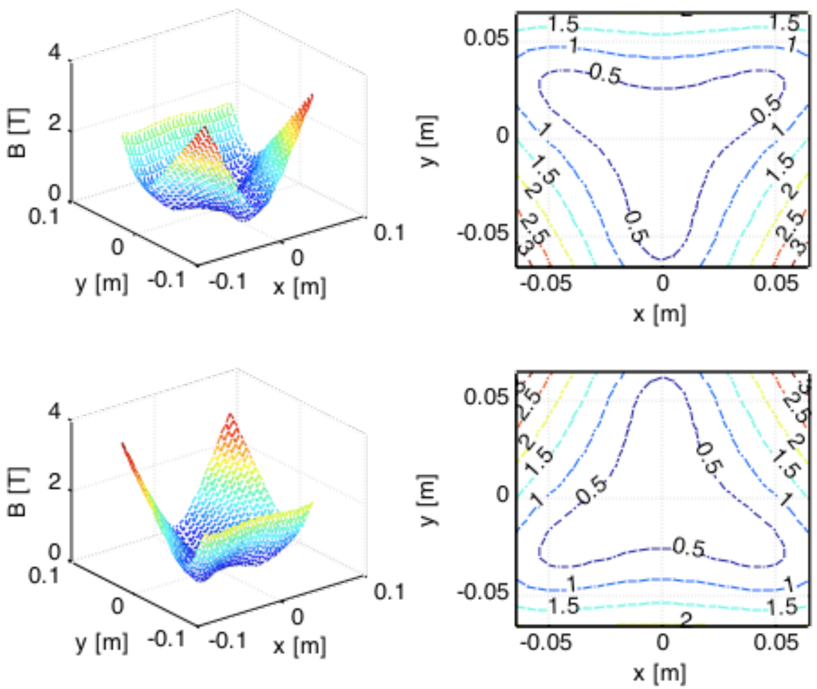

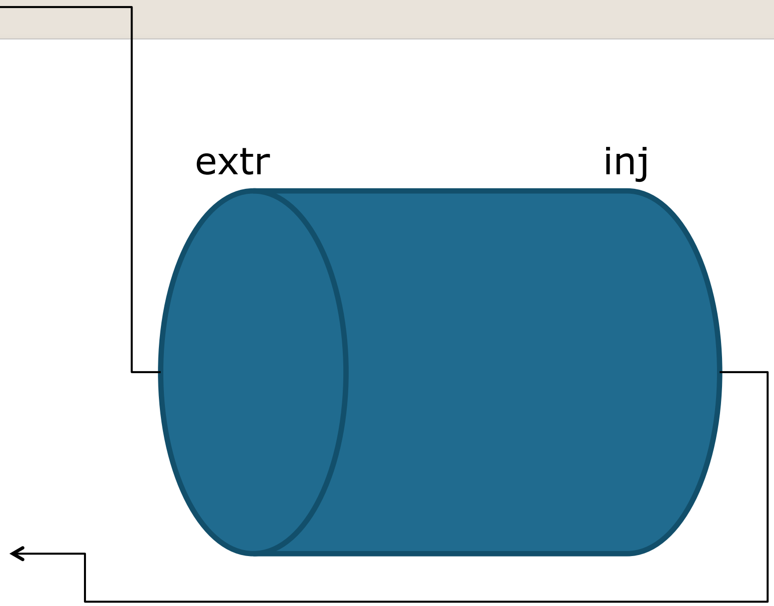


```
[X,Y]=meshgrid(-0.065:0.005:0.065,-0.065:0.005:0.065);

Bz=B0+B1.*z.^2;
Bx=-B1.*X.*z+2*S.*X.*Y;
By=-B1.*Y.*z+S.*(X.^2-Y.^2);
Bparallel=sqrt(Bx.^2+Bz.^2);
Bort=sqrt(Bx.^2+By.^2);

mesh(X,Y,Bort);
```

Evaluate domain

Plotting field

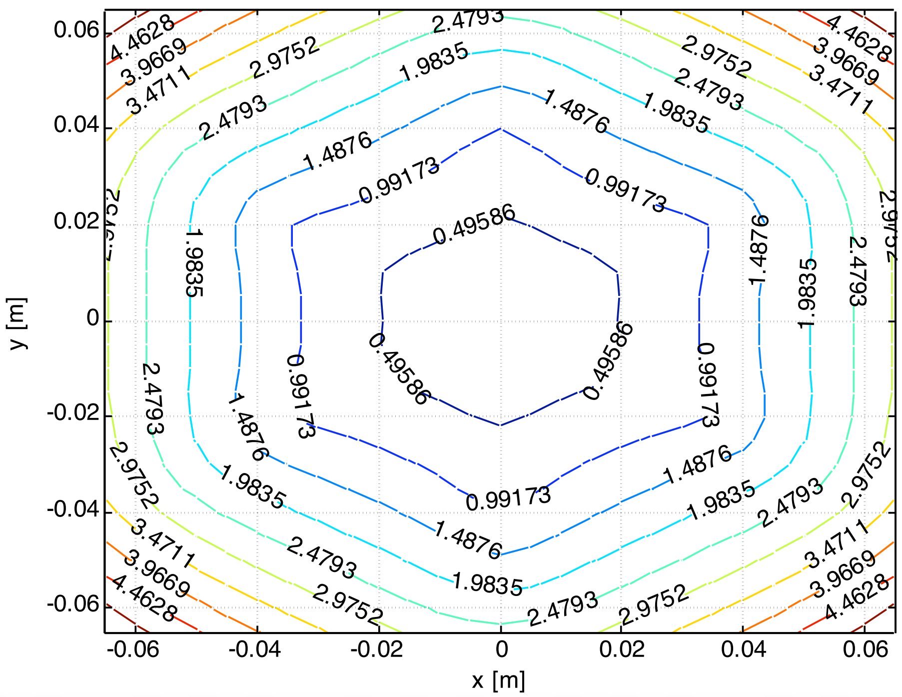

Modeling of electron and ion dynamics with Monte-Carlo calculations: **The SERSE magnetic field**

$$B_x = \boxed{-B_1 xz} + \boxed{2Sxy}$$

$$B_y = \boxed{-B_1 yz} + \boxed{2S(x^2 - y^2)}$$

$$B_z = \boxed{\begin{cases} -B_0 + B_{inj} z^2 & \forall z < 0 \\ -B_0 + B_{ext} z^2 & \forall z > 0 \end{cases}}$$

Hexapolar field

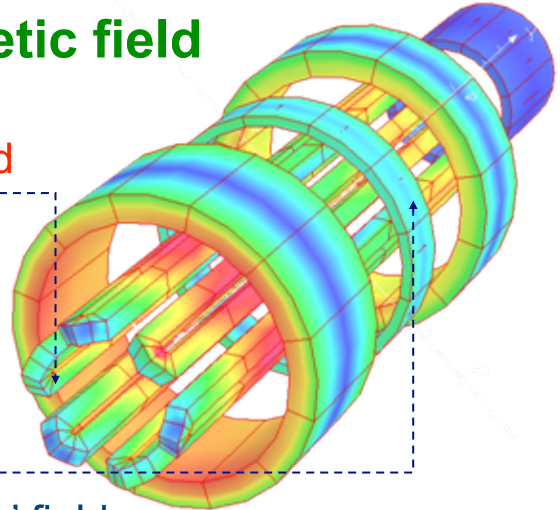

Solenoids' field

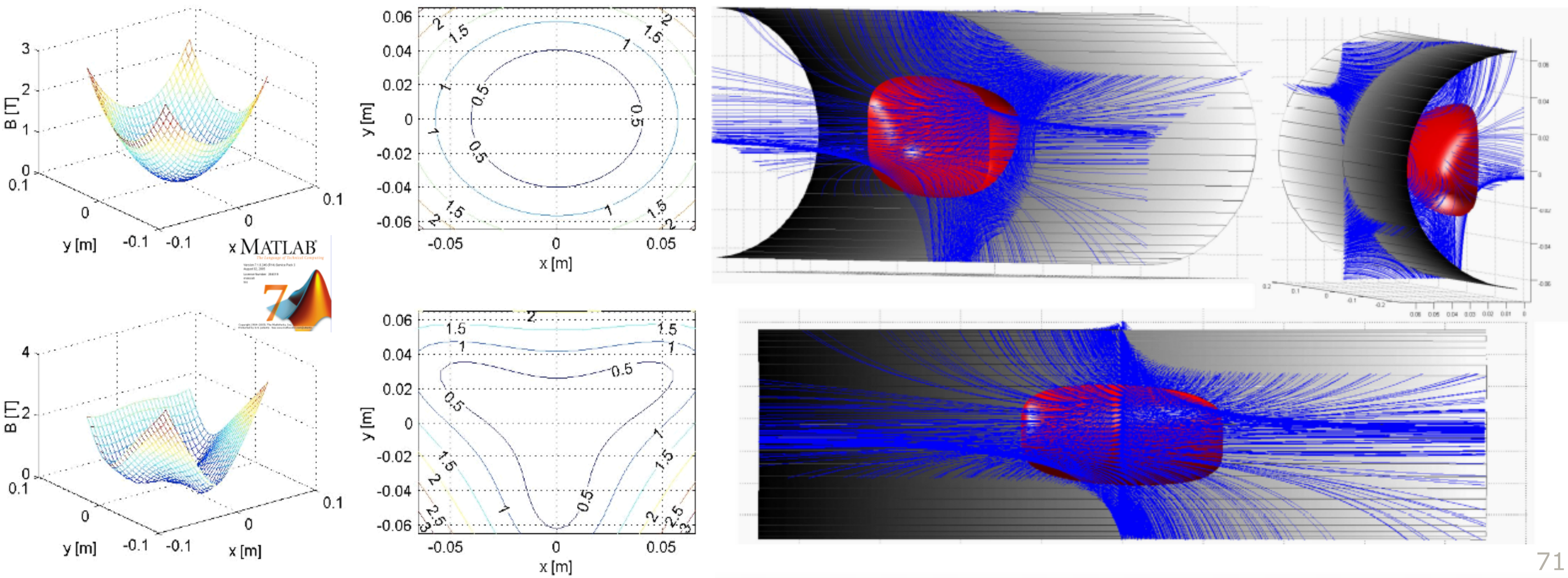

Resonant Absorption of Electromagnetic Waves

Magnetized plasma are electromagnetically Anisotropic: the dielectric tensor accounts for wave propagation properties at different angles

$$\longrightarrow \begin{pmatrix} \epsilon'_{xx} & \epsilon'_{xy} & 0 \\ \epsilon'_{yx} & \epsilon'_{yy} & 0 \\ 0 & 0 & \epsilon'_{zz} \end{pmatrix}$$

$$k'_\theta = \frac{\omega}{c}\left[1 - \frac{X(1+iZ-X)}{(1+iZ)(1+iZ-X) - \frac{1}{2}Y_T^2 + \sqrt{\frac{1}{4}Y_T^4 + Y_L^2(1+iZ-X)^2}}\right]^{\frac{1}{2}}$$

$$k''_\theta = \frac{\omega}{c}\left[1 - \frac{X(1+iZ-X)}{(1+iZ)(1+iZ-X) - \frac{1}{2}Y_T^2 - \sqrt{\frac{1}{4}Y_T^4 + Y_L^2(1+iZ-X)^2}}\right]^{\frac{1}{2}}$$

Waves propagating along B are distinguished by two k vectors, according to polarization

Resonant Absorption of Electromagnetic Waves

The simplified version of the equation of motion provides the analytical solution for electron velocity when resonance conditions are fulfilled

$$m_e \frac{d\vec{v}}{dt} = q_e\vec{E} - m_e\vec{v}\omega_{eff} + q_e\vec{v} \times \vec{B}_0$$

Circular polarization

DX:

$$|v_x|^2 = \frac{q_e^2}{m_e^2}A^2 \frac{\omega_{eff}^2 + (\omega + \omega_g)^2}{(\omega_g^2 - \omega^2 + \omega_{eff}^2)^2 + 4\omega^2\omega_{eff}^2}$$

$$|v_y|^2 = \frac{q_e^2}{m_e^2}A^2 \frac{\omega_{eff}^2 + (\omega + \omega_g)^2}{(\omega_g^2 - \omega^2 + \omega_{eff}^2)^2 + 4\omega^2\omega_{eff}^2}$$

F(ω)

Circular polarization

SX:

$$|v_x|^2 = \frac{q_e^2}{m_e^2}B^2 \frac{\omega_{eff}^2 + (\omega - \omega_g)^2}{(\omega_g^2 - \omega^2 + \omega_{eff}^2)^2 + 4\omega^2\omega_{eff}^2}$$

$$|v_y|^2 = \frac{q_e^2}{m_e^2}B^2 \frac{\omega_{eff}^2 + (\omega - \omega_g)^2}{(\omega_g^2 - \omega^2 + \omega_{eff}^2)^2 + 4\omega^2\omega_{eff}^2}$$

Resonant Absorption of Electromagnetic Waves

Electron velocity for the R wave

Trend of F(ω) as a function of ω/ω_g:

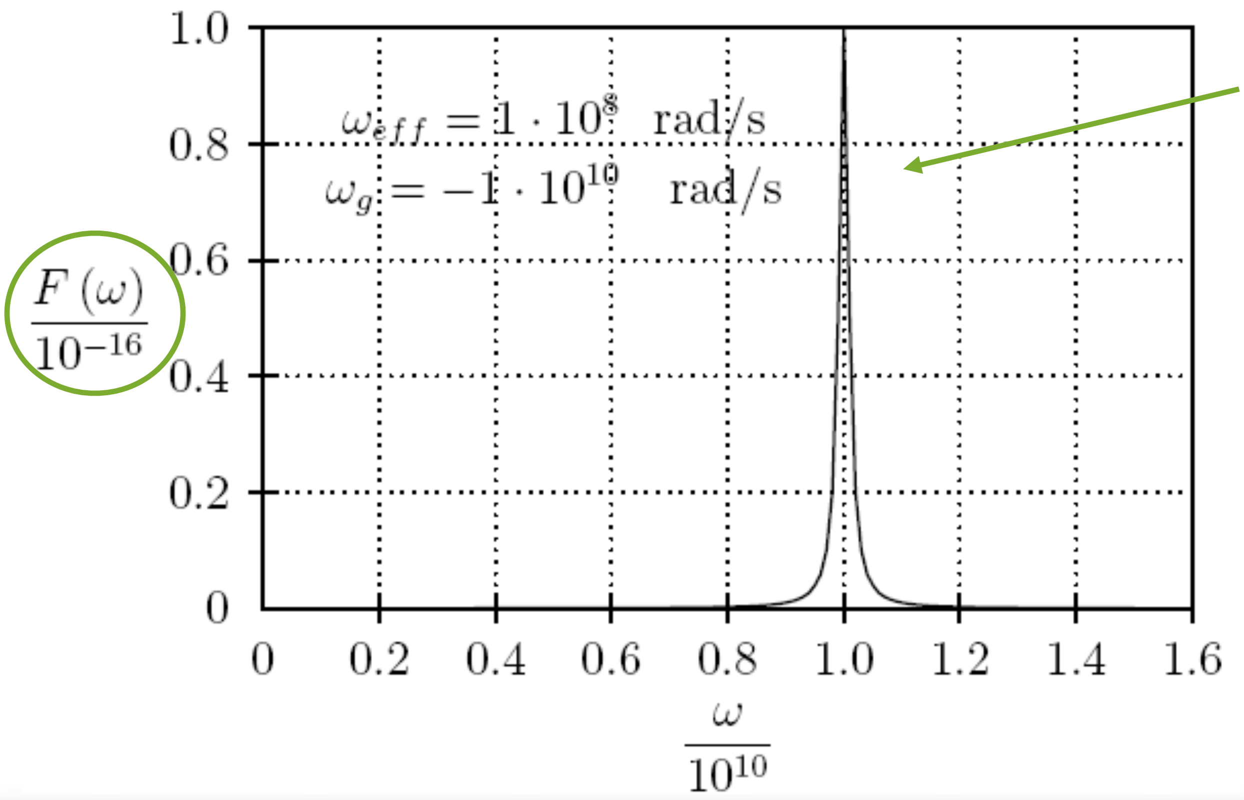

Electron Cyclotron Resonance @ $\omega=\omega_g$

Electron energy increase due to resonant interaction with the magnetic field

Microwave coupling
experimental measurements

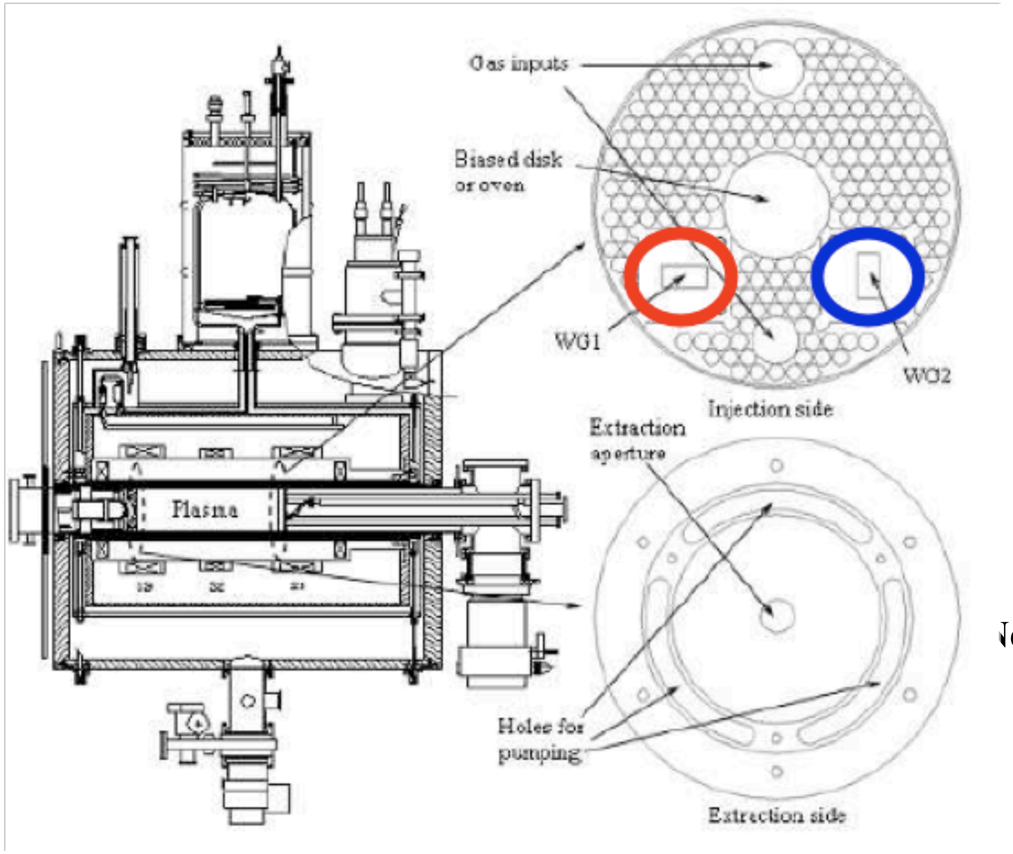

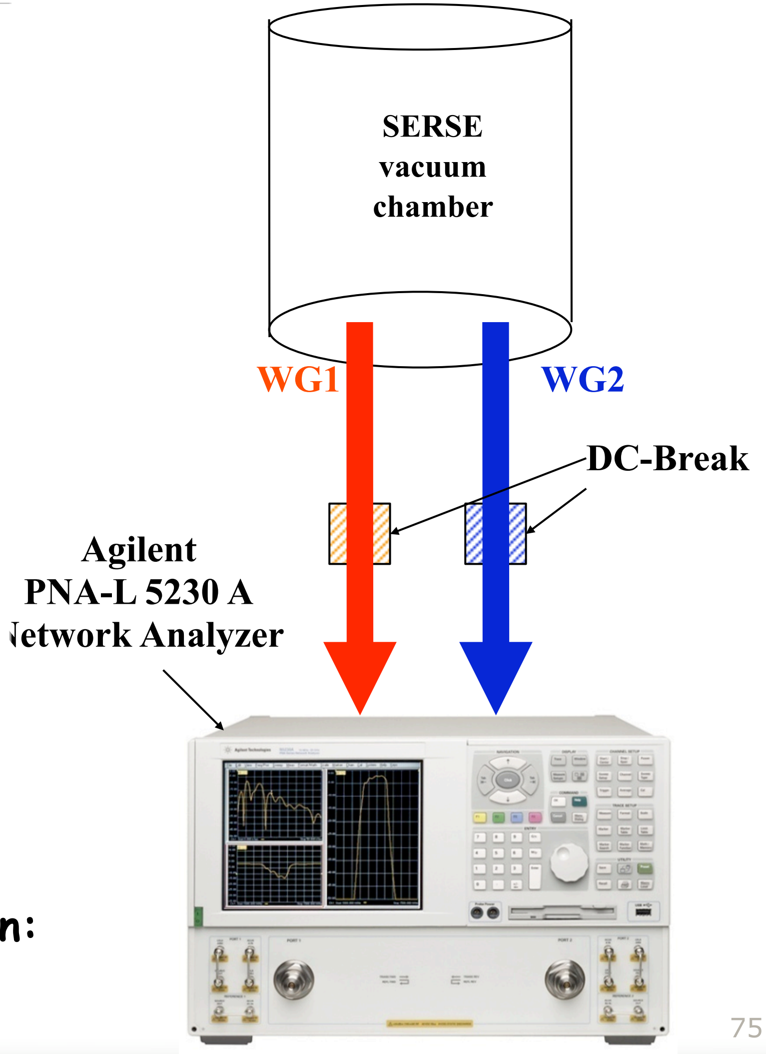

Two different ports for the MW injection:
WG1, WG2.

Microwave coupling
Cavity model

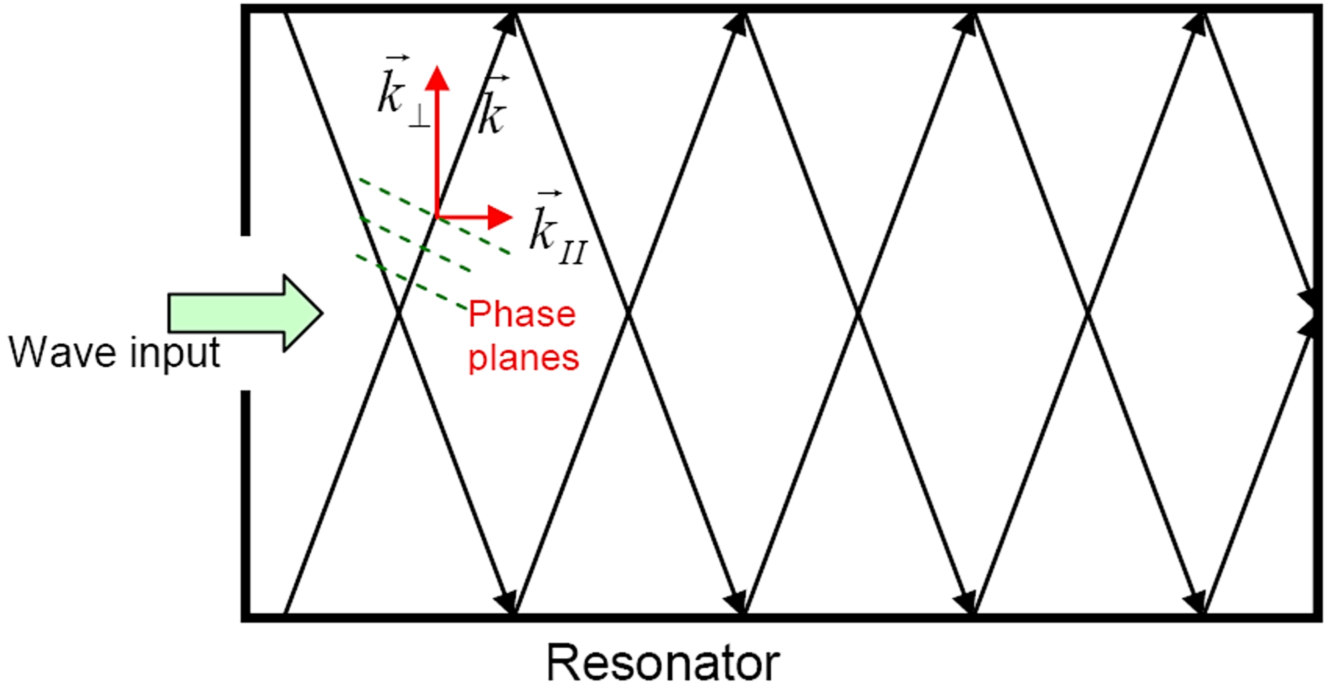

❖The electromagnetic field must obey to boundary conditions inside a metallic chamber;

❖The TEM structure of plane waves propagating in vacuum is destroyed;

❖The wave becomes a standing wave and allowed frequency are discretized;

Microwave coupling

experimental measurements for an air-filled cavity

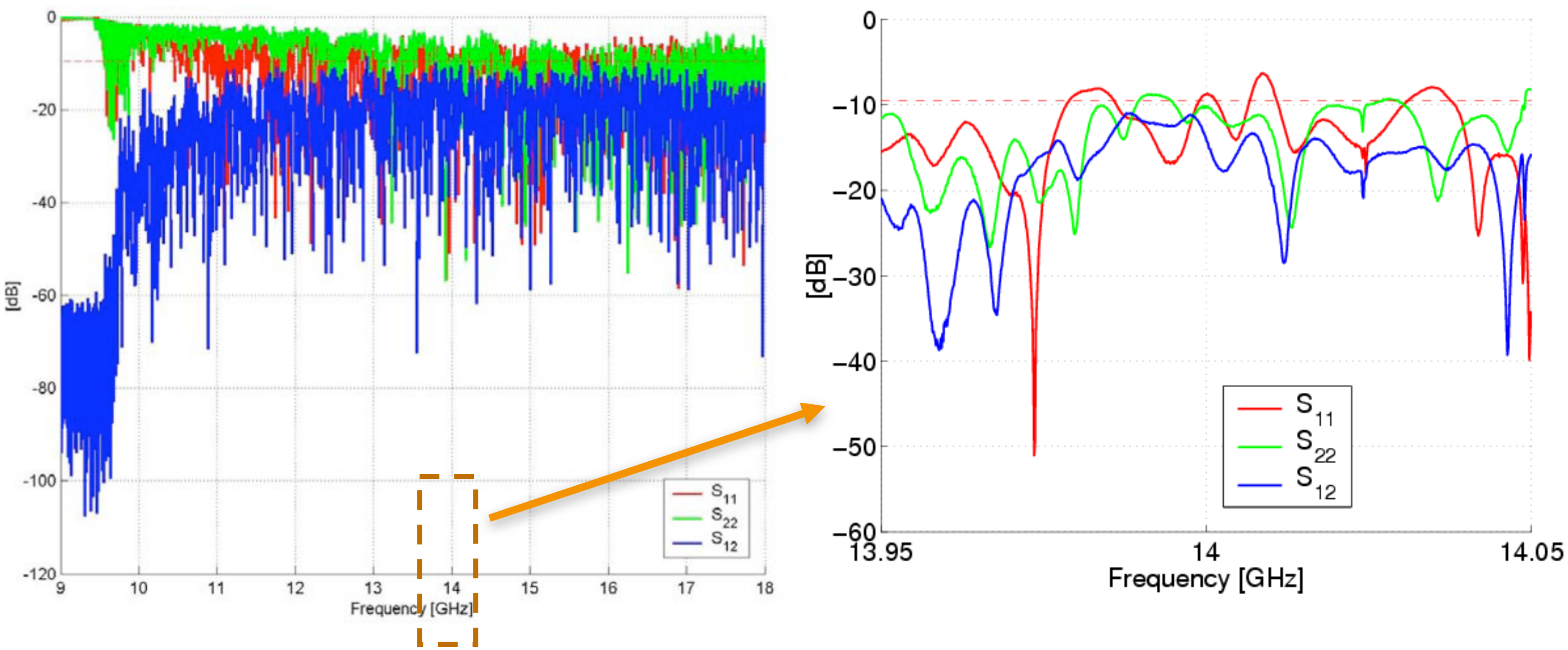

- *Defined modes excited in the plasma chamber*
- *Coupling is different for the two MW ports*

Theoretical determination of the modes distribution

TM modes in vacuum

Resonant frequency

$$f_{n\nu r} = \frac{c}{2\pi}\sqrt{\left(\frac{x_{n\nu}}{a}\right)^2 + \left(\frac{r\pi}{l}\right)^2}$$

Quality factor

$$Q_0 = \mu\sqrt{\frac{\pi\,\sigma\, f_{n\nu r}}{\mu_p}}\,\frac{1}{\left[\frac{2}{l}+\frac{1}{a}\right]} \qquad r \neq 0$$

$$FWHM = \frac{f_{n\nu r}}{Q_0}$$

TE modes in vacuum

Resonant frequency

$$f_{n\nu r} = \frac{c}{2\pi}\sqrt{\left(\frac{x'_{n\nu}}{a}\right)^2 + \left(\frac{r\pi}{l}\right)^2}$$

Quality factor

$$Q_0 = a\,\mu\sqrt{\frac{\pi\,\sigma\, f_{n\nu r}}{\mu_p}}\,\frac{\left\{\left[\left(\frac{r\pi}{l}\right)^2 + h_{n\nu}^2\right]\left[1-\left(\frac{n}{h_{n\nu}\,a}\right)^2\right]\right\}}{\left[h_{n\nu}^2 + 2\frac{r^2\pi^2 a}{l^3} + \frac{r^2\pi^2 n^2}{h_{n\nu}^2\, a\, l^2}\left(\frac{1}{a}-\frac{2}{l}\right)\right]}$$

Spectral distribution of modes inside an air filled cavity

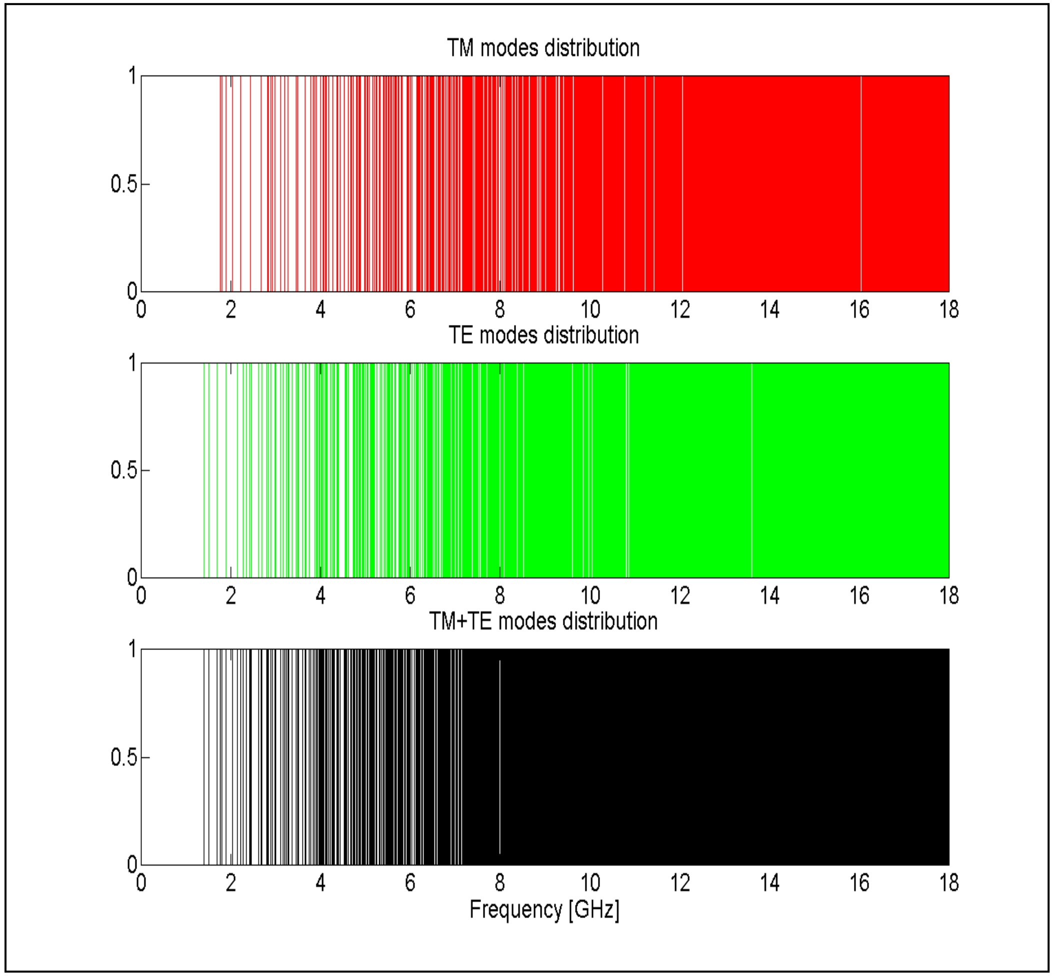

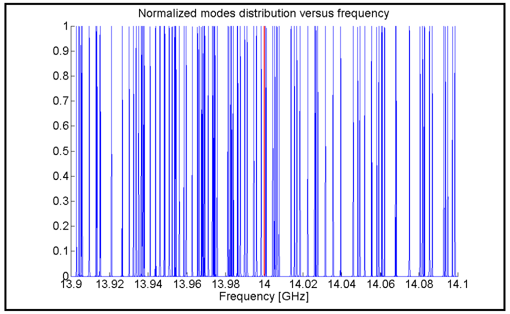

14GHz

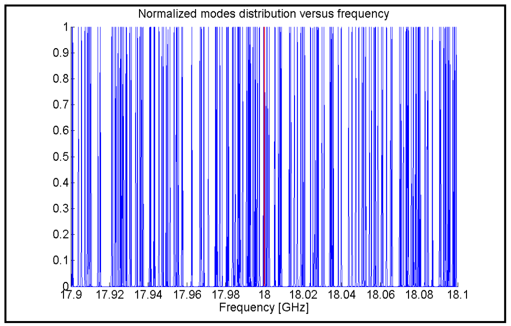

18GHz

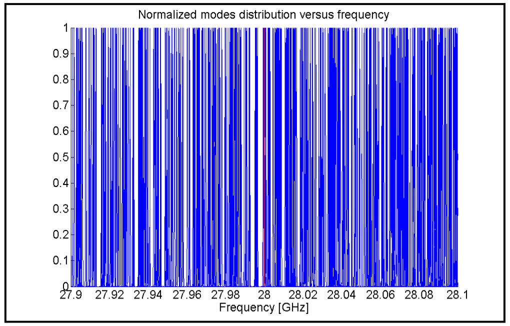

28GHz

Numerical approach for calculating the caivty EM field

HFSS™

- Based on the Finite Element Method
- It is indicated for efficient simulation of cilindrical objects
- It discretizes the calculation domain into tetraedrons
- By using the PML boundary conditions, it supports eigenmode simulation of partially open structures.

CST Microwave Studio™

- Based on the Finite Integration Technique, working on time domain
- It is indicated for efficient simulation of cylindrical objects
- It doesn't support the eigenmode simulation of partially open structures

HFSS numerical study
air-filled cavity

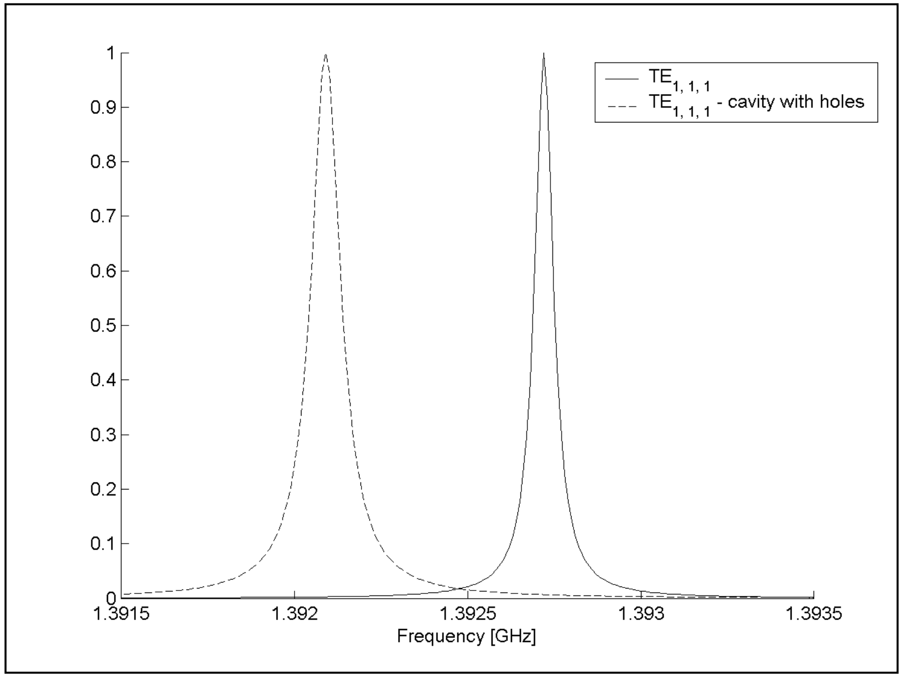

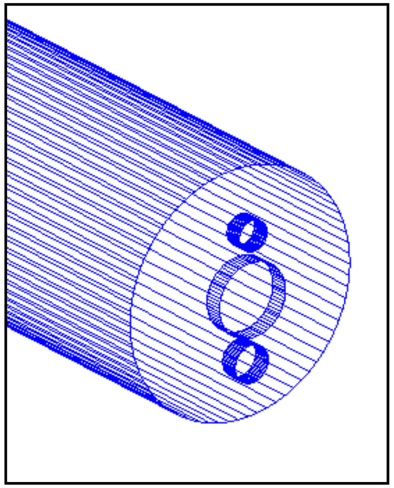

MODE	$\nu_{p\,q\,r}$ [GHz]	Q	FWHM [kHz]
$TE_{1\,1\,1}$ - analytical	1.39197045	2147	64.819
$TE_{1\,1\,1}$ - HFSS	1.39272	2144	64.941
$TE_{1\,1\,1}$ - HFSS with	1.39209	1350	103.072

Electromagnetic field calculation: Resonant Chamber Model

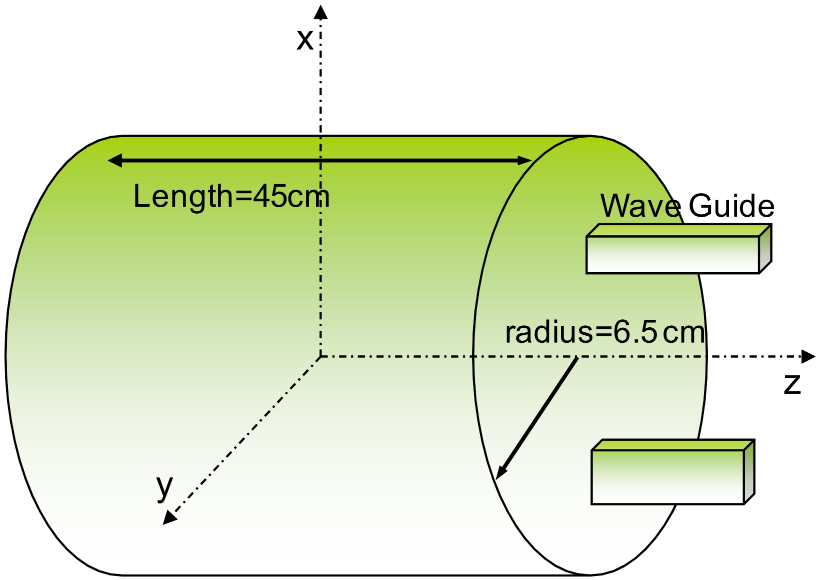

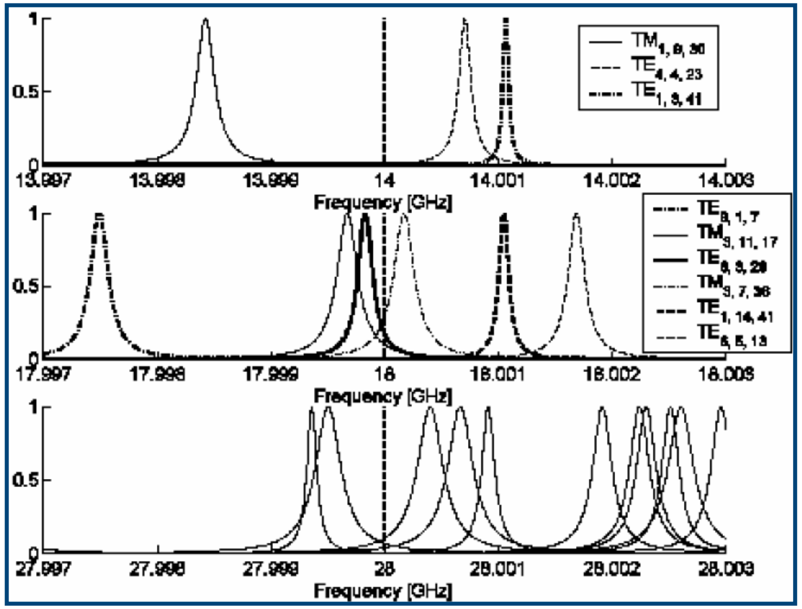

$$
\begin{aligned}
E_x &= A_n \frac{\mu\omega}{h} \sin\left(\frac{r\pi z}{l}\right) J_n' \sin[(n-1)\phi] + J_{n+1} \sin n\phi \cos n\phi \cos(\omega t + \varphi) \\
E_y &= A_n \frac{\mu\omega}{h} \cos\left(\frac{r\pi z}{l}\right) J_n' \sin[(n-1)\phi] + J_{n+1} \sin n\phi \sin n\phi \cos(\omega t + \varphi) \\
H_x &= -A_n \frac{\pi r}{hl} \cos\left(\frac{r\pi z}{l}\right) J_n' \cos[(n-1)\phi] + J_{n+1} \sin n\phi \sin n\phi \sin(\omega t + \varphi) \\
H_y &= A_n \frac{\pi r}{hl} \cos\left(\frac{r\pi z}{l}\right) J_n' \sin[(n-1)\phi] + J_{n+1} \sin n\phi \cos n\phi \sin(\omega t + \varphi) \\
H_z &= -A_n \sin\left(\frac{r\pi z}{l}\right) J_n' \cos n\phi \sin(\omega t + \varphi)
\end{aligned}
$$

Resonant Frequencies

$$
\boxed{\omega = c\sqrt{\frac{r^2\pi^2}{l^2} + h^2}}
$$

```
%autovalore modo TE 4,4,23
h=x_n_ni/a;
rho=sqrt(x(1).^2+x(2).^2);
arg_bessel=h.*rho;                                    %argomento funzioni di bessel per
   il modo TE 4,4,23
phi_var=atan(x(2)./x(1));
freqRF=(c/(2*pi))*sqrt((x_n_ni/a)^2+((r*pi)/l)^2);   %frequenza di risonanza per il
   modo TE 4,4,23
omegaRF=2*pi*freqRF;

%% definisco la derivata prima della funzione di bessel corrispondente al modo
   eccitato
global BesseljMap4 BesseljMap5
Bj=BesseljMap4(int32(arg_bessel*1e5));
bessel_der=(n./arg_bessel).*Bj-BesseljMap5(int32(arg_bessel*1e5));

% componenti dei campi elettrico e magnetico associati all'onda e.m.
mu_0=4*pi*1e-7;                                       % permeabilità  magnetica del
   vuoto
% equazioni dei campi relative al modo TE 4,4,23
Ex_em=((mu_0*omegaRF)/h).*sin((r*pi.*x(3))./l).*Amplitude.*((n./
   (h.*rho)).*Bj.*sin(n.*phi_var).*cos(phi_var)-
   bessel_der.*cos(n.*phi_var).*sin(phi_var)).*cos(omegaRF*t);
Ey_em=((mu_0*omegaRF)/h).*sin((r*pi.*x(3))./l).*Amplitude.*((n./
   (h.*rho)).*Bj.*sin(n.*phi_var).*sin(phi_var)
   +bessel_der.*cos(n.*phi_var).*cos(phi_var)).*cos(omegaRF*t);
Bx_em=-((mu_0*r*pi)/(l*h)).*cos((r*pi.*x(3))./l).*Amplitude.*((n./
```

Electromagnetic Field

Electromagnetic Field

Inner "empty-cavity" electric field distribution for the $TE_{4\,4\,23}$ mode close to 14 GHz

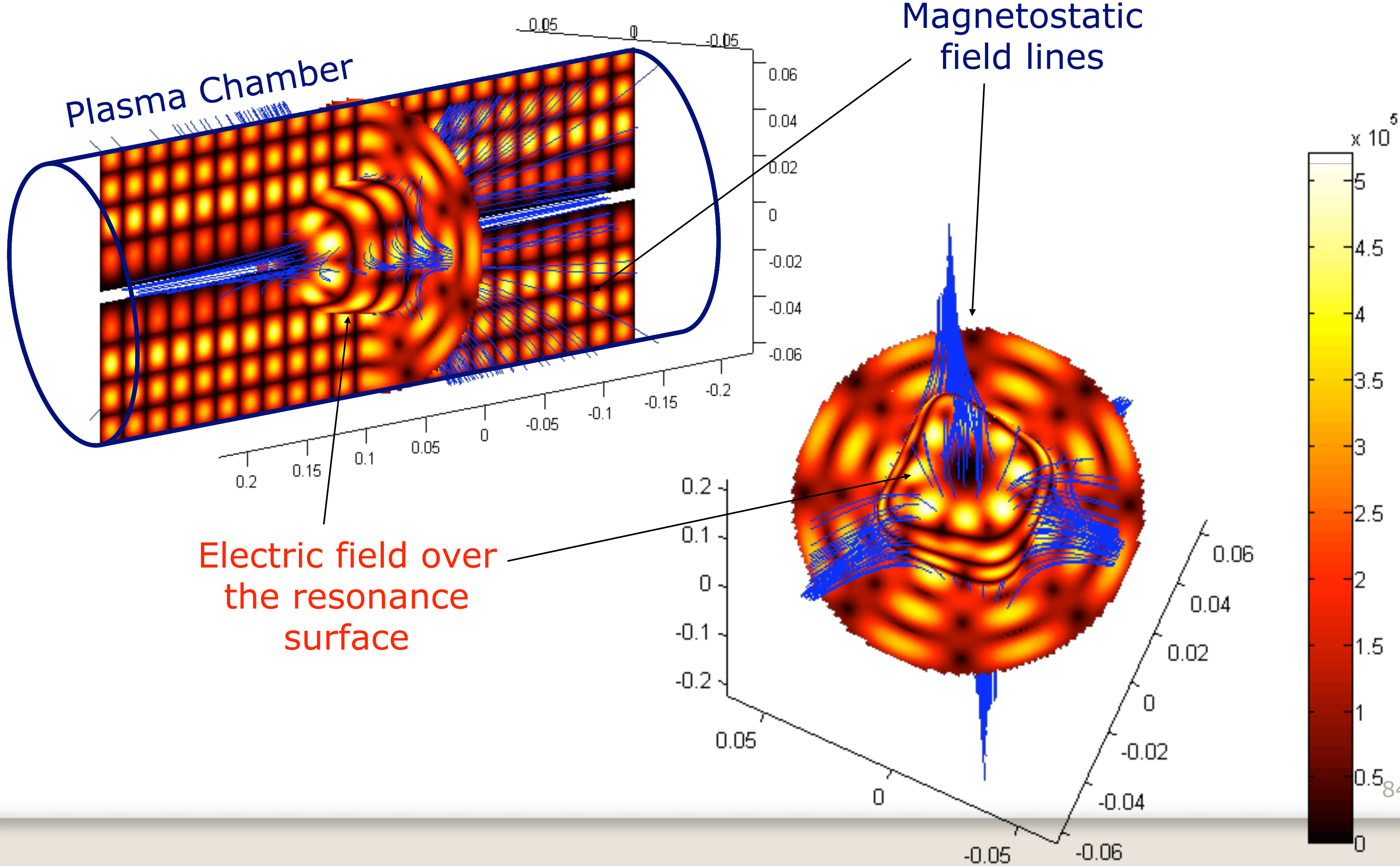

Initial conditions

Simulation of electron and ion distribution at t=0

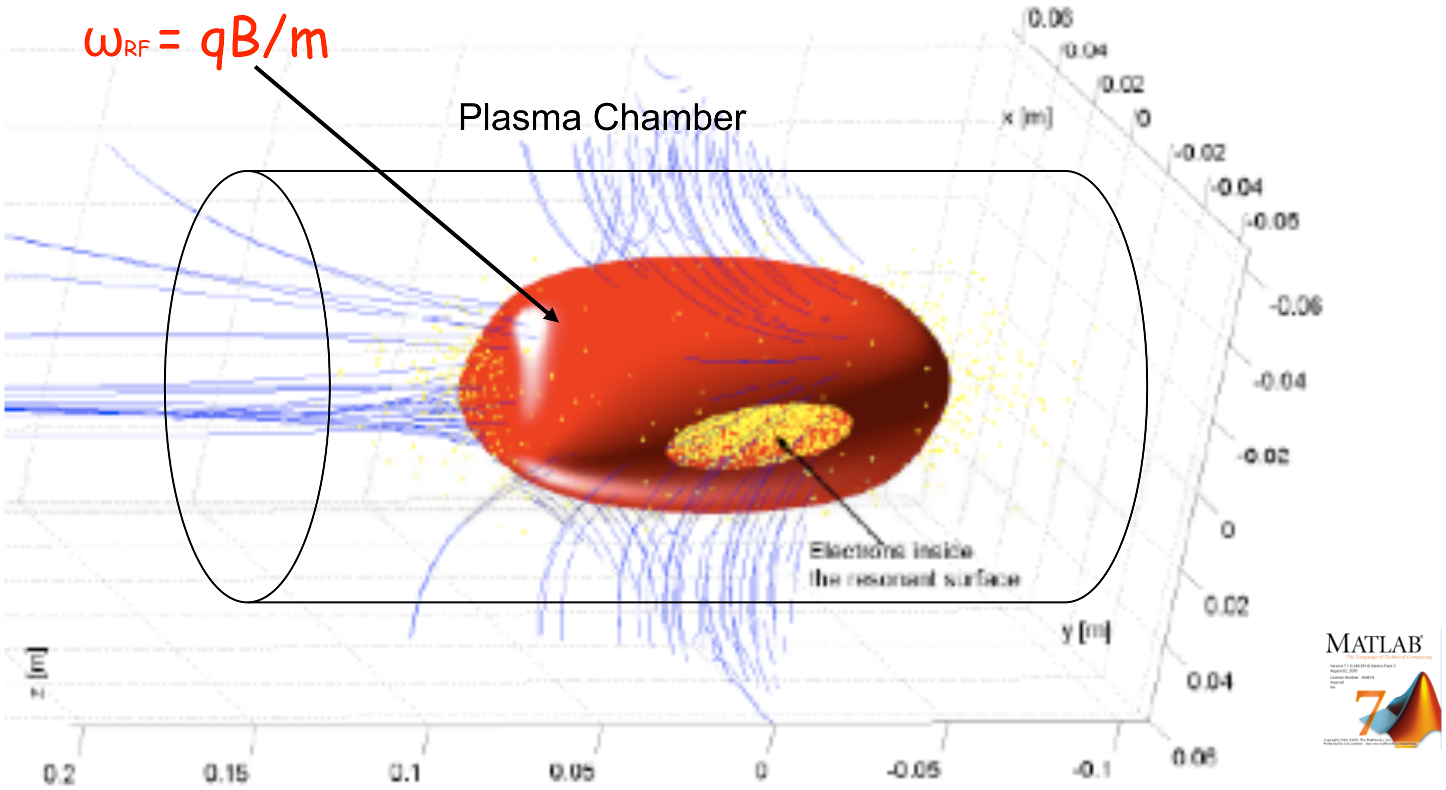

RED	Resonant Surface
BLUE	Magnetic Field lines
YELLOW	Plasma Electrons

Dominant collisions

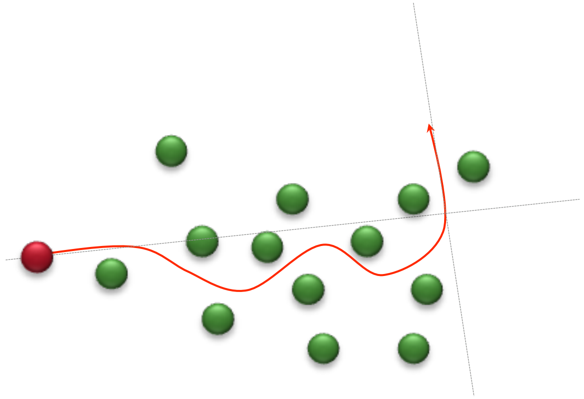

The most common collisions in fully ionized – hot plasmas are the multi-electrostatic, Spitzer collisions with a total scattering angle of 90°

e-e/i-i ("like particles" scattering) collisions dominate over e-i/i-e collisions ("unlike particles" scattering)

Collision frequency

$$\begin{cases} \nu_{90^\circ}^{ee} & = \dfrac{1}{\tau_{sp}} = 5\cdot 10^{-6} n \dfrac{\ln\left(\dfrac{\Lambda_D}{b}\right)}{T_e^{\frac{3}{2}}} \\ \nu_{90^\circ}^{ei} & = \dfrac{1}{\tau_{sp}} \sim 2\cdot 10^{-6} z n \dfrac{\ln\left(\dfrac{\Lambda_D}{b}\right)}{T_e^{\frac{3}{2}}} \\ \nu_{90^\circ}^{ii} & = \dfrac{1}{\tau_{sp}} \sim z^4 \left(\dfrac{m_e}{m_i}\right)^{\frac{1}{2}} \left(\dfrac{T_e}{T_i}\right)^{\frac{3}{2}} \nu_{90^\circ}^{ee} \end{cases}$$

Carachteristic scattering time

$$\begin{cases} \tau_m^{ee} & \sim \quad \tau_{90^\circ}^{ee} \sim \tau_{90^\circ}^{ei} \\ \tau_m^{ii} & \sim \quad \tau_{90^\circ}^{ii} \sim \left(\dfrac{m_i}{m_e}\right)^{\frac{1}{2}} \tau_{90^\circ}^{ei} \\ \tau_m^{ei} & \sim \quad \tau_m^{ie} \sim \dfrac{m_i}{m_e} \tau_{90^\circ}^{ei} \end{cases}$$

$$\tau_m^{ee} \sim \tau_{90^\circ}^{ee} \text{ and } \tau_m^{ei} \gg \tau_{90^\circ}^{ei}$$

Dominant collisions

Numerical technique for single particle 90° collisions

1. The most probable collision type are the electrostatic i-i and e-e multiple collisions with velocity rotation of 90°
2. Collision position is determined by comparing a randomly extracted number in the range 0-1 with the collision probability

$$(0 < rnd < 1) < P(t) = 1 - \exp\left(-\frac{t}{\tau_{coll}}\right)$$

The collision time is given by:

$$\tau_{coll} = \frac{M_{i,e}^2 2\pi\varepsilon_0^2 v_{i,e}^3}{n_e z^4 e^4 \ln\Lambda}$$

Where the plasma density is an input parameter

$$n_{ECRIS}(x,y,z) = 0.3 n_{cutoff} + \Sigma_i h n_{cutoff} \exp\left\{-\frac{\left[B_{tot}(x,y,z) - (B_{ECR} - ki)\right]^2}{k^2}\right\}$$

This formula is the initial parameterization of plasma distribution (preliminary 2D PIC simulations were used)

Numerical evaluation of Spitzer collisions

Collision evaluation procedure

Fixing integration time

Evaluating the position (density) inside the chamber

Extracting collision probability at time *t* and density *n(x,y,z)*

Comparing the collision probability with a randomly extracted number.

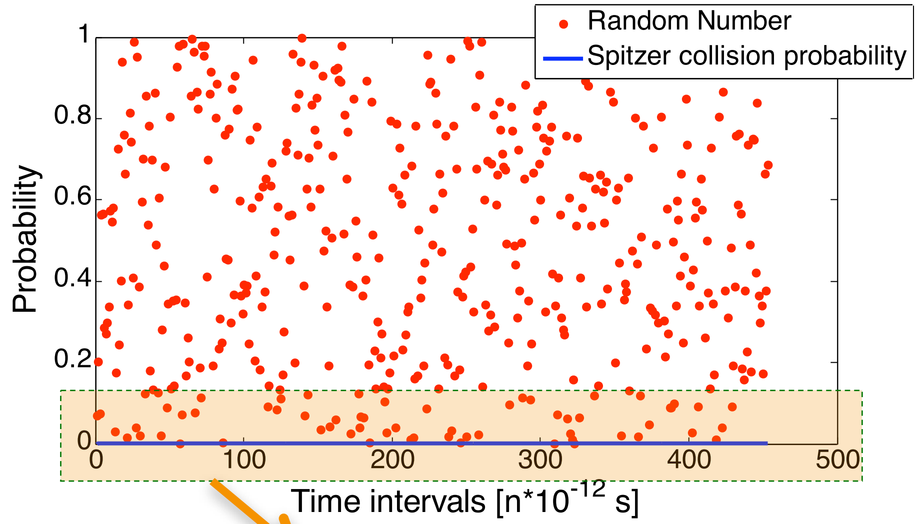

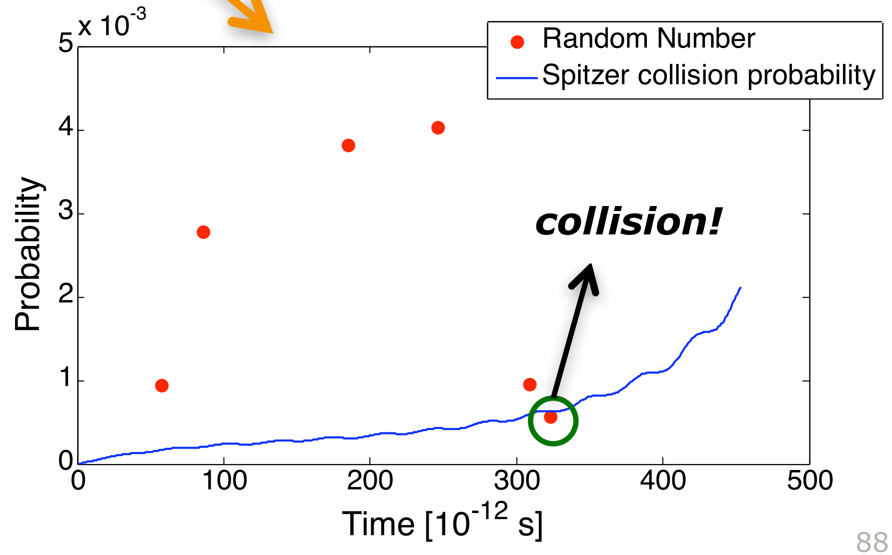

90° collisions code implementation

$$V_1 = \begin{pmatrix} v_{x_1} & v_{y_1} & v_{z_1} \end{pmatrix}$$

$$V_2 = \begin{pmatrix} v_{x_2} & v_{y_2} & v_{z_2} \end{pmatrix}$$

$$\begin{cases} V_1 \cdot V_2 = 0 \\ |V_1| = |V_2| \end{cases} \longrightarrow \text{Energy conservation}$$

$$\begin{cases} v_{x_1} v_{x_2} + v_{y_1} v_{y_2} + v_{z_1} v_{z_2} = 0 \\ |V_1| = \sqrt{v_{x_2}^{\;2} + v_{y_2}^{\;2} + v_{z_2}^{\;2}} \end{cases}$$

$$\begin{cases} v_{x_2} = -\dfrac{v_{y_1} v_{y_2} + v_{z_1} v_{z_2}}{v_{x_1}} \\ V_1^2 = v_{x_2}^{\;2} + v_{y_2}^{\;2} + v_{z_2}^{\;2} \end{cases}$$

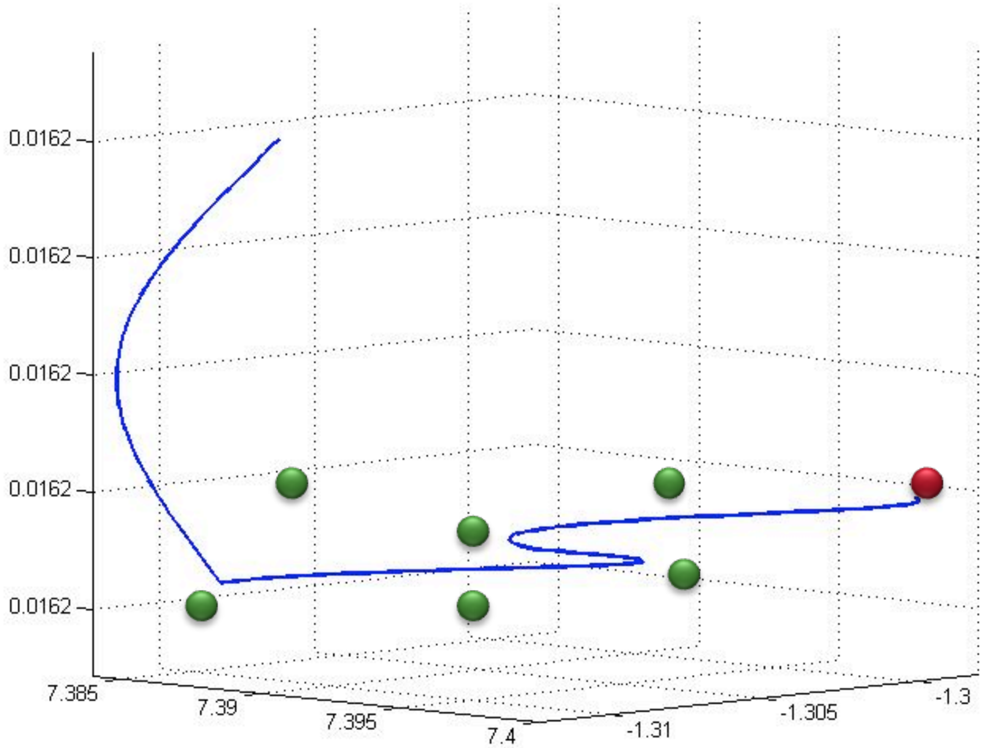

$$\begin{cases} v_{x_2} = -\dfrac{v_{y_1} v_{y_2} + v_{z_1} v_{z_2}}{v_{x_1}} \\ \left(\dfrac{v_{y_1}^{\;2}}{v_{x_1}^{\;2}} + 1\right) v_{y_2}^{\;2} + \left(\dfrac{2 v_{y_1} v_{z_1} v_{z_2}}{v_{x_1}^{\;2}}\right) v_{y_2} + \dfrac{v_{z_1}^{\;2} v_{z_2}^{\;2}}{v_{x_1}^{\;2}} + v_{z_2}^{\;2} - V_1^2 = 0 \end{cases}$$

3 Variables + 2 Conditions = One free parameter = z_2

90° collisions code implementation

Vz_2 = rand(1)*2*V-V

-V < Vz_2 < V

Editor - D:\Assegno\assegno x simulazioni\proAssegnoMatlab\montecarlo elettroni\urtoa90gradi_5.m

```
function [X02]=urtoa90gradi_5(X01)
V1=[X01(4),X01(5),X01(6)];              % Vector 1 before rotation
V=sqrt(sum(V1.^2));                     % Vector 1 module
D=-1;
while D<0                               % check discriminator value
    Vz2=rand(1)*2*V-V;                  % random parameter (-V,V)
    a=(V1(2)/V1(1))^2+1;                % ax^2+bx+c=0 coefficients
    b=2*V1(2)*V1(3)*Vz2/V1(1)^2;
    c=Vz2^2+(V1(3)*Vz2/V1(1))^2-V1(1)^2-V1(2)^2-V1(3)^2;
    D=b^2-4*a*c;                        % discriminator
end
Vy2=(-b+sqrt(D))/(2*a);                 % one solution of quadratic equation
Vx2=-(V1(2)*Vy2+V1(3)*Vz2)/V1(1);       %
V2=[Vx2,Vy2,Vz2];                       % Vector 2 (simply ortogonal to first vector)
```

θ = rand(1)*2*π-π

-π < θ < π

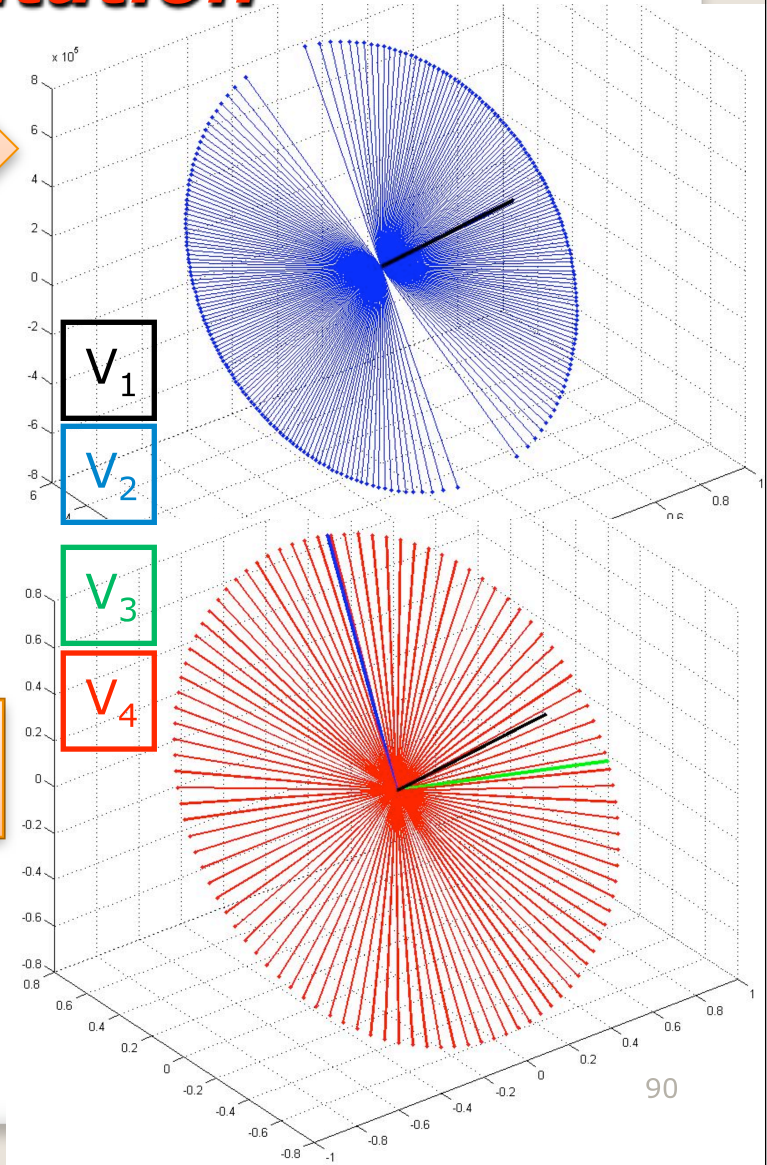

Electron Resonant acceleration

$$\vec{E} = \hat{x}E_0 \cos\left(\frac{\omega}{c}z - \omega t + \phi\right)$$
$$\vec{H} = \hat{y}\frac{E_0}{\mu c} \cos\left(\frac{\omega}{c}z - \omega t + \phi\right)$$

Electron acceleration proceeds in a timescale of 1-2 nsec

The energy exchange depends on the wave-to-electron phase relationship.

ECR zone crossing; the resonance takes place only where $B=B_{ECR}$

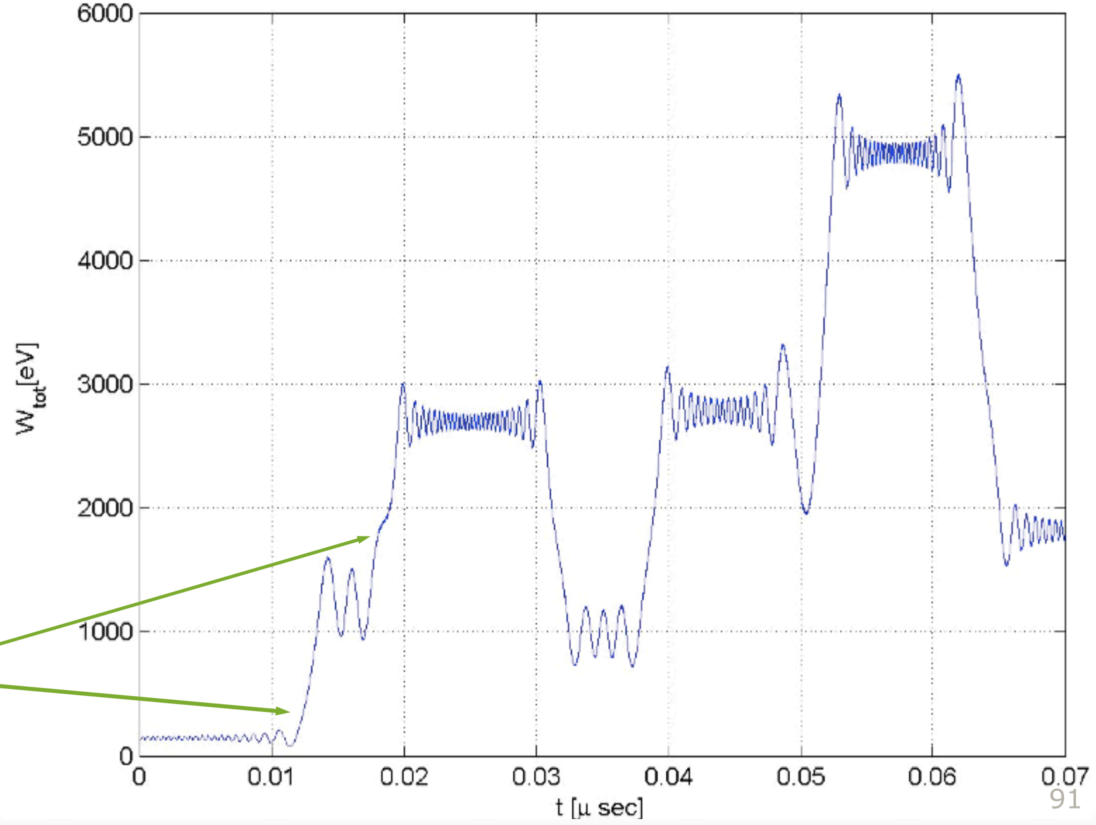

Simulated Electron Energy Distribution Function (EEDF)

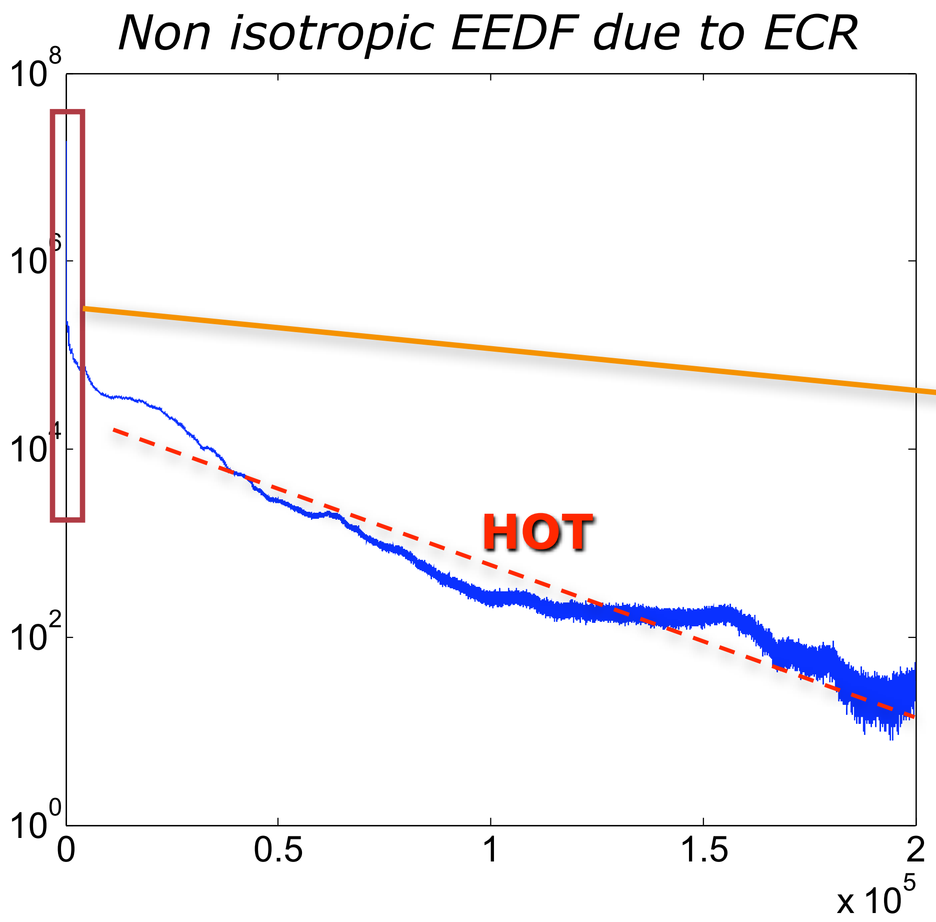

Non thermalized plasma:

HOT population T>25 keV

COLD population T~3-5 eV

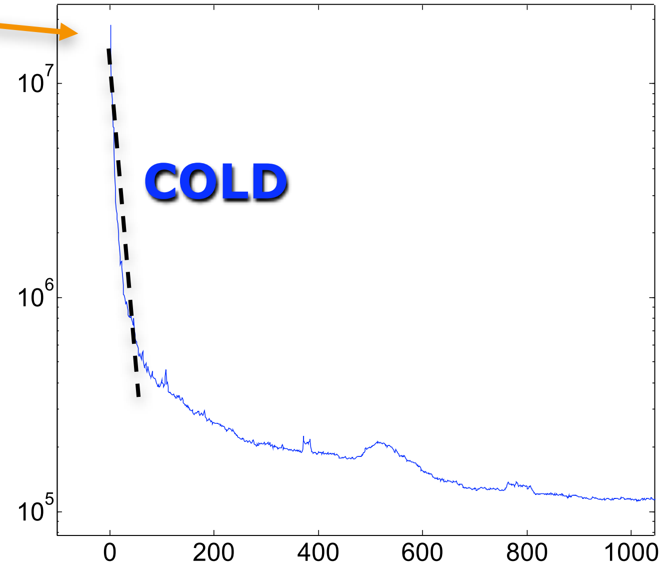

Magnetic confinement

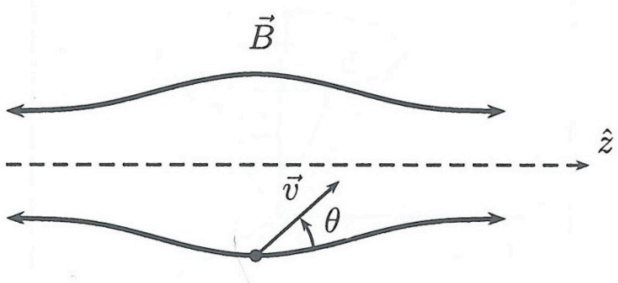

$$\frac{B}{B_{inv}} = \frac{v_{\perp}^2}{v^2} = \sin^2\theta$$

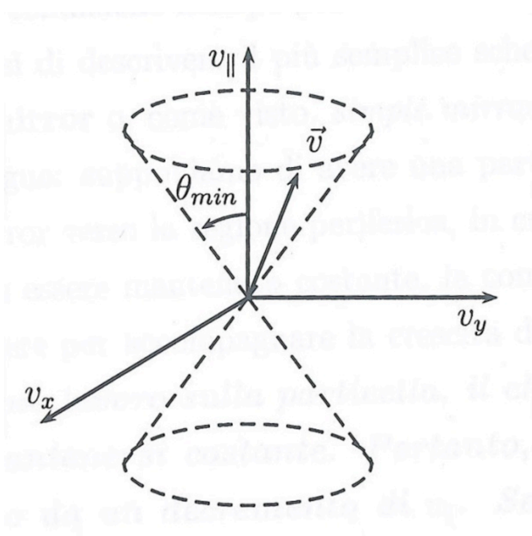

Confinement parameter

$$\Gamma = \frac{v_{\perp}^{2}}{v^2}\frac{B_{\max}}{B}$$

$$\begin{cases} \Gamma > 1 & \textit{confined} \\ \Gamma < 1 & \textit{not confined} \end{cases}$$

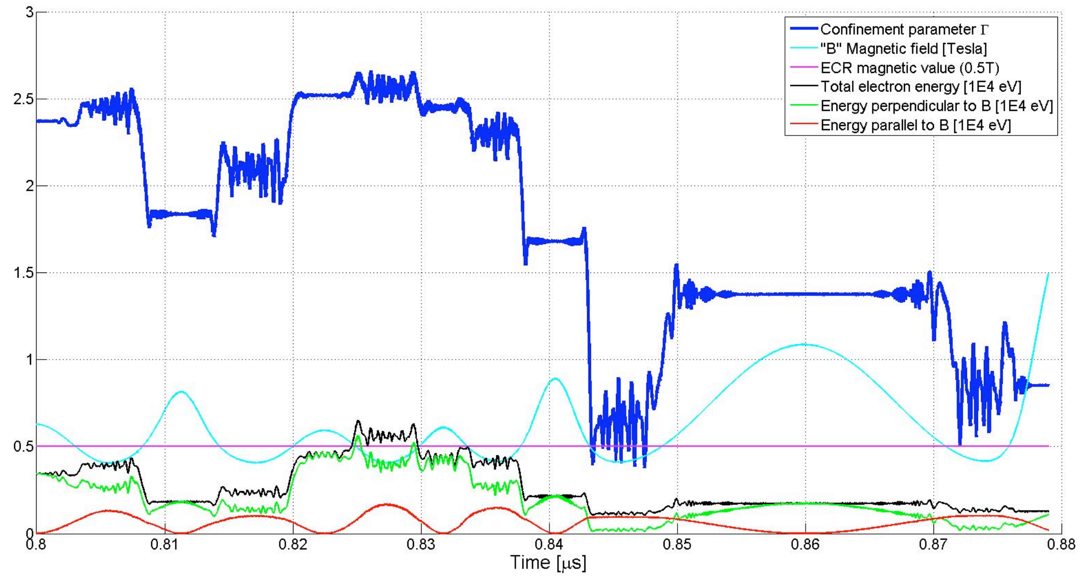

Two causes of deconfinement

1° Electron Cyclotron Resonance: modifing $v_{\perp}$

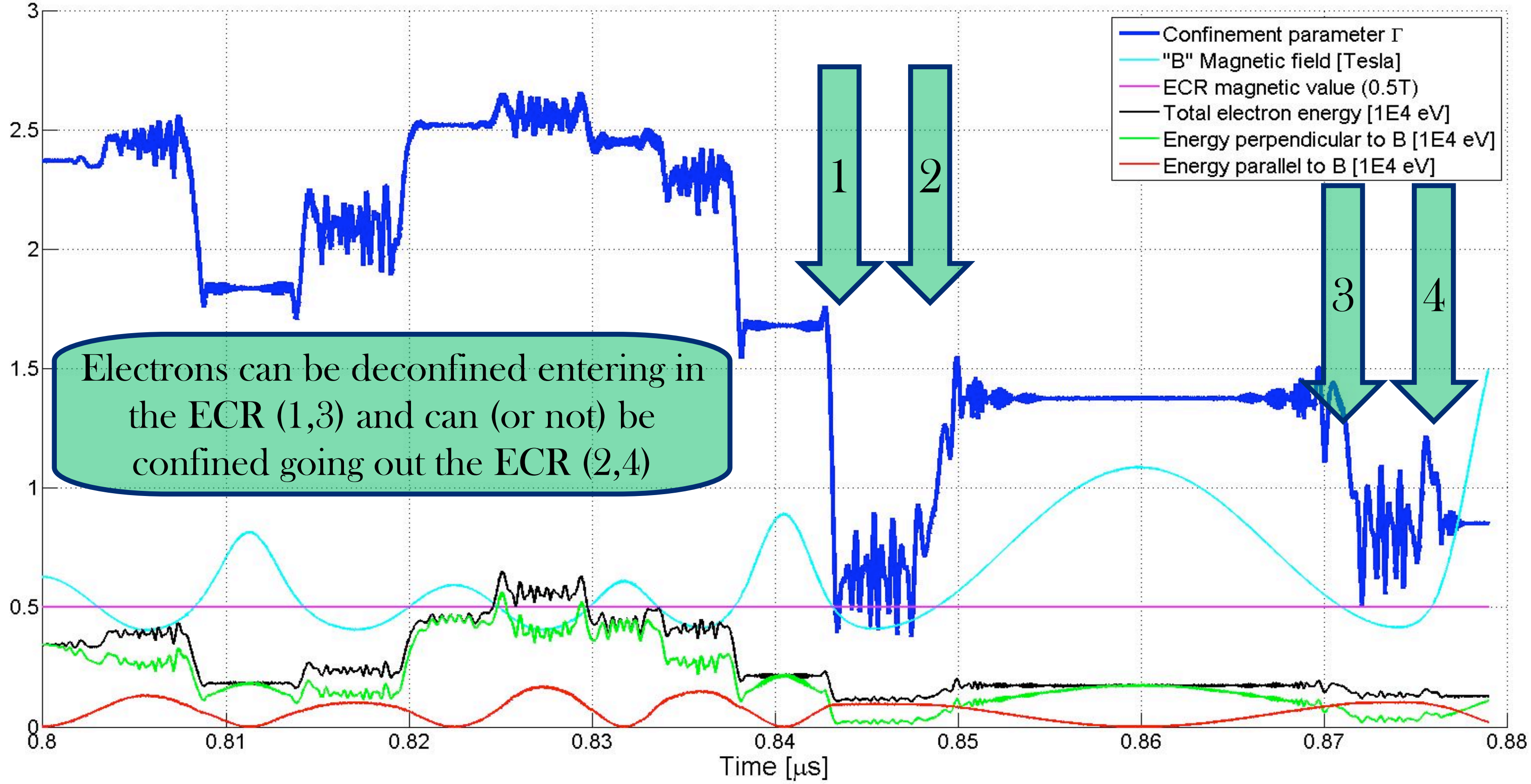

Two causes of deconfinement

2° Spitzer collision: 90° elastic coulomb collision

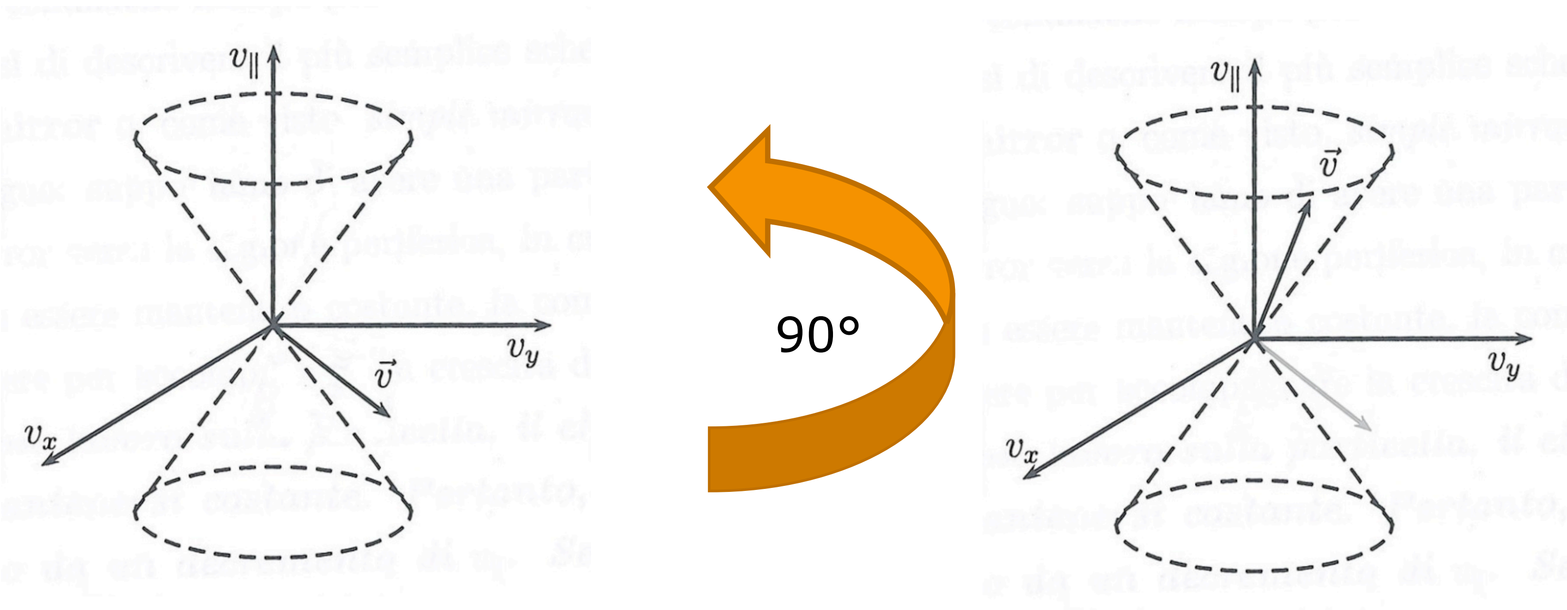

confined *not confined*

Electron expulsion by Spitzer collisions

$$Event_{LastCollision} = \left(x_{lc} \quad y_{lc} \quad z_{lc} \quad Vx_{lc} \quad Vy_{lc} \quad Vz_{lc} \quad t_{lc} \right)$$

$$Event_{ChamberWall} = \left(x_{cw} \quad y_{cw} \quad z_{cw} \quad Vx_{cw} \quad Vy_{cw} \quad Vz_{cw} \quad t_{cw} \right)$$

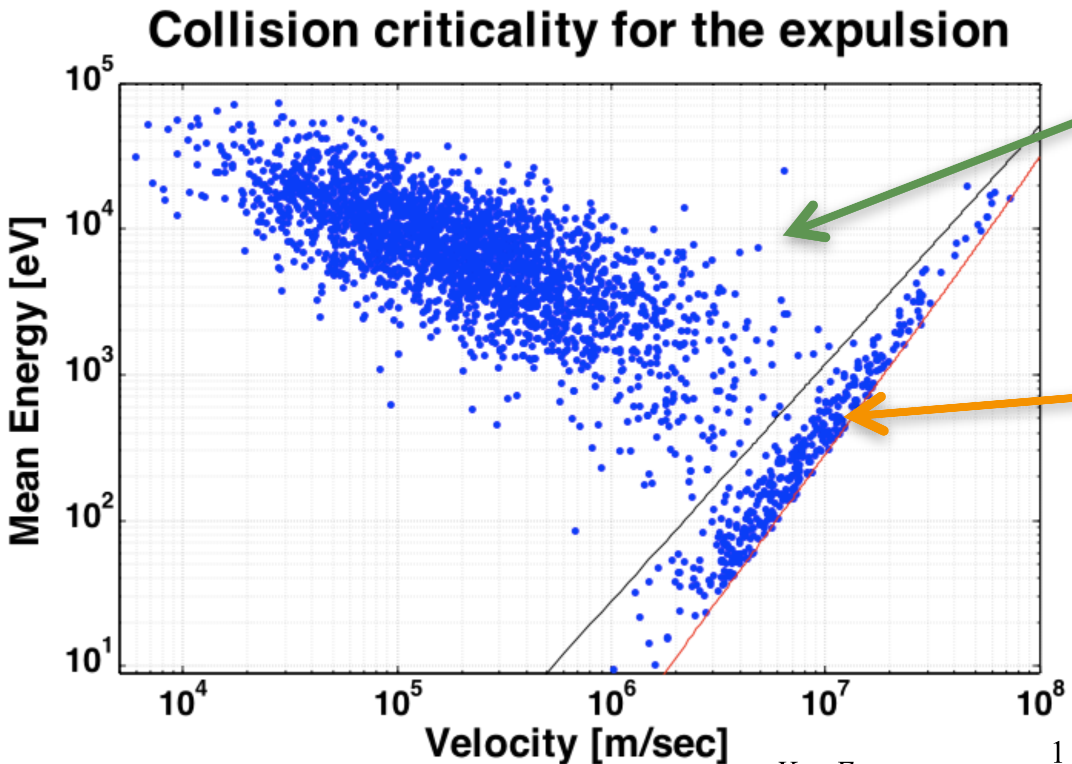

Particles expelled by non-adiabatic interaction at ECR and/or "pitch angle" scattering

Particles directly expelled by 90° collisions

$$X = E_{Hypotetical\ Straight} = \frac{1}{2} m \left(\frac{\Delta r}{\Delta t} \right)^2 = \frac{1}{2} m \left(\frac{(x_{cw} - x_{lc})^2 + (y_{cw} - y_{lc})^2 + (z_{cw} - z_{lc})^2}{\Delta t^2} \right)$$

$$Y = \left\langle E_{Real\ Trajectory} \right\rangle = \frac{1}{2} m \left(\left\langle Vx^2_{lc \to cw} \right\rangle + \left\langle Vy^2_{lc \to cw} \right\rangle + \left\langle Vz^2_{lc \to cw} \right\rangle \right)$$

Electron expulsion by Spitzer collisions

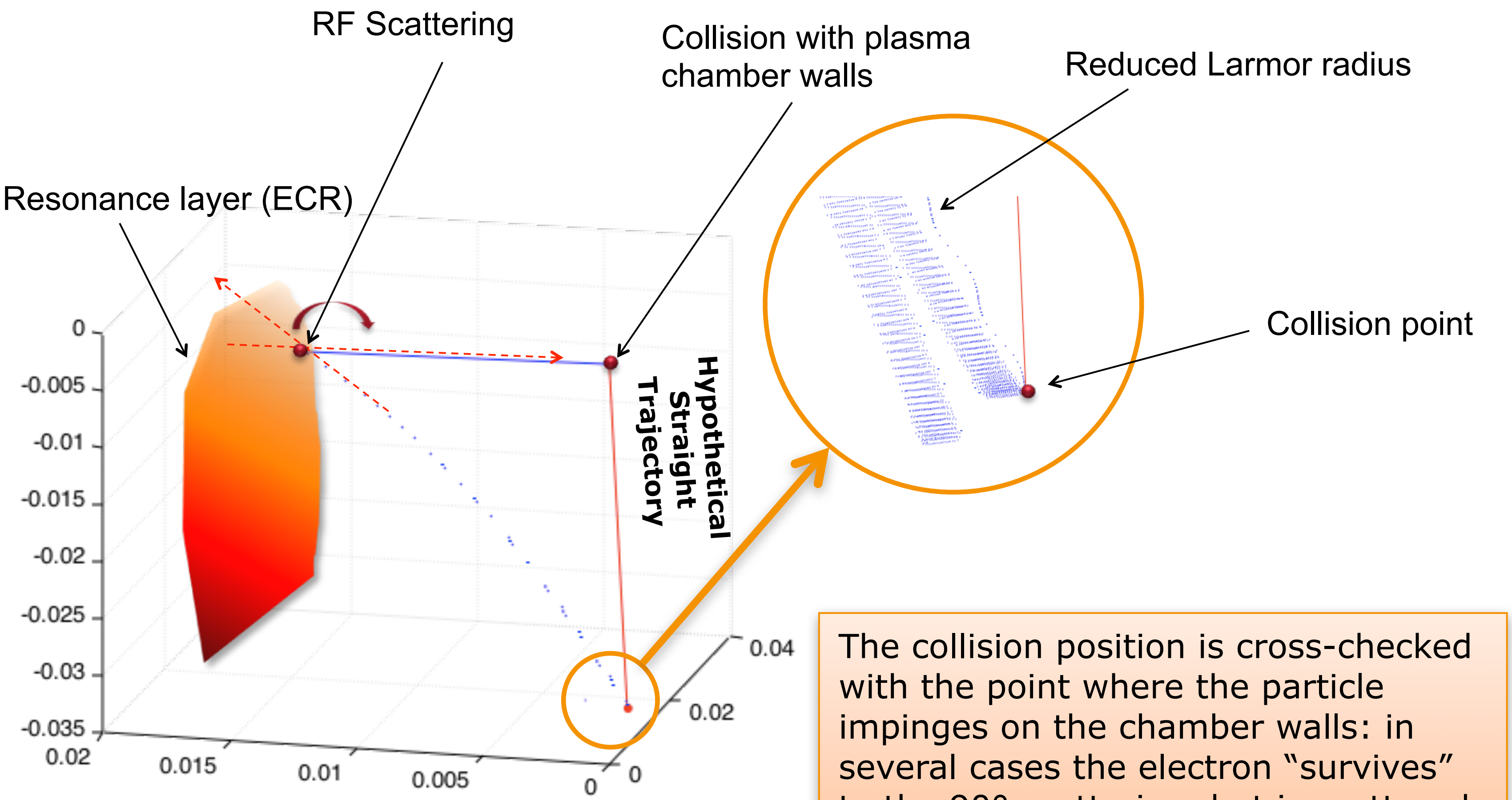

The collision position is cross-checked with the point where the particle impinges on the chamber walls: in several cases the electron "survives" to the 90° scattering, but is scattered by the RF field at the resonance

Definition of 3D density/energy maps

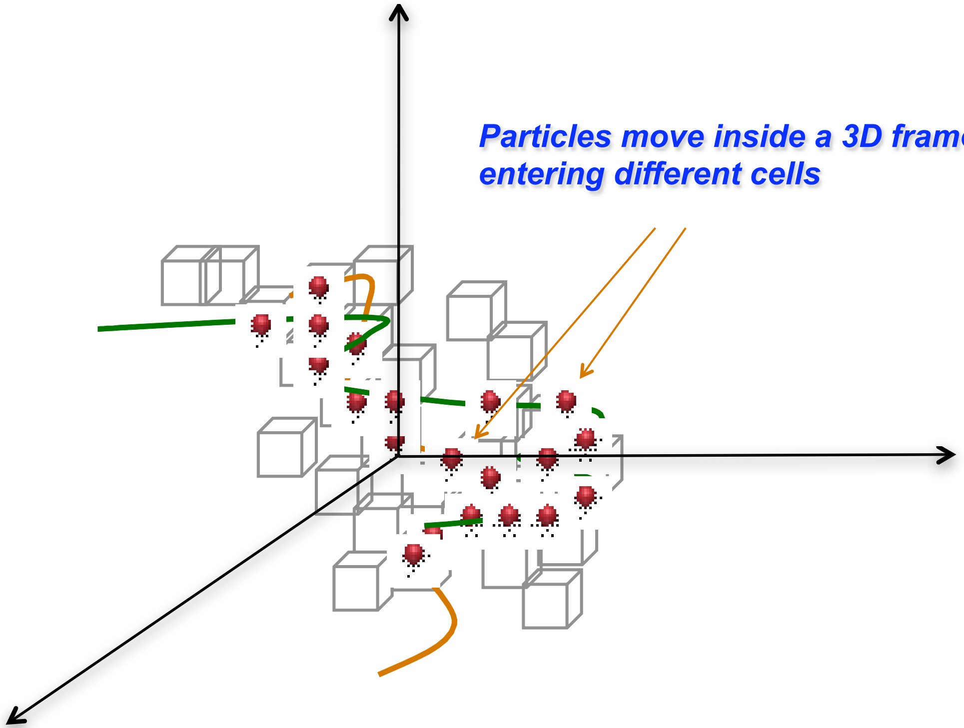

The plasma chamber domain is subdivided into 130x130x450=7·10^6 cells
(mm precision)

3D *false color* representation of the density

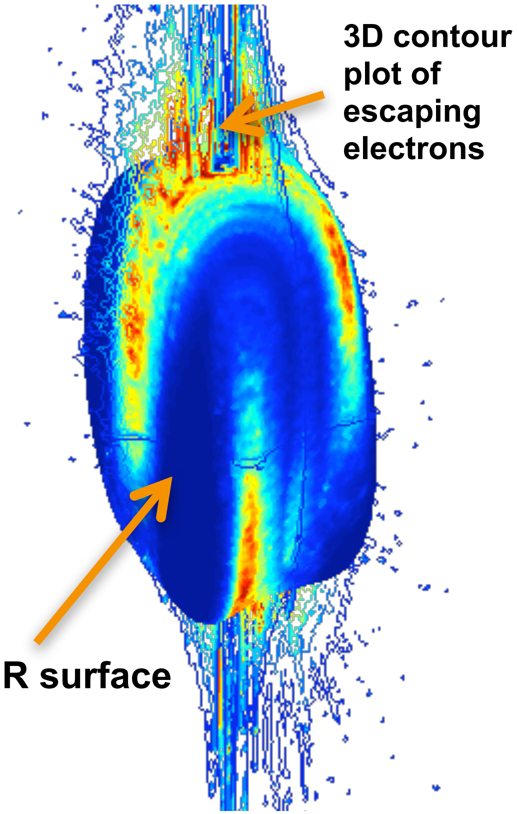

The density distribution can be then plotted by the `slice,contour3D,surf` routines. Slicing on arbitrary surface is also possible.

Self-consistency implementation

$$\frac{d\vec{v}}{dt} = \frac{q}{m_0\gamma}\left[\vec{E} + \vec{v}\times B - \frac{\vec{v}\cdot\vec{E}}{c^2}\vec{v}\right]$$

Solving the time-independent Vasov equation, including single particle collisions

$$\frac{\partial f_\alpha}{\partial t} + \vec{v}\cdot\vec{\nabla} f_\alpha + \frac{q_\alpha}{m_\alpha}\left(\vec{E} + \frac{\vec{v}\times\vec{B}}{c}\right)\cdot\vec{\nabla}_{\vec{v}} f_\alpha = 0$$

Step-by-step current

Step-by-step plasma density

$$\begin{aligned}
\vec{\nabla}\cdot\vec{E} &= 4\pi\sum_\alpha \overline{n}_\alpha q_\alpha \boxed{\int f_\alpha d\vec{v}} + 4\pi\rho_{ext} \\
\vec{\nabla}\times\vec{B} &= \frac{1}{c}\frac{\partial\vec{E}}{\partial t} + \frac{4\pi}{c}\sum_\alpha \overline{n}_\alpha q_\alpha \boxed{\int \vec{v} f_\alpha d\vec{v}} + \frac{4\pi}{c}\vec{J}_{ext} \\
\vec{\nabla}\times\vec{E} &= -\frac{1}{c}\frac{\partial\vec{B}}{\partial t}
\end{aligned}$$

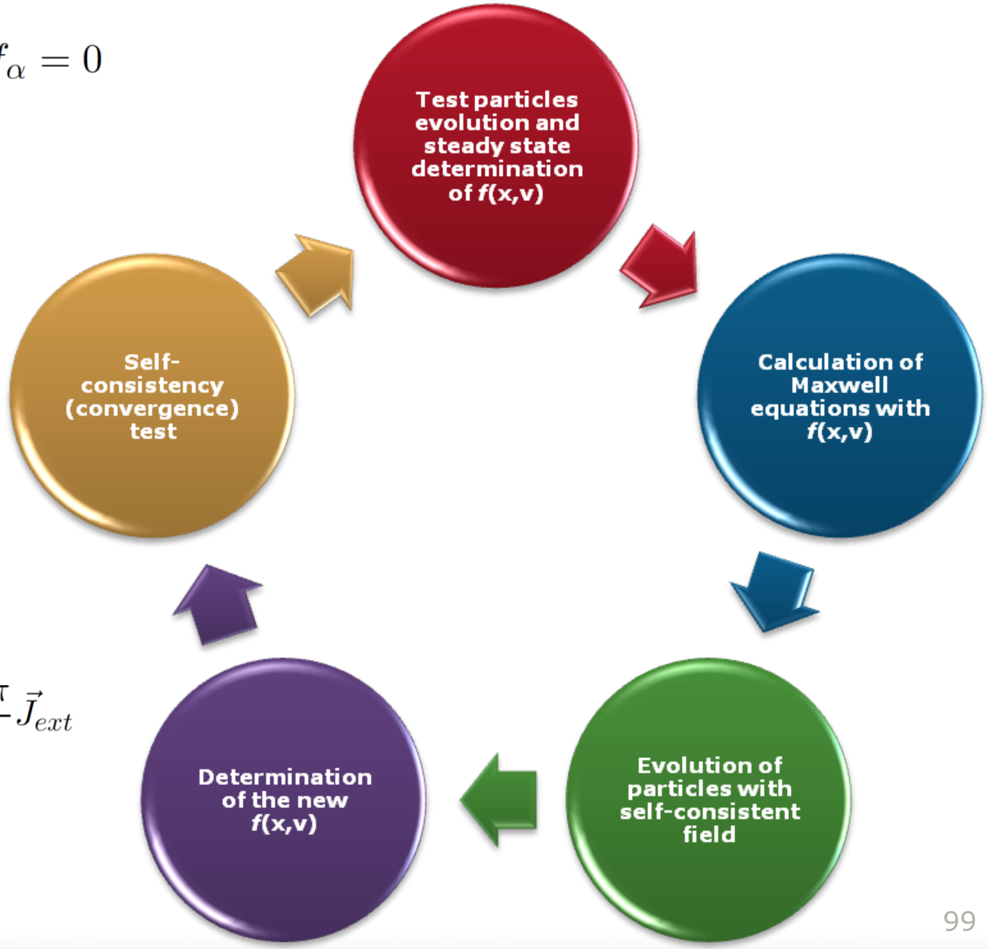

Simplified ray tracing

A first way to get self-consistency

Simulation strategy

A simplified ray tracing calculation has been implemented to follow **EM-waves path in the non-isotropic – non-homogeneous plasma**. The validity of the numerical approach has been tested with empty cavity, reproducing the well known pattern characterizing resonant modes.

As first approximation, all rays can start from the same input position without any loss of generality.

The frame of the free **Ray**:

$$\mathbf{R_x(i) = R_x(i-1) + \Delta R\cos(\vartheta(i-1))}$$

$$\mathbf{R_y(i) = R_y(i-1) + \Delta R\sin(\vartheta(i-1))}$$

Position of the **Ray** at iteration *i* depends on the position and on the angle at iteration *i-1*

The frame of the resonator is divided in square cells, larger than $\Delta R_{x,y}$

The square cells allow to count how many rays crossed their surface

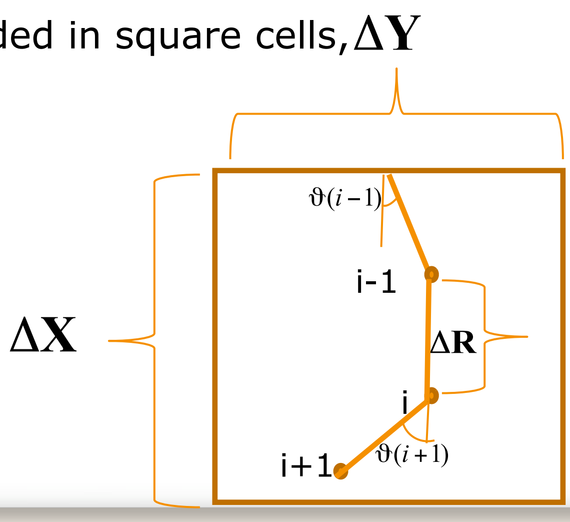

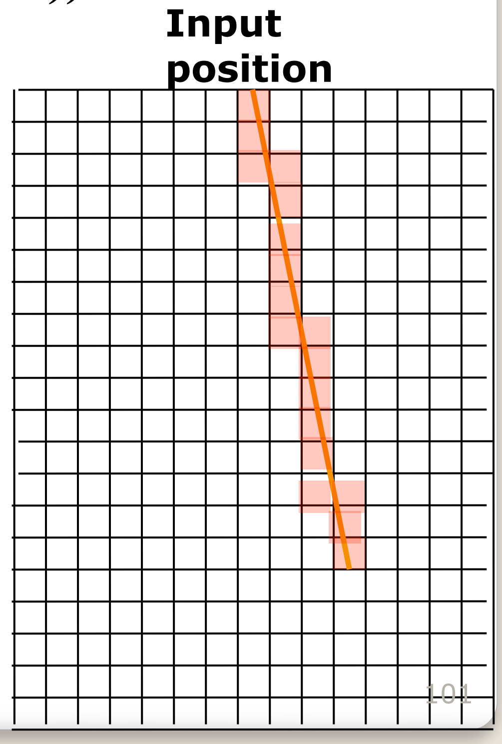

Simulation strategy

Wave amplitude is a complex function whose phase depends by the total path of the wave:

$$A(r) = \mathrm{C}e^{-2\pi i f\, r/c}$$

Different rays reach the same square after covering different distances:

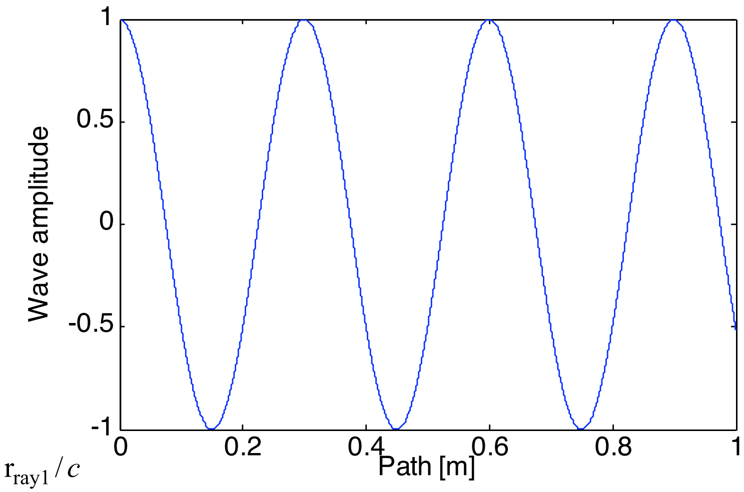

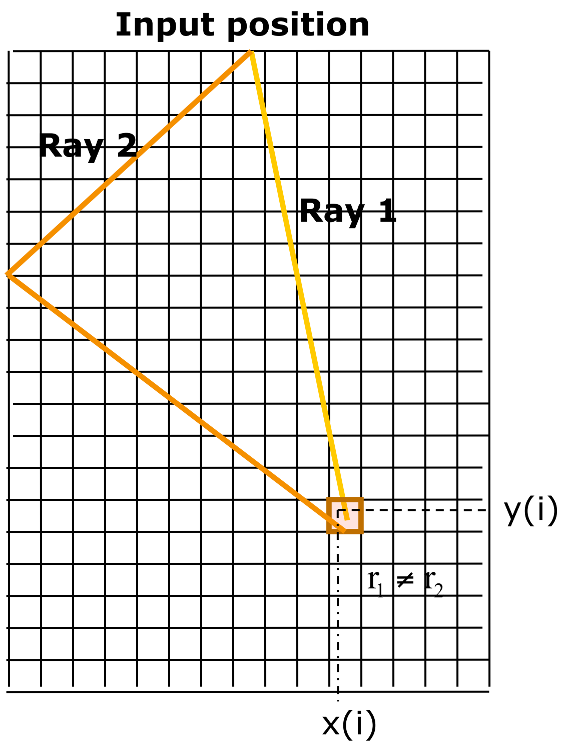

After 1° ray

$$A(x(i), y(i)) = \mathrm{C}e^{-2\pi i f\, r_{ray1}/c}$$

$$\left|E(x(i), y(i))\right|^2 = \left|\mathrm{C}e^{-2\pi i f\, r_{ray1}/c}\right|^2$$

Electric field amplitude

After 2° ray:

$$A'(x(i), y(i)) = A(x(i), y(i)) + \mathrm{C}e^{-2\pi i f\, r_{ray2}/c}$$

$$\left|E(x(i), y(i))\right|^2 = \left|A(x(i), y(i)) + \mathrm{C}e^{-2\pi i f\, r_{ray2}/c}\right|^2$$

After *n* rays we have:

$$\left|E(x(i), y(i))\right|^2 = \left|\sum_{rays} \mathrm{C}e^{-2\pi i f\, r_{rays}/c}\right|^2$$

Total electric field amplitude per cell

INFN Istituto Nazionale di Fisica Nucleare

Simulating the Ray propagation in plasma

Let's come back to the propagation laws of Microwave ray:

$$\mathbf{R_x(i) = R_x(i-1) + \Delta R\cos(\vartheta(i-1))}$$
$$\mathbf{R_y(i) = R_y(i-1) + \Delta R\sin(\vartheta(i-1))}$$

The angle at iteration **i** depends on the angle at iteration **i -1** by means of the Snell laws

$$\sin\vartheta(\mathbf{i})\times\mathbf{n(i)} = \sin\vartheta(\mathbf{i-1})\times\mathbf{n(i-1)}$$

Where **n(i)** is the refraction index of the medium:

$$\mathbf{n}^2 = 1 - \frac{2X(1-X)}{2(1-X)Y^2\sin^2(\vartheta) \pm \left[Y^4\sin^4(\vartheta) + 4(1-X)^2Y^2\cos^2(\vartheta)\right]^{\frac{1}{2}}}$$

Appleton-Hartree formula for the anisotropic plasma refraction index

$$\mathbf{X} = \frac{\omega_p^2}{\omega^2}$$

Normalized density

$$\mathbf{Y} = \frac{\omega_c}{\omega}$$

Normalized magnetic field

X and **Y** ***depend on the electron density of the plasma*** at position **i** and on magnetic field on position **i**

Preformed electron density and magnetic field maps are needed!!

Simulating the Ray propagation in plasma

In empty resonators n=1 , so

$$\vartheta(i) = \vartheta(i-1)$$

In plasma filled cavities, generally

$$\vartheta(i) \neq \vartheta(i-1)$$

Ray tracing calculation in a simplified magnetic field (typical of proton sources) and density structure

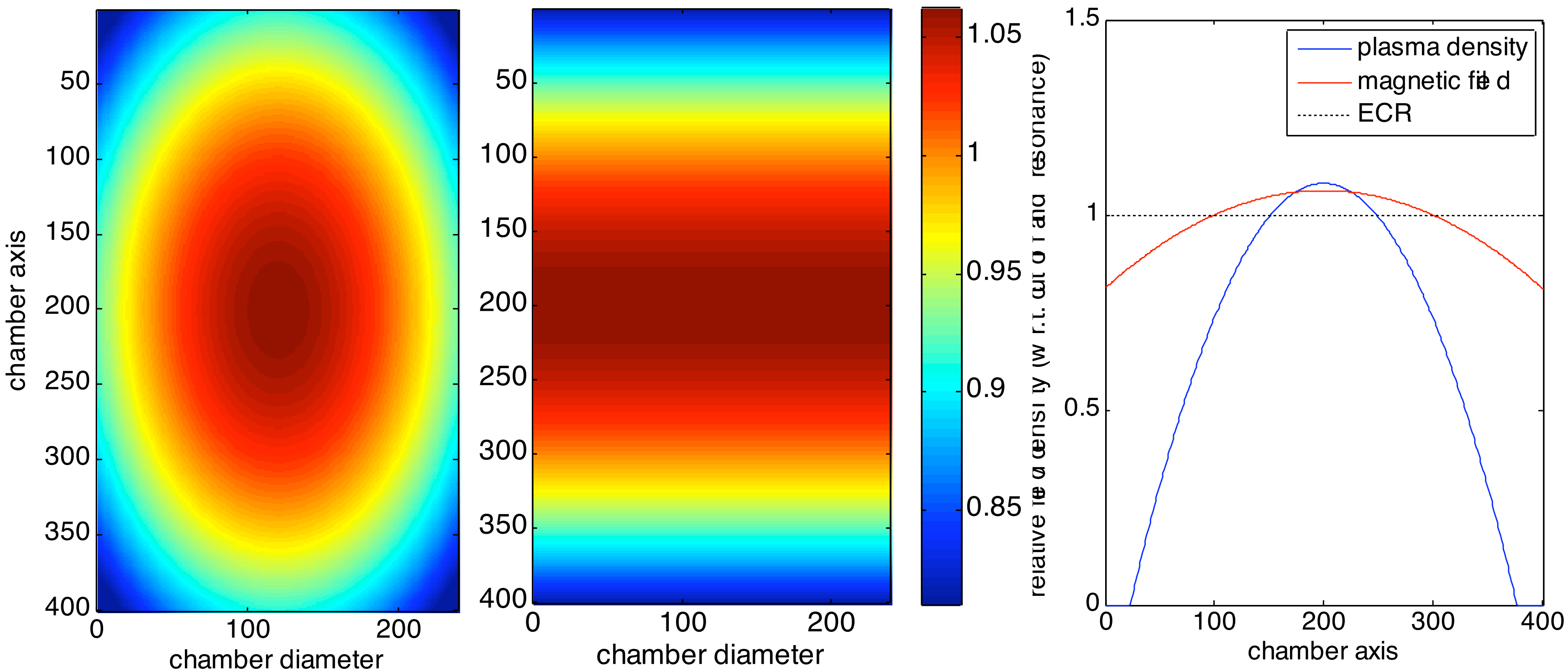

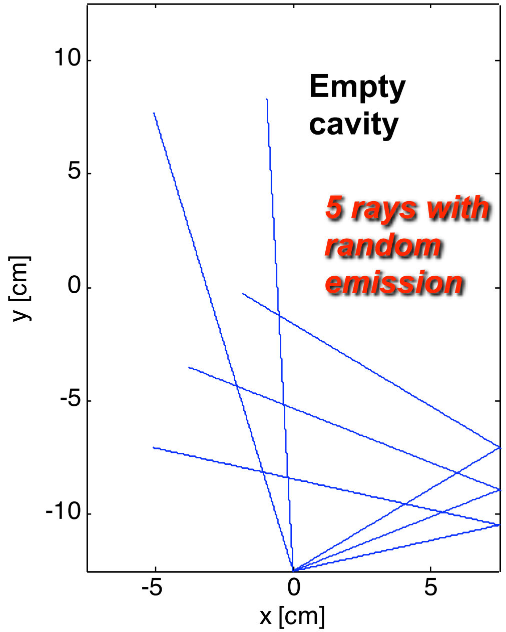

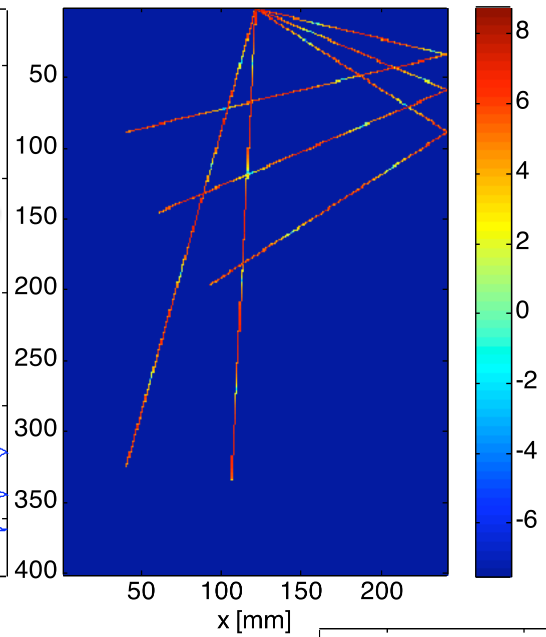

Simulating the Ray propagation in plasma

False colors highlight the s.b.s. wave amplitude modulation

The high density plasma distorts significantly the rays paths.

The high density plasma core is arduously reachable by the wave

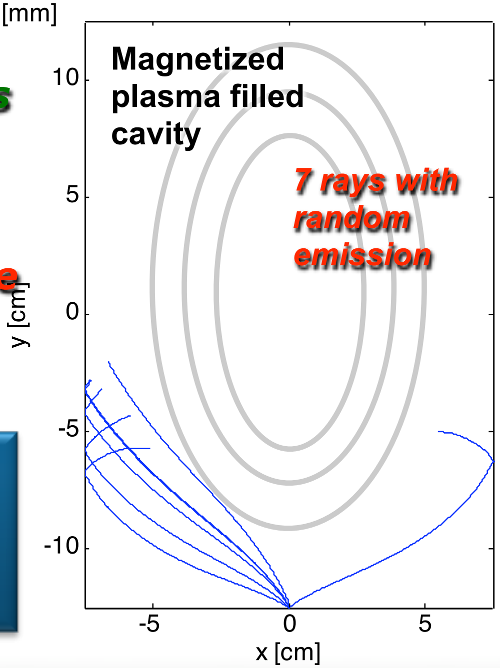

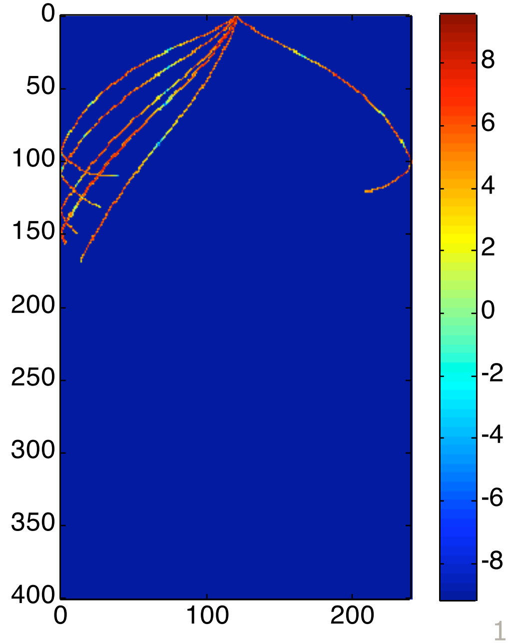

Simulations suggest that alternative heating schemes are needed to deposit energy into the plasma core

Case 1: Empty resonator

Empty resonators are characterized by n=1 -----> $\vartheta(i) = \vartheta(i-1)$

Mode $TE_{2,0}$ f=1.1992 GHz

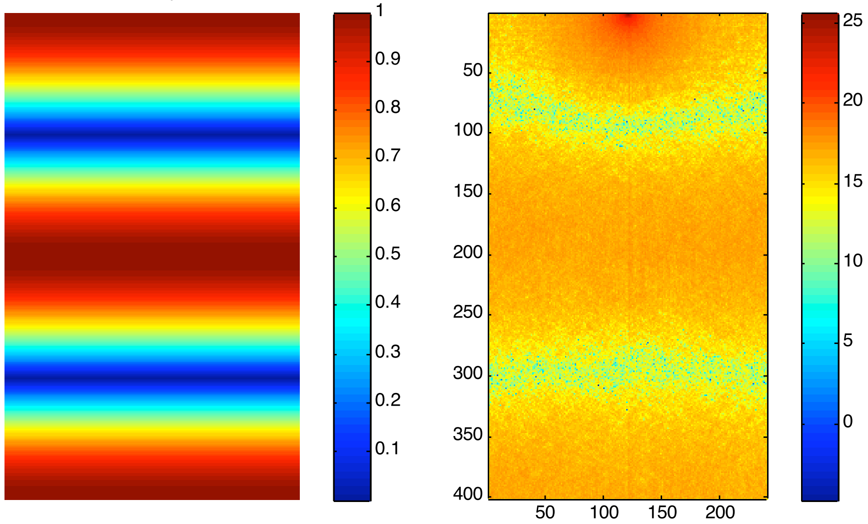

Position of the microwaves input must ever coincide with a maximim of the E.M field ----> second index have to be even

Modes having odd second index cannot exist in *real* resonators.

Mode $TE_{2,1}$ f=1.561 GHz

Mode $TE_{4,2}$ f=3.1219 GHz

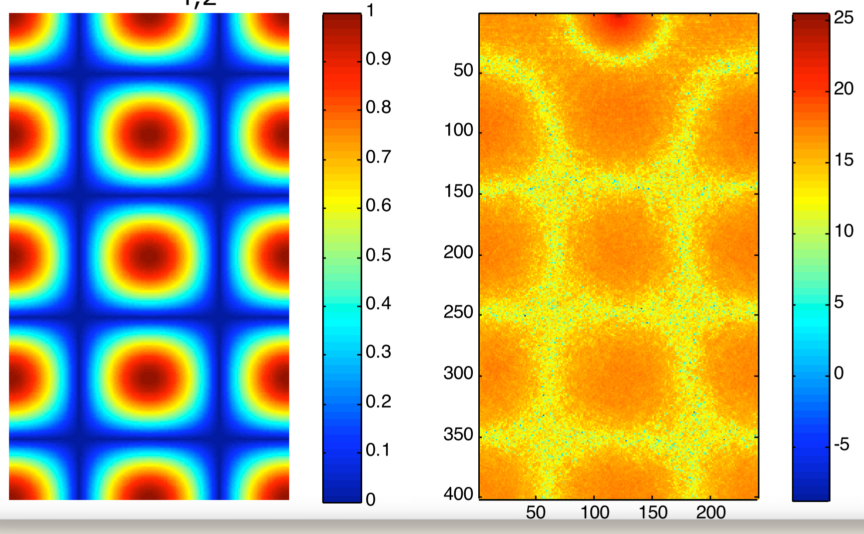

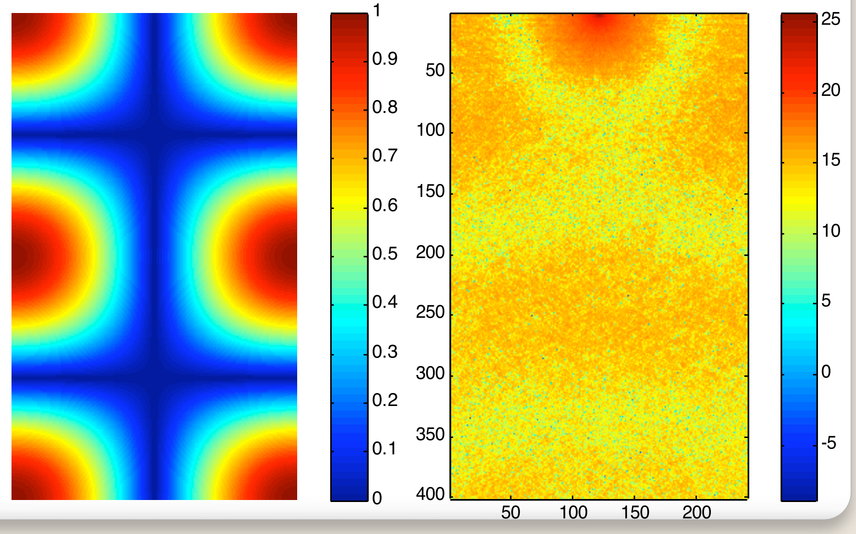

Case 2: Plasma filled cavities

In plasma filled cavities the microwaves are absorbed at the resonances and reflected at cut-off surfaces, depending on the value of electron density and magnetic field:

Resonance condition:

$$\cos^{-1}\left(\frac{\mathbf{X}+\mathbf{Y}^2-1}{XY^2}\right)^{\frac{1}{2}} = 0$$

Reflection condition:

$$\mathbf{n} < 0$$

It's not so simple to solve the problem for reflection. It's necessary to valuate the surface of reflection.
The numerical method allows to find regions in which the resonance occurs

Numerical results:

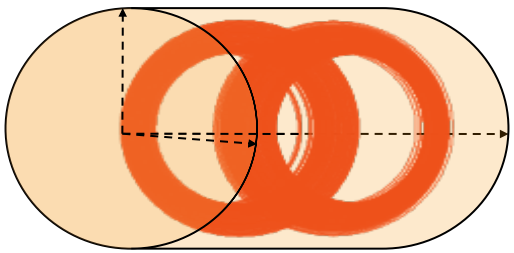

f=2.45 GHz

Experimental Evidences:

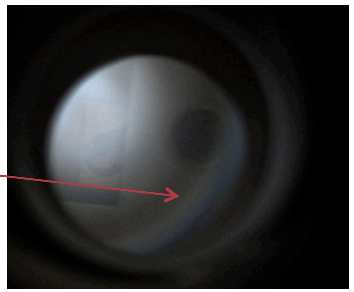

Numerical results:

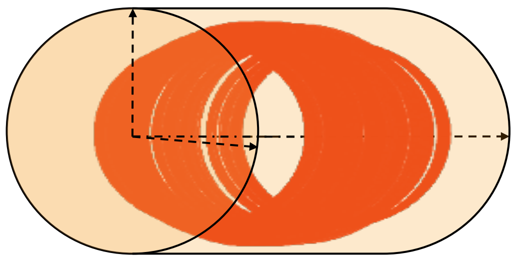

f=3.76 GHz

Experimental Evidences:

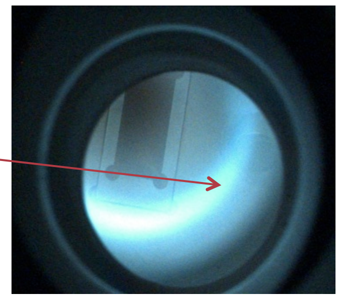

Importance of Modeling

Explanation of the impact of magnetic field and pumping wave frequency on ion and electron dynamics

FINE TUNING OF ECRIS PARAMETERS (B , *f*)

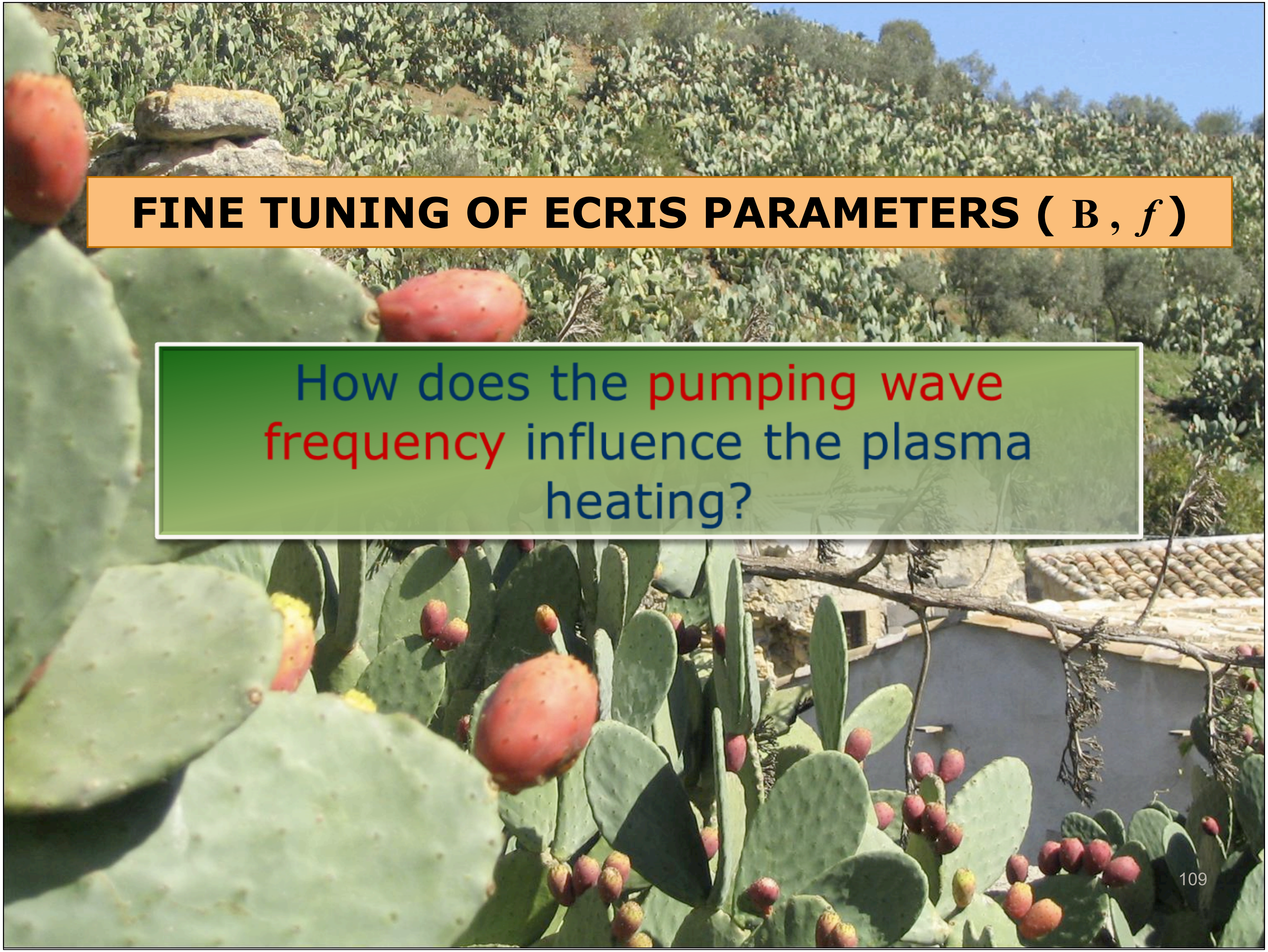

How does the pumping wave frequency influence the plasma heating?

Importance of modes coupling with plasma

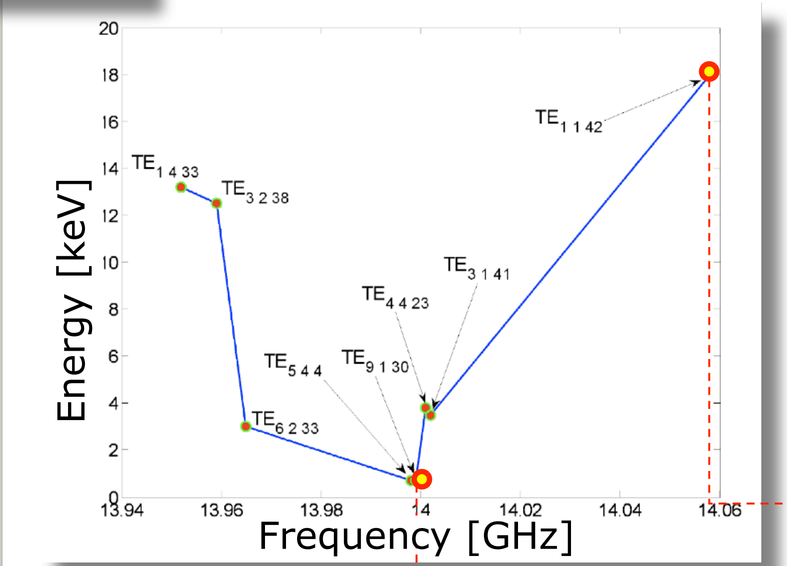

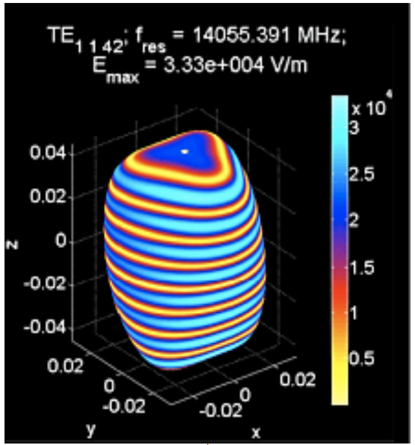

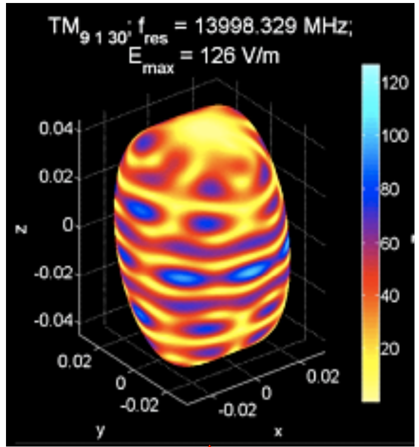

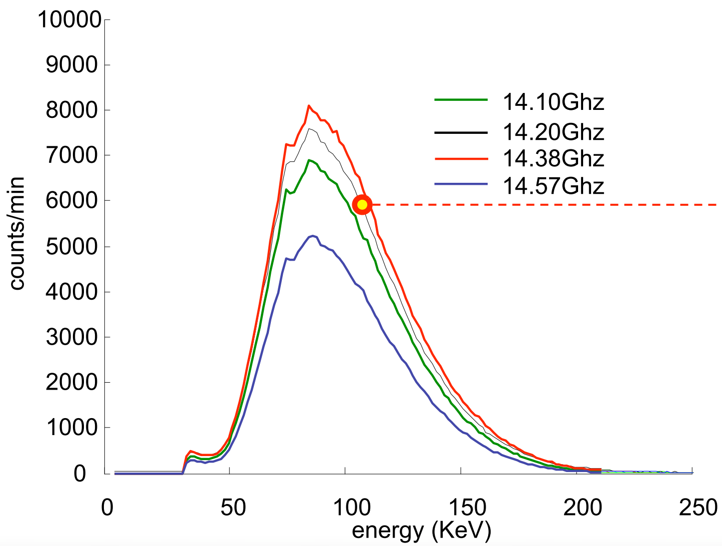

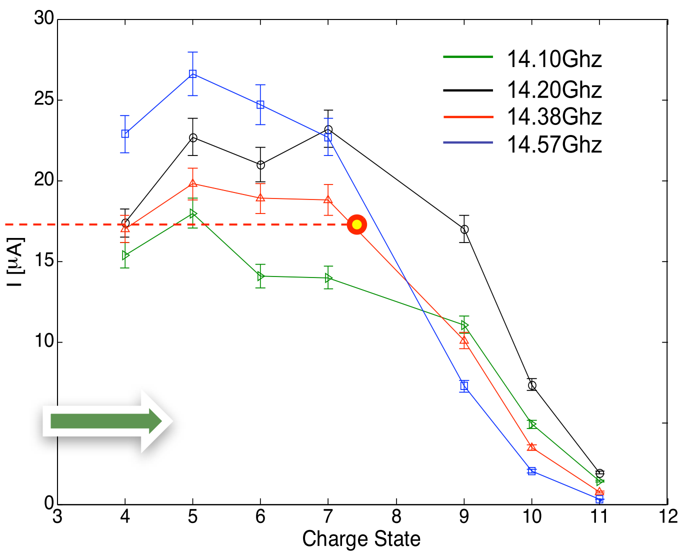

FTE plays a main role in fixing heating rapidity, but it only moderately affects the X-ray production at high energy. CSD is uncorrelated with X-rays

Explanation of frequency tuning effect

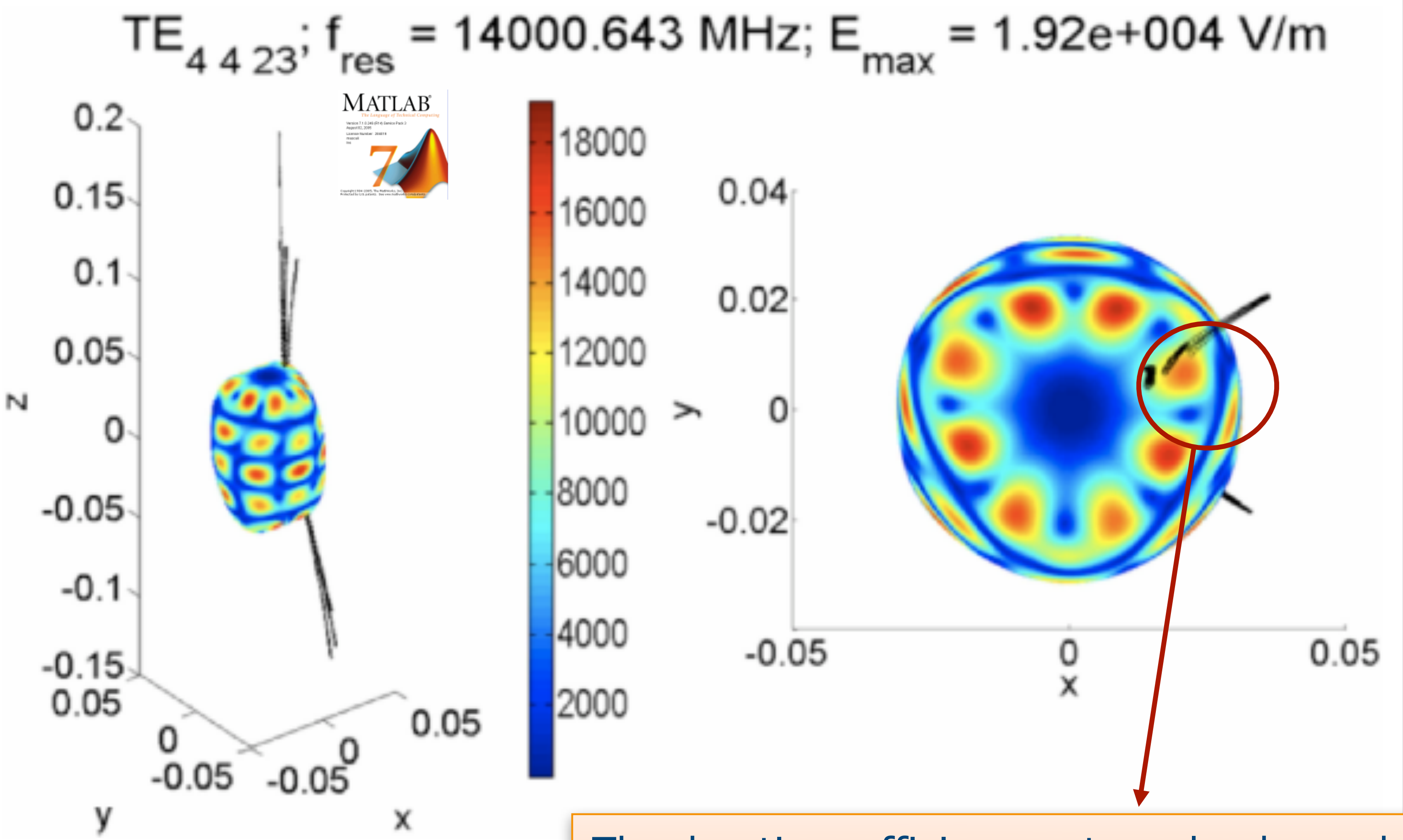

The heating efficiency strongly depends on the microwave pattern. The electrons cross the resonance surface in particular regions according to the field lines structure.

Localization of electrons energy absorption regions

[D. Mascali et al., *Oral presentation at 19th ECRIS Workshop*, Grenoble, 2010]

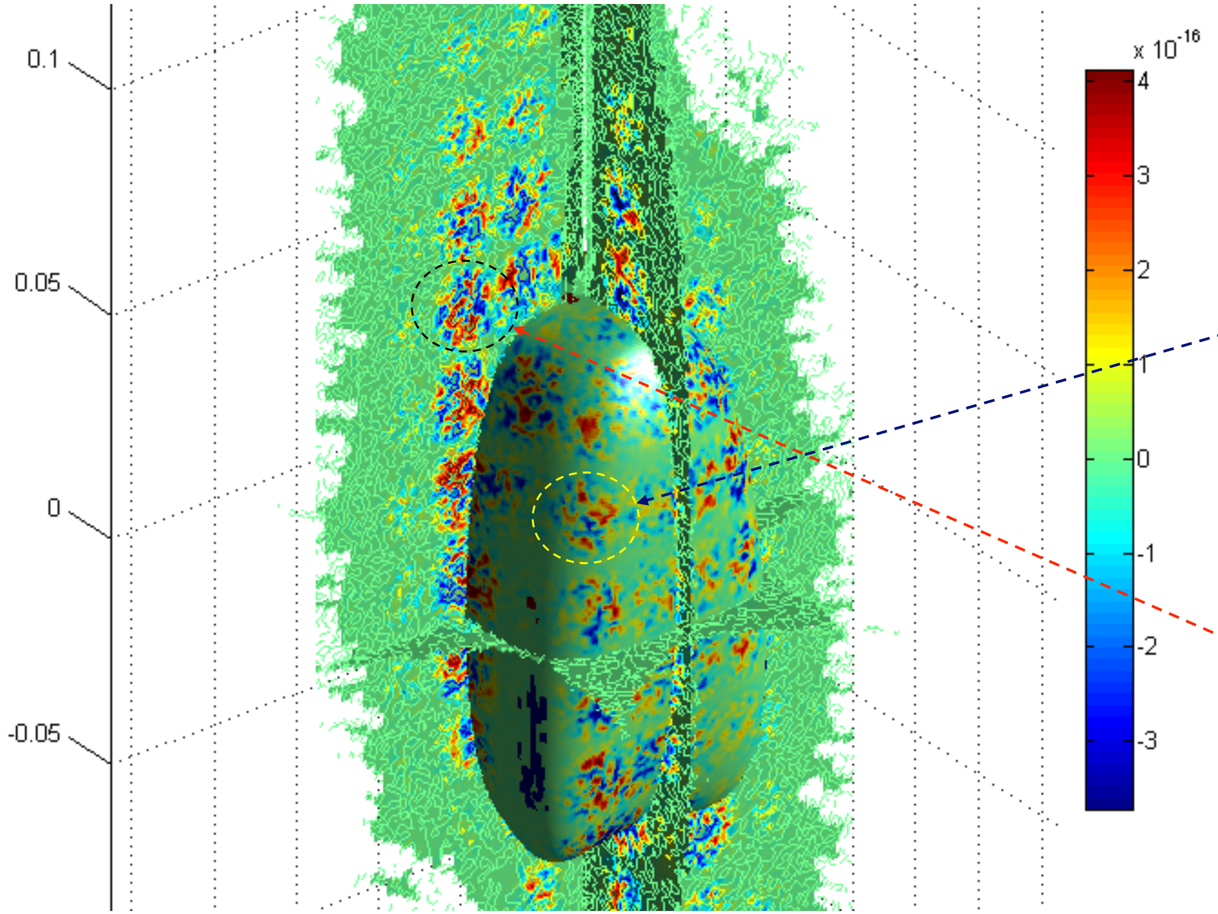

Interaction of the wave with the plasma takes place in some localized areas over the resonance surface. Particles gain or loss energy locally, being positive for electrons the net balance.

Energy exchange takes place also in off-resonance regions.

Off resonance interaction between wave and electrons must be more deeply investigated: relativistic effects (Doppler, mass)? It may be linked to ultra-hot electrons…

Impact of the modes on the density

The pattern of the electromagnetic field influences also the plasma density distribution

Electric field pattern

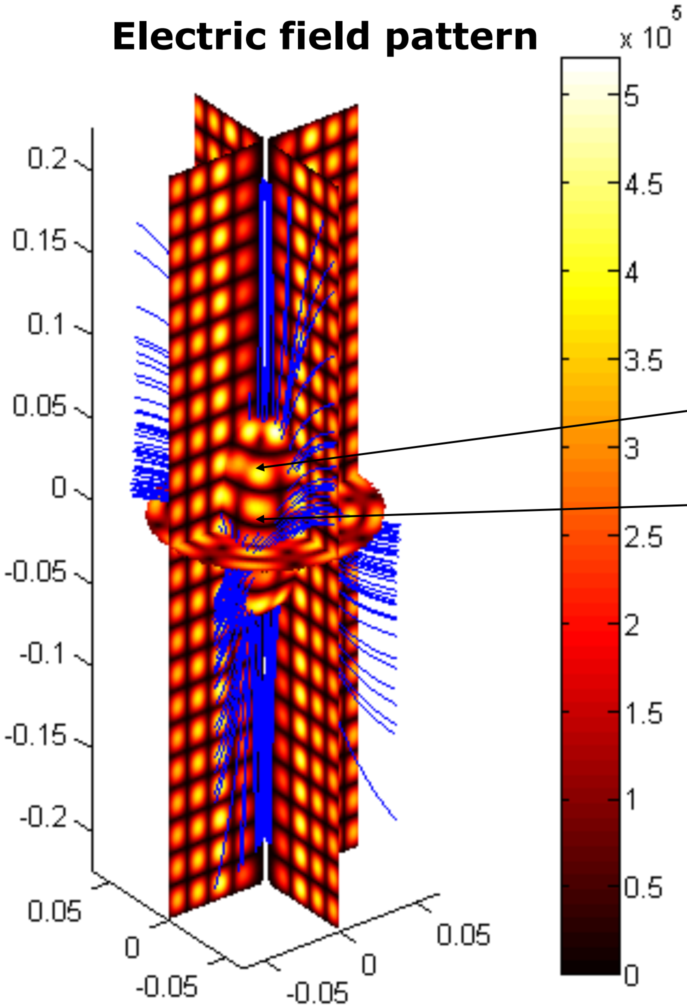

Plasma density distribution in proximity of ECR surface

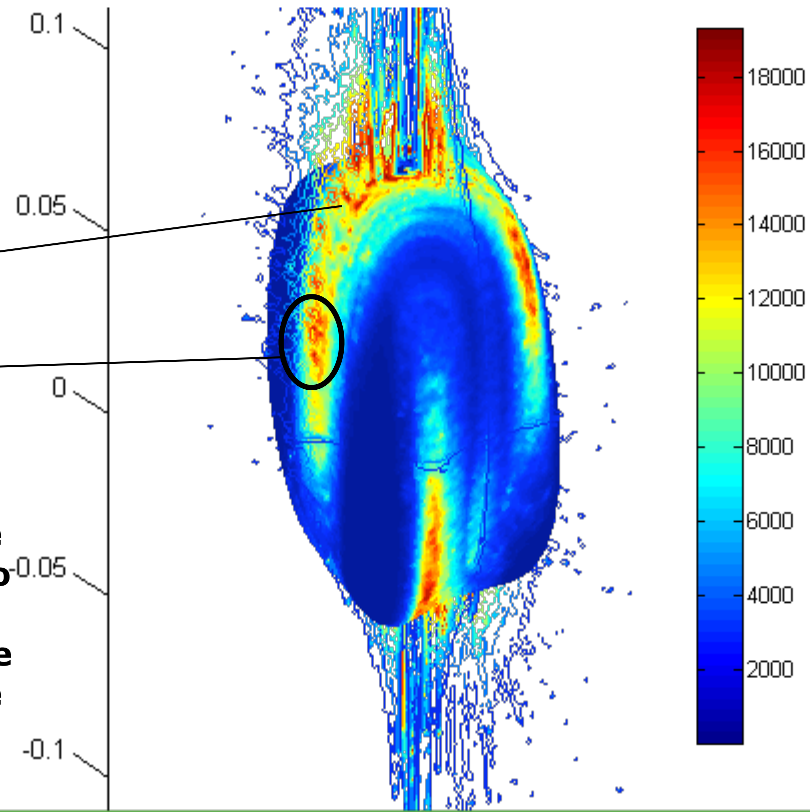

Density structure reflects to some extent the structure of the standing wave

NOTE that the plasma is almost completely confined inside the resonance surface

Profile of electron density for the different energy domains

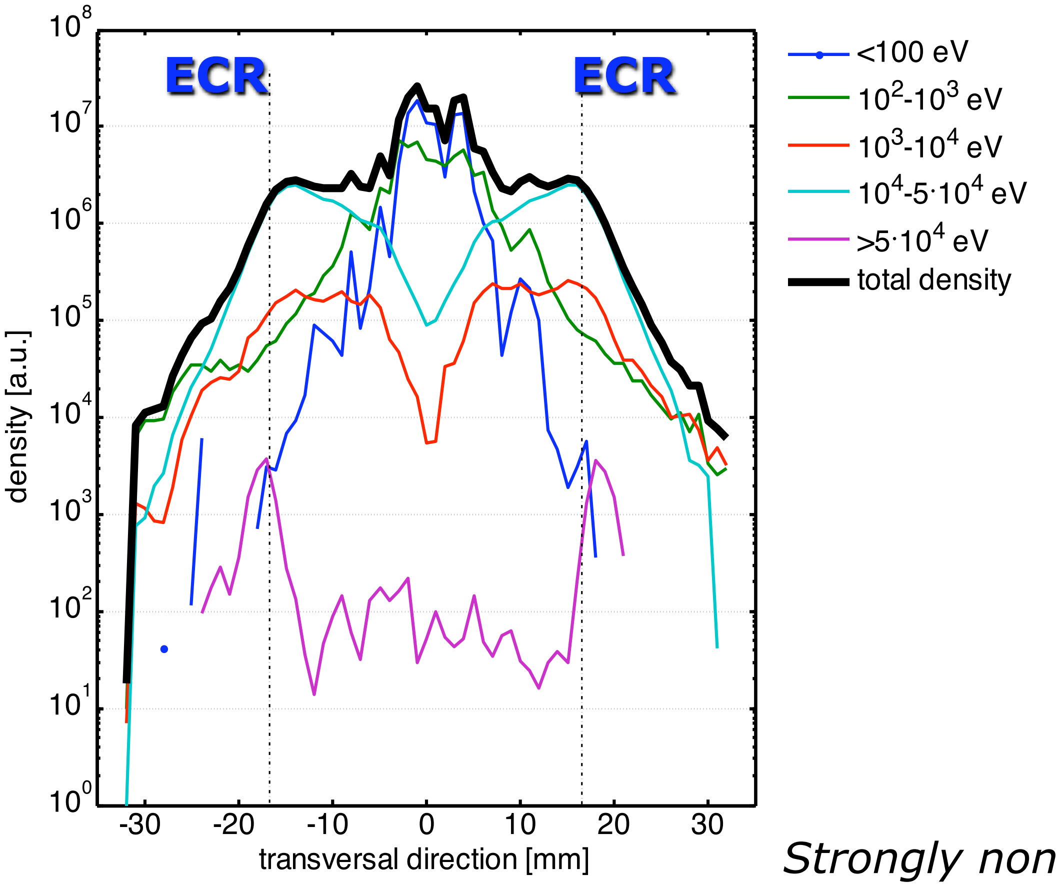

The simulated structure of the electron density provides information on:

- ***Regions of ion generation***
- ***Properties of plasma heating***
- ***Mechanisms of plasma confinement***

Strongly non-homogeneous distribution of the electrons inside the plasma chamber → due to the action of the electromagnetic wave through ECR

INFN Istituto Nazionale di Fisica Nucleare

SIMULATED 3D STRUCTURE OF THE PLASMA

Simulations based on a 3D Monte-Carlo collisional approach reveal that the plasma almost totally accumulates inside the ECR surface (**PLASMOID GENERATION**).

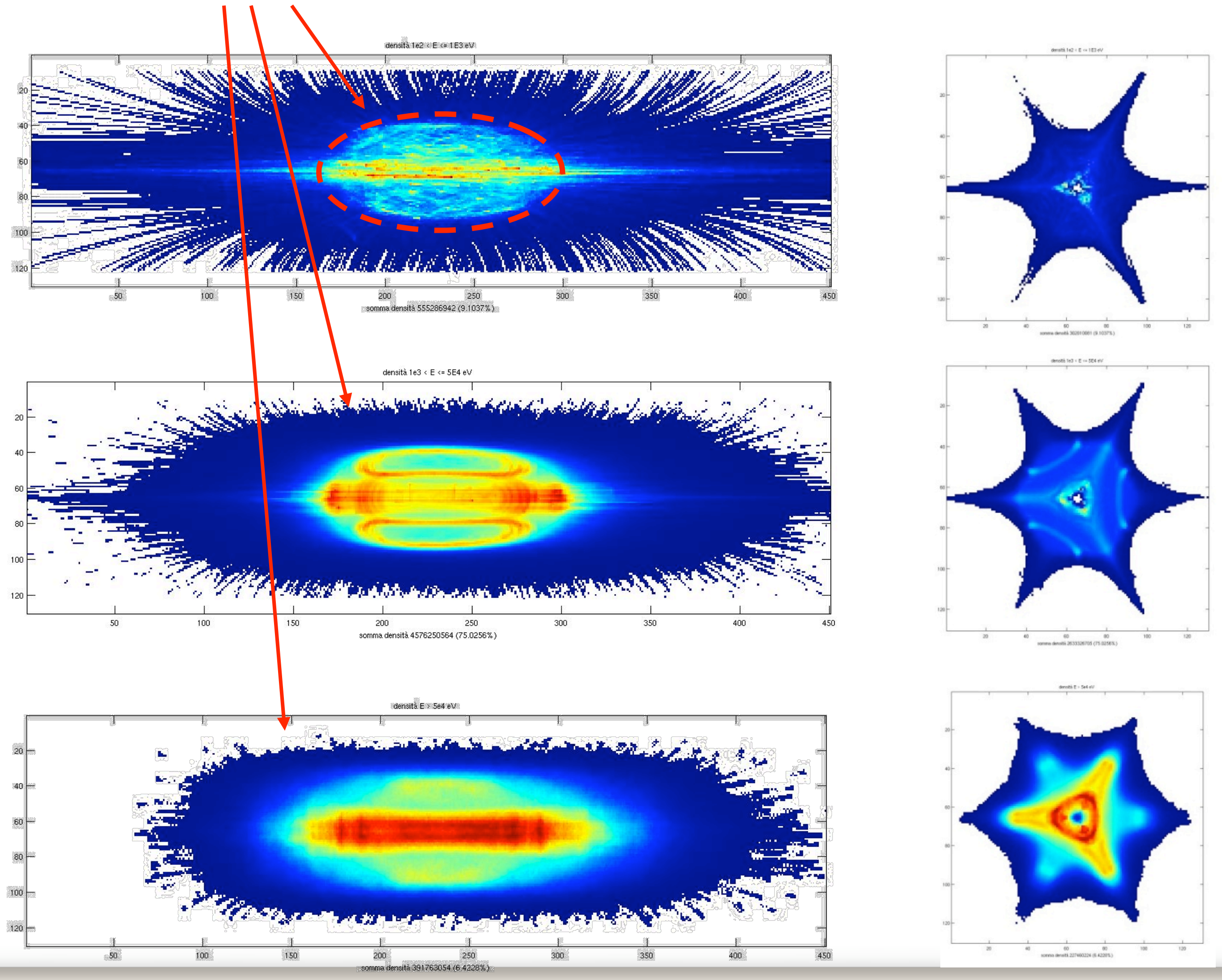

0.001<E<1 keV

1<E<50 keV

E>50 keV

[D. Mascali, K. Wiesemann, L. Neri L. Celona, S. Gammino and G. Ciavola, *in preparation for Phys. Rev. E*]

Explanation of plasma plugging inside the plasmoid

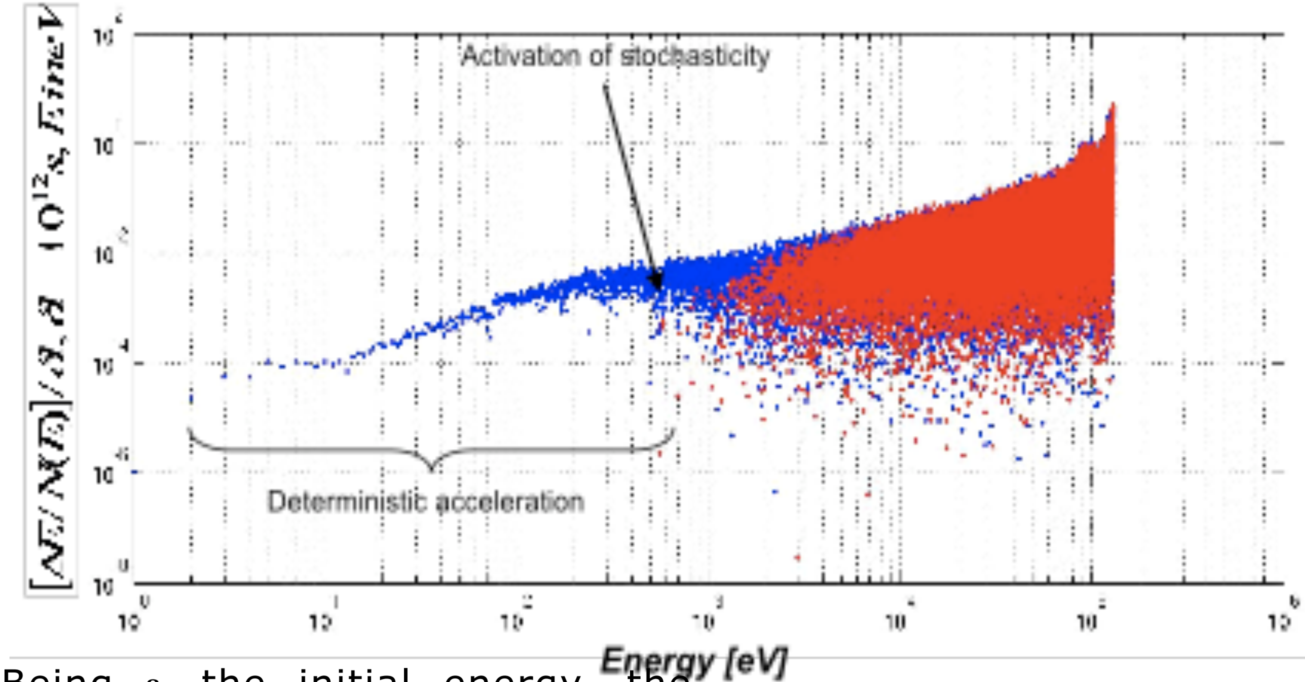

BLUE: Accelerated
RED: Decelerated

✓Low energy electrons (up to 3 10^3 eV) preferably gain energy when passing through the resonance;

✓most of them are reflected the just at the resonance;

Being ε_i the initial energy, the energy after the resonance crossing will be given by the following equation:

$$\varepsilon = \varepsilon_i + \Delta\varepsilon + \boxed{2\cos(\phi_0 - \phi_p)\sqrt{\varepsilon_i \times \Delta\varepsilon}}$$

term which accounts of the stochasticity in the wave-particle interaction

$$2\cos(\phi_0 - \phi_p)\sqrt{\varepsilon_i \times \Delta\varepsilon} << \varepsilon_i + \Delta\varepsilon$$

$$\boxed{\varepsilon \approx \varepsilon_i + \Delta\varepsilon}$$

For low enough initial energies (E<1 keV), the acceleration is purely deterministic

Towards self-consistency: ion formation

Ions initial position can be extracted where high energy electrons are placed. Net ion-electron density determines fluctuations in plasma quasi-neutrality (first step towards self-consistency).

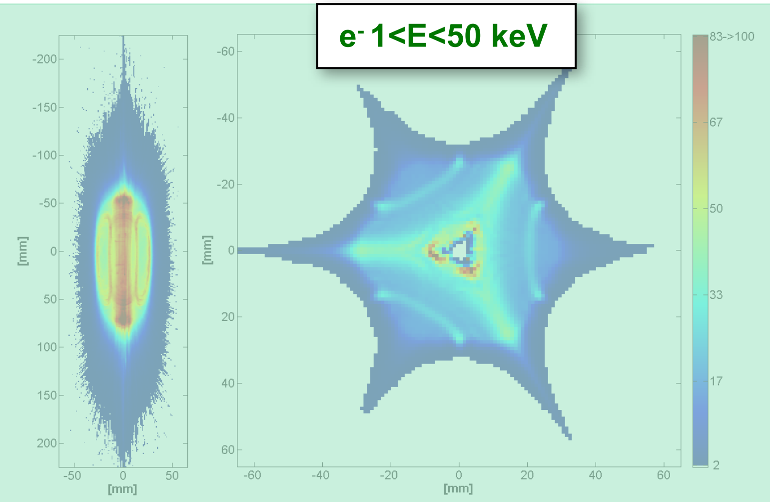

Electrons distribution fixes regions of ion generation

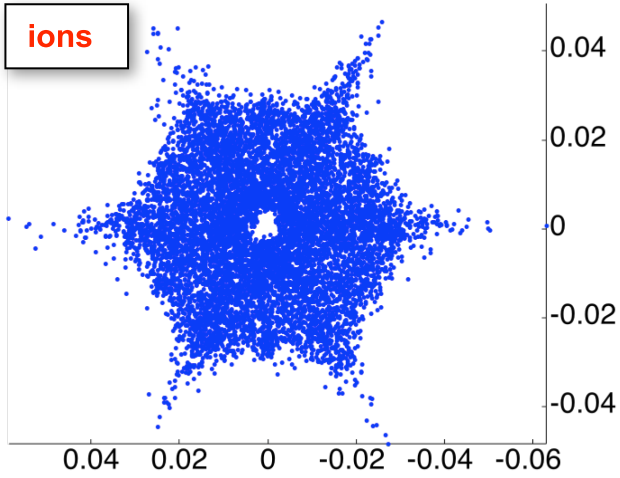

Ions were simulated asuniquely subjected to collisions and eventually to the magnetic field

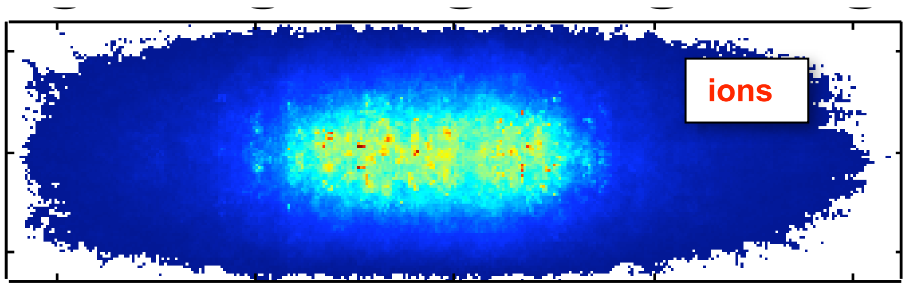

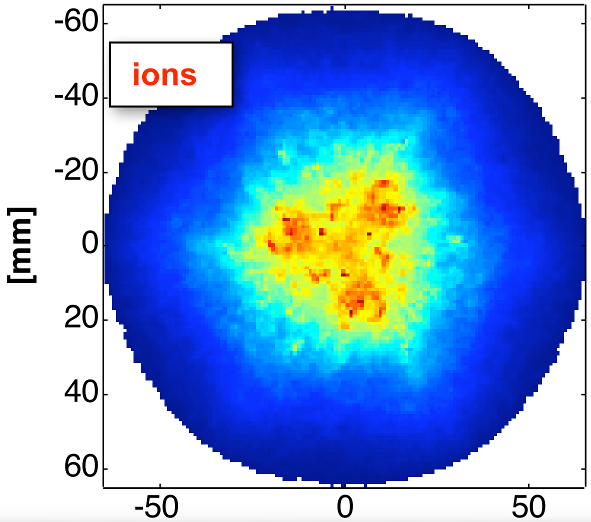

[D. Mascali, K. Wiesemann, L. Neri, L. Celona, S. Gammino and G. Ciavola, *in preparation for Phys. Rev. E*]

An example of Self-Consistency

The DL formation at the plasmoid edge

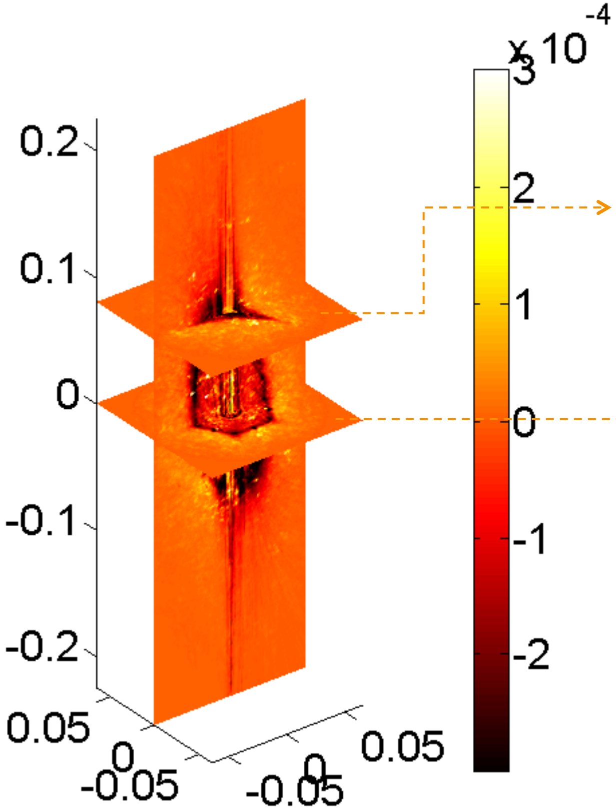

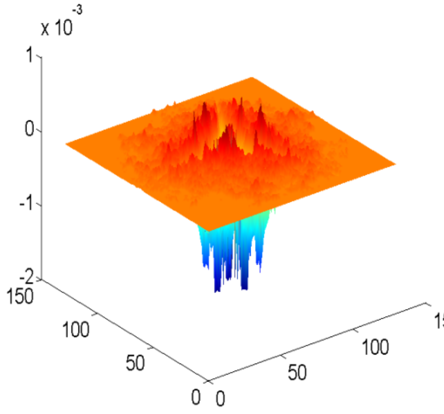

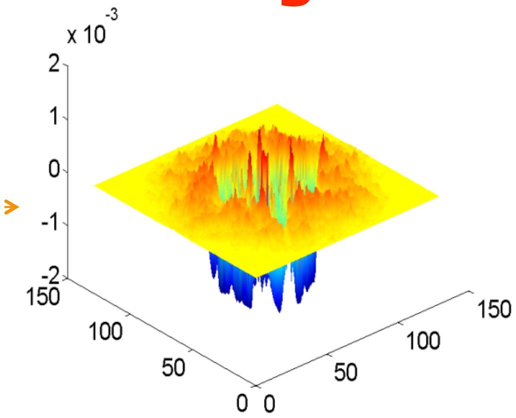

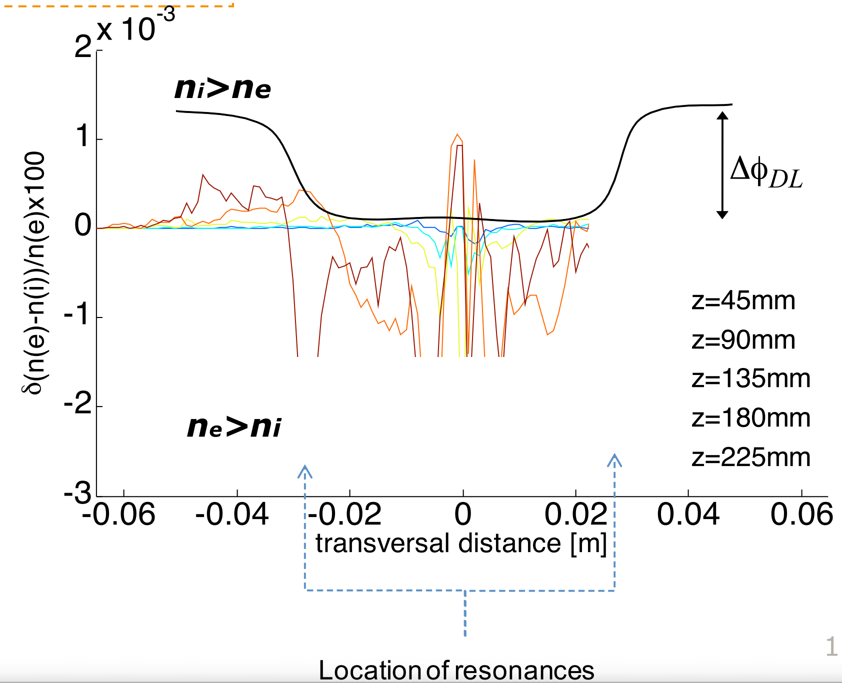

Electrons are retained by the RF plug effect, while ions tend to diffuse across ECR layer due to their larger inertia and collisionality.

The DL potential arises radially to preserve quasi-neutrality in high magnetic field side.

[D. Mascali, *invited at 14th International Conference on Ion Sources – ICIS 2011, Rev. Sci. Instrum. 83, 02A336 (2012)*]

Explanation of frequency impact on the ion beam structure

Hollow beams are a consequence of plasma depletion in the near axis region

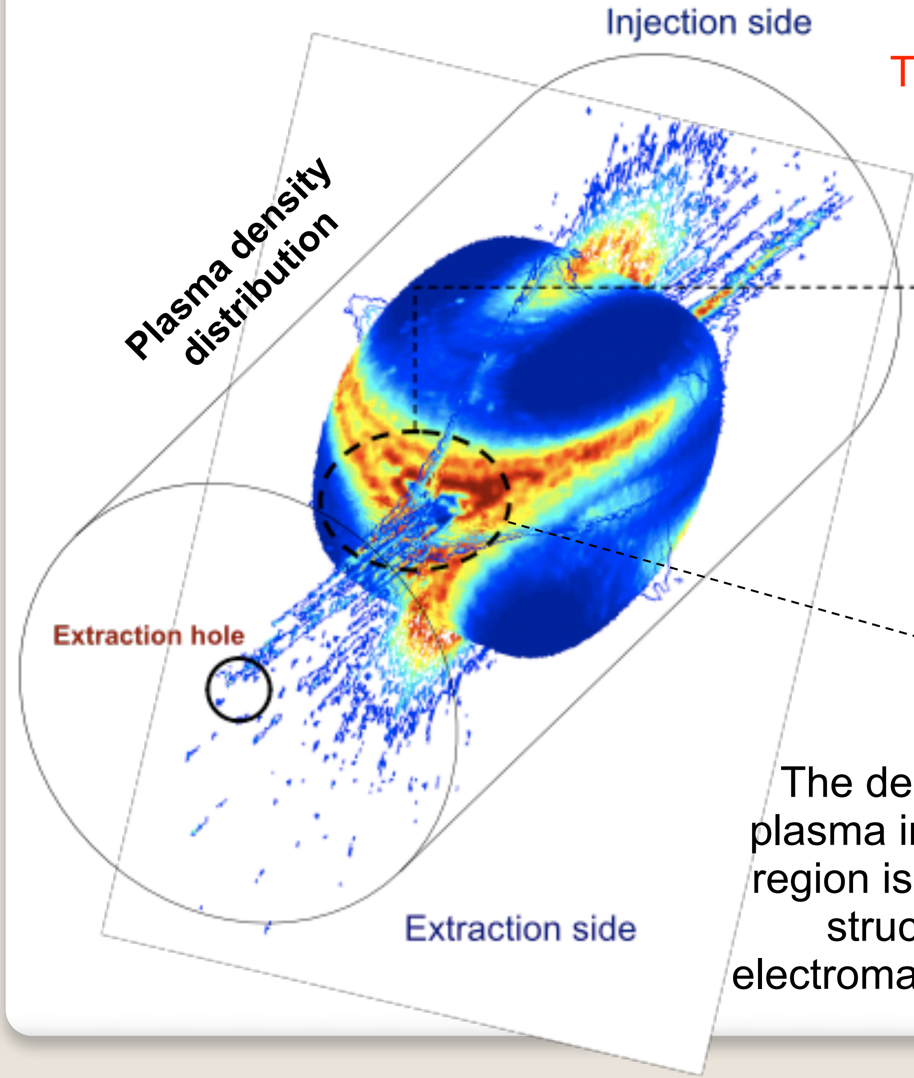

The density distribution explains why for some frequencies the beams appear hollow

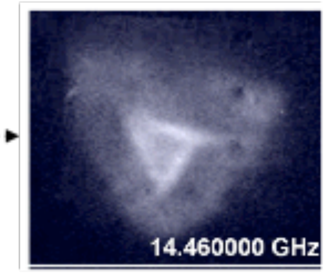

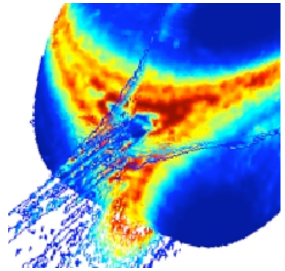

The depletion of plasma in near axis region is due to the structure of electromagnetic field.

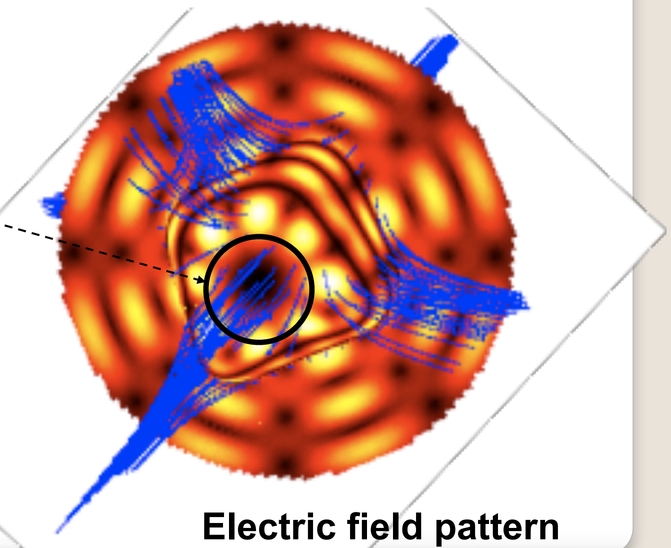

Electric field pattern

Huge impact of FTE on ion dynamics and beam formation

Jyvaskyla ECRIS

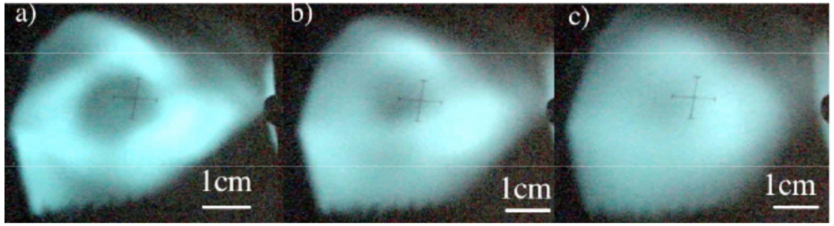

GSI-ECRIS (CAPRICE)

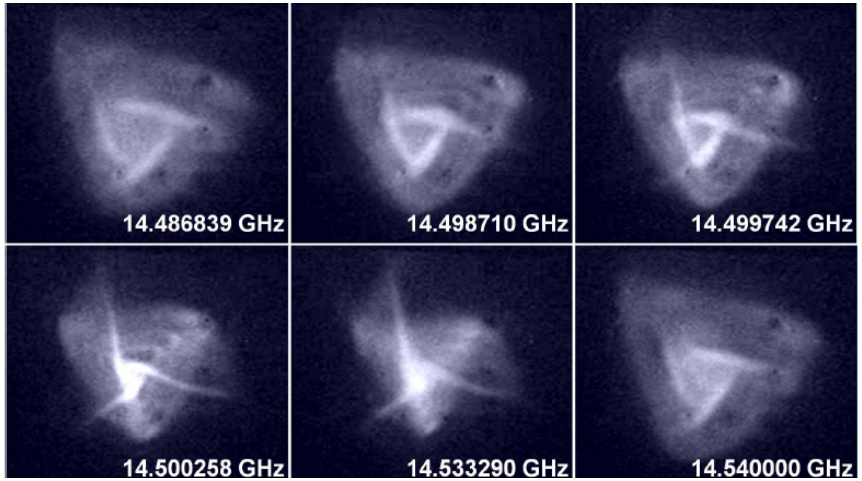

Hollow beam formation is a common feature of most of ECRIS.
Transversal beam shape confirms ions are magnetized in outer plasmoid region

Near axis density depletion takes place because of low EM field. **Most of the resonant modes at f>10GHz exhibit holes in near axis zone**

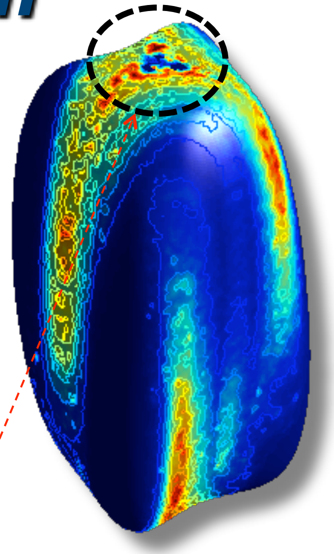

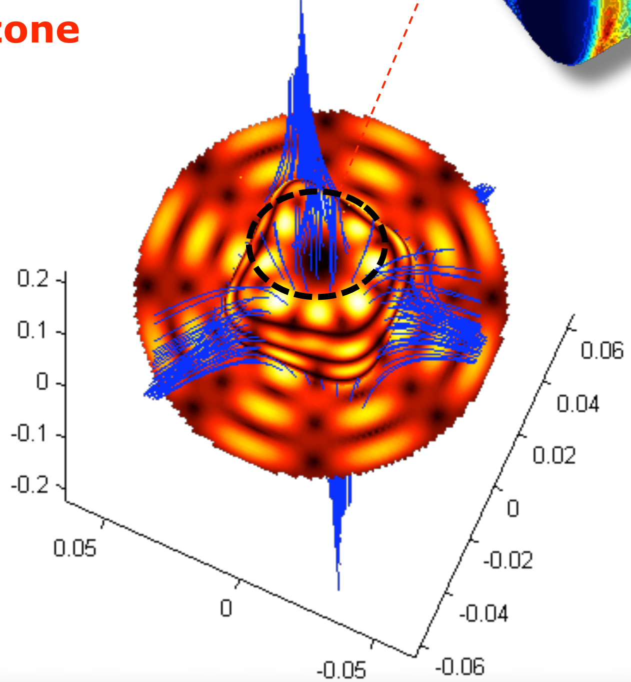

Preliminary results on self-consistent Ion Dynamics

Corrugation of the primary plasma surface

At first approximation it was assumed to be the same of the electromagnetic field pattern

[D. Mascali et al. *Plasma ion dynamics and beam formation in Electron Cyclotron Resonance Ion Sources*, Rev. Sci. Instrum.]

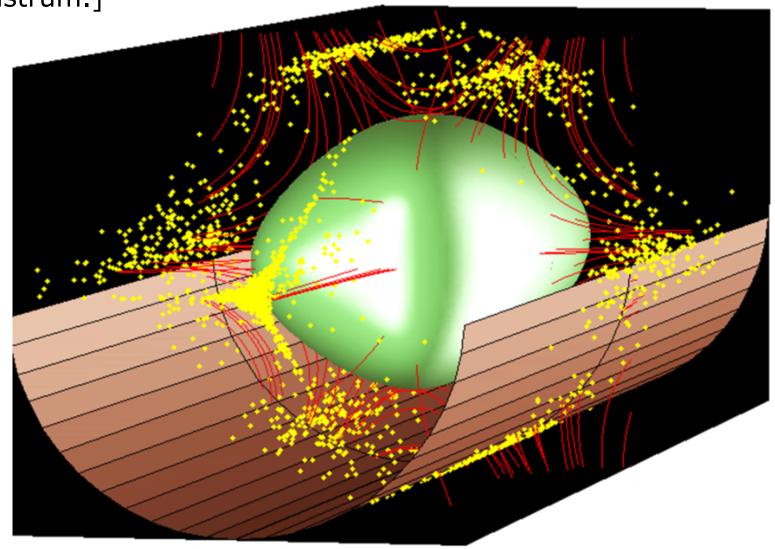

Simulated Ar^{10+}
Smooth primary plasma surface
30 V of PP-SP electrostatic potential

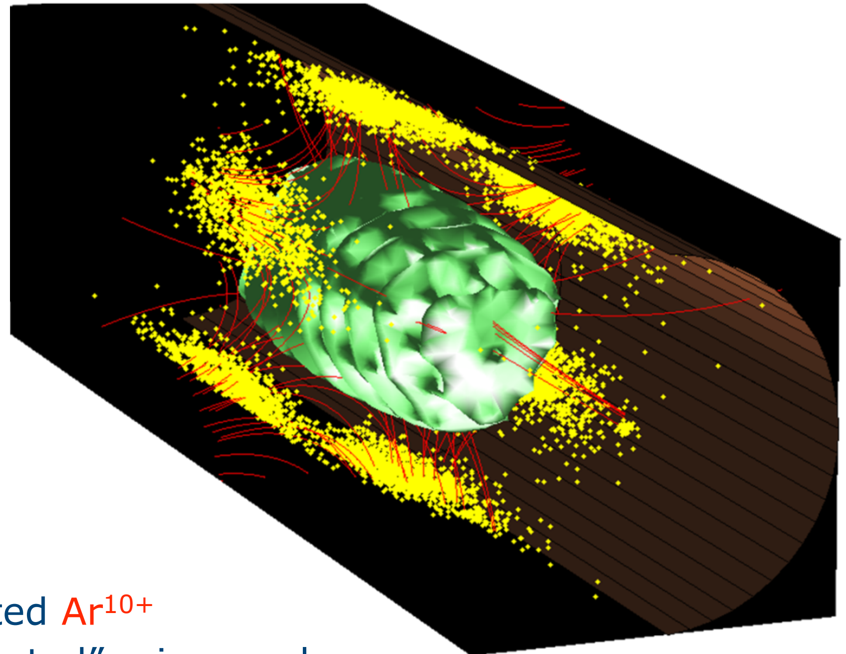

Simulated Ar^{10+}
"Corrugated" primary plasma surface
30 V of mean PP-SP potential

Ion lifetime depends strongly on corrugation, mean value of accelerating potential and inner resonance plasma density. Recent simulations estimate τ_i~0.5-3 ms, according to density fluctuations.

Thank you for your attention!!

R&D on Ion Sources team: Santo Gammino, Luigi Celona, Giovanni Ciavola, David Mascali, Lorenzo Neri, Giuseppe Castro, Federico Di Bartolo, Rossella Di Giugno, Claudia Caliri, Luciano Allegra